

Cancerous Tumor Ablation Using Different Microwave Ablation Applicators

Doctoral Thesis

by

Vellavalapalli Satish

(2017MEZ0024)



**DEPARTMENT OF MECHANICAL ENGINEERING
INDIAN INSTITUTE OF TECHNOLOGY ROPAR**

September, 2023

Cancerous Tumor Ablation Using Different Microwave Ablation Applicators

A Thesis Submitted
In Partial Fulfilment of the Requirements
for the Degree of

DOCTOR OF PHILOSOPHY

by

**Vellavalapalli Satish
(2017MEZ0024)**



**DEPARTMENT OF MECHANICAL ENGINEERING
INDIAN INSTITUTE OF TECHNOLOGY ROPAR**

September, 2023


Vellavalapalli Satish: *Cancerous Tumor Ablation Using Microwave Ablation Applicators*

**Copyright © 2023, Indian Institute of
Technology Ropar All Rights Reserved**

DEDICATED
TO
FAMILY & FRIENDS

Declaration of Originality

I hereby declare that the work which is being presented in the thesis entitled **CANCEROUS TUMOR ABLATION USING DIFFERENT MICROWAVE ABLATION APPLICATORS** has been solely authored by me. It presents the result of my own independent investigation/research conducted during the time period January 2018 (joining the Ph.D. program) January 2023 (Ph.D. Thesis submission) under the supervision of Dr. Ramjee Repaka, Associate Professor, Department of Mechanical Engineering. To the best of my knowledge, it is an original work, both in terms of research content and narrative, and has not been submitted or accepted elsewhere, in part or in full, for the award of any degree, diploma, fellowship, associateship, or similar title of any university or institution. Further, due credit has been attributed to the relevant state-of-the-art and collaborations (if any) with appropriate citations and acknowledgments, in line with established ethical norms and practices. I also declare that any idea/data/fact/source stated in my thesis has not been fabricated/ falsified/ misrepresented. All the principles of academic honesty and integrity have been followed. I fully understand that if the thesis is found to be unoriginal, fabricated, or plagiarized, the Institute reserves the right to withdraw the thesis from its archive and revoke the associated Degree conferred. Additionally, the Institute also reserves the right to appraise all concerned sections of society of the matter for their information and necessary action (if any). If accepted, I hereby consent for my thesis to be available online in the Institute's Open Access repository, inter-library loan, and the title & abstract to be made available to outside organizations.


12/09/2023

Signature

Name: Vellavalapalli Satish
Entry Number: 2017MEZ0024
Program: Doctor of Philosophy.
Department: Department of Mechanical Engineering
Indian Institute of Technology Ropar
Rupnagar, Punjab 140001


Date: 12/09/2023

Acknowledgments

I wish to express my gratitude to Dr. Ramjee Repaka, Associate Professor, Department of Mechanical Engineering, who, gave freely of his time, influenced virtually every aspect of this thesis. I also wish to thank the chair of my thesis advisory committee, Prof. Navin Kumar, and the other members of the group, Dr. Himanshu Tyagi, Dr. Anupam Agrawal, and Dr. Subrahmanyam Murala, for their valuable advice during my period of work. I also thank my fellow research Scholars at IIT Ropar, Rakesh Kumar, Purna Abhishek, Ananth Bhardwaj, Pranav Johri and Rajesh Kumar for their comments and assistance at various stages of the research work. Assistance in carrying out the research and writing of this project was extended by a number of people to whom I am grateful.

I would like to thank the authorities of IIT Ropar for their support by providing research labs and other facilities without which my project would never have been completed. I also acknowledge the Science and Engineering Research Board (SERB), GoI, for partially supporting this work. For errors and omissions in the work, however, the author assumes complete responsibility.

I profusely thank my parents, who indirectly helped me in the execution of my Ph.D. research work.


12/09/2023

Vellavalapalli Satish

2017MEZ0024

Certificate

This is to certify that the thesis titled **Studies on Cancerous Tumor Ablation Using Different Microwave Ablation Applicators**, submitted by **Vellavalapalli Satish (2017MEZ0024)** for the award of the degree of **Doctor of Philosophy** of Indian Institute of Technology Ropar, is a record of bonafide research work carried out under my (our) guidance and supervision. To the best of my knowledge and belief, the work presented in this thesis is original and has not been submitted, either in part or full, for the award of any other degree, diploma, fellowship, associateship or similar title of any university or institution.

In my (our) opinion, the thesis has reached the standard fulfilling the requirements of the regulations relating to Ph.D. Degree.



Signature of the Supervisor

Dr Ramjee Repaka

Department of Mechanical Engineering

Indian Institute of Technology Ropar

Rupnagar, Punjab 140001

Date: 12/09/2023

Lay Summary

According to the Global Cancer Observatory and World Health Organization, cancer incidence and mortality rates are very high, making it the leading disease in the world. Even in developed countries like America, one out of four deaths are due to cancer, which constitutes the second highest mortality rate after heart disease. Despite significant progress in understanding, diagnosing, treating, and preventing the disease in the past decades, cancer still remains the major threat to human beings. Localized tumor ablation therapies gain their importance more than surgical resection in cancer treatment, with more satisfactory results with less recurrence rate. MWA is a newly developed minimally invasive thermal ablation technique primarily used in the treatment of HCC. During MWA procedure, the trocar (antenna or applicator) is being inserted into the tumor either transcutaneously or laparoscopically with the help of available image guidance techniques. Large tumors can be treated efficiently by MWA technique using multiple trocars (two or three) or by repositioning a single trocar. Multiple trocars must be inserted simultaneously in clinical practices to achieve a large ablation zone. The clinical trials of microwave ablation techniques lack imaging guidance techniques, which results in difficulty in monitoring and controlling the ablation range. Further, it isn't easy to achieve accurate trocar positioning with the ablation region in real-time applications.

Based on the mortality rates caused by the cancer, the present thesis work considers the six major organs affected by cancer: lung, breast, stomach/gastric, liver, liver (with colon metastasis), and kidney for MWA procedure. In this section various parameters (such as input power and treatment time) that influence the outcome of microwave ablation, with a focus on importance of apt positioning of the trocar into the tissue during the procedure have been discussed. The present work addresses one of the major problems clinicians faces, i.e., the proper placement of the trocar due to poor imaging techniques and human error, resulting in incomplete tumor ablation and increased surgical procedures. The highest values of the ablation region have been observed for the liver, colon metastatic liver and breast cancerous tissues compared to the other organs at the same operating conditions. A slight inapt positioning of trocar (either linearly and angular insertion) results in ablation of a large volume of healthy tissue. The positioning of the trocar is more important for the breast, liver, and kidney, as they produce a more rapid zone of heating in a shorter span of time. The organs lung, stomach, and kidney organs exhibit lesser deformations, with low volumetric tissue contractions of 0.14 mm, 0.11 mm, and 0.8 mm, respectively, as compared to the deformation values of other organs. The outcome of the present study may help in better clinical output. Moreover, the liver organ has been chosen as the focus of this work in order to address the precise positioning of the trocar during the MWA technique.

Most of the studies available on MWA were conducted at 2.45 and 0.915 GHz frequencies. However, more research is going on to explore the use of frequencies above 2.45 GHz in MWA techniques. The use of High frequency in MWA techniques increases flexibility in probe design and in developing better treatment planning procedures. As per the guidance from the Industrial, Scientific and Medical (ISM) Radio Band guidelines, the frequencies of 2.5, 5.89 and 24 GHz, can be used in medical applications. In this study 2.45 (nearly 2.5) and 6 (nearly 5.87) GHz frequency operated trocars have been considered for microwave ablation. The present study has been designed to assess the ablation region obtained using multiple MWA trocars both numerically and experimentally. Further, multiple trocars have been inserted into the tissue in parallel and non-parallel positions operating at 2.45 GHz and 6 GHz frequencies. An internally cooled trocar operated at a frequency of 2.45 and 6 GHz has been modelled in the present study. Experimental analysis has been performed on egg white with added albumin protein since it expedites real-time monitoring of the ablation region obtained during the microwave ablation technique. Even though multiple trocars increase ablation volume, inapt positioning leads to the ablation of healthy tissue. The problem, as mentioned, can be overcome by using non-parallel trocar positioning. Further, the angle of the trocar insertion and the energy among the trocars (frequency, time and power) will be decided based on the tumour's precise location in the tissue.

In addition to this, a novel microwave trocar design has been proposed and considered in the present study wherein single antenna is being replaced with multiple tines supplied with energy at available conventional and high frequencies. Once the trocar is inserted into the tissue, the dual tine array can be deployed according to the tumor size and required ablation region. Each tine operates at a frequency of 2.45/6 GHz with a microwave power of 15 W and an ablation time of 10 min (considered for all cases). This novel trocar is expected to treat tumors of nearly 3 cm in diameter and of irregular shapes, restrict damage to the healthy tissues and achieve more concentrated ablation regions. Precise position of trocar into the tissue is one of the major problems clinicians face during thermal ablation procedure. Inadequate position of trocar leads to incomplete tumor ablation and further increases the operational procedure. The present model is expected to overcome the problem associated with the inapt positioning of the trocar.

Abstract

While there are several chronic diseases more destructive to life than cancer, none is more feared. Despite significant progress in understanding, diagnosing, treating, and preventing the disease in the past decades, cancer still remains the major threat to human beings. Microwave ablation (MWA) modality is a newly emerged minimally invasive thermal therapy technique for the treatment of various malignant tumors up to 3 cm in diameter. The ablation region obtained during MWA mainly depends on the type and efficiency of the trocar as well as the energy transfer from the generator to the biological tissue. The trocar plays an essential role in the MWA system by governing the energy distribution during tissue ablation. The present study analysed the microwave ablation of cancerous tumors located in six vital organs and estimated the significance of tissue properties in relation to the importance of appropriate positioning of the trocar during treatment. The six major organs are lungs, breast, stomach/gastric, liver, liver (with colon metastasis), and kidney. The input power (100 W) and ablation times (4 minutes) with apt and inapt positioning of the trocar have been considered to compare the ablation volume of various cancerous tissues. The highest values of the ablation region have been observed for the liver, colon metastatic liver and breast cancerous tissues compared with other organs at the same operating conditions. The positioning of the trocar is more important for the breast, liver, and kidney, as they produce a more rapid zone of heating in a shorter span of time. The present study addresses one of the major problems clinicians face: the proper placement of the trocar due to poor imaging techniques and human error, resulting in incomplete tumor removal and increased surgical procedures. In addition, the present work also consists of a new MWA trocar design proposed to overcome the above-mentioned issues. A numerical analysis of MWA using the new medical applicator (also referred to as trocar or antenna) in L and U shaped has been presented in this work. The novel microwave applicator consists of a flexible dual tine trocar, with each tine supplied with energy at equal and/or different frequencies, 2.45/6 GHz. Once the trocar is inserted into the tumor, the flexible tines can be deployed independently with varying lengths. With the proposed trocar design, large size ablation zones can be obtained by varying the frequency of the supplied energy and the deployment length of the tines. Various combinations of supplied energy and deploying lengths result in tumor ablations ranging from 2.7 to 4 cm in diameter. Supplying energy at high-frequency (6 GHz) to the trocar results in ablating tumors (> 4 cm) with spherical ablation region. The use of high-frequency energy in MWA (6 GHz) further addresses the issue of collateral damage to the tissue and the low spherical shaped ablation region associated with the MWA procedure at 2.45 GHz frequency. In addition, the present study has been designed to assess the ablation region obtained using multiple MWA trocars both numerically and experimentally. Further, multiple trocars have been inserted into the tissue in parallel and non-parallel positions operating at 2.45 GHz and 6 GHz frequencies. Internal trocar cooling mechanism has been considered in this study.

Experimental analysis has been performed on egg white with added albumin protein. It has been found from the present study that MWA operated at 2.45/6 GHz with the non-parallel position of multiple trocars into the tissue leads to a considerable increase in the ablation region as compared to the parallel insertion of trocars. Hence, it may be concluded that non-parallel insertion of trocars is suitable to treat irregular-shaped large cancerous tumours (>3 cm). The non-parallel simultaneous insertion of trocars can overcome the healthy tissue ablation issue as well as the problem associated with indentation.

List of Publications from Thesis

Journals

- 1) **Vellavalapalli Satish**, Ramjee Repaka (2022). "Microwave Ablation Trocar Operated at Dual Tine Dual-Frequency: A Numerical Analysis". Journal of Engineering and Science in Medical Diagnostics and Therapy (JESMDT).; 6(2): 021002. ASME. <https://doi.org/10.1115/1.4056410>.
- 2) **Vellavalapalli Satish**, Ramjee Repaka (2023). "Microwave Ablation Trocar for Ablating Cancerous Tumors: A Numerical Analysis". Medical & Biological Engineering & Computing Journal (MEBC). Springer. <https://doi.org/10.1007/s11517-023-02781-7>.
- 3) **Vellavalapalli Satish**, Ramjee Repaka. "Safety and Efficacy of Intracavitary Microwave Ablation in hepatic gland tumors: Numerical and In-vitro Studies". Proceedings of the Institution of Mechanical Engineers, Part H: Journal of Engineering in Medicine. 2023;0(0). <https://doi.org/10.1177/09544119231179136>.
- 4) **Vellavalapalli Satish**, Ramjee Repaka. "The Influence of Microwave Ablation Parameters on The Positioning of Trocar in Different Cancerous Tissues: A Numerical Study" (Under Review, Electromagnetic Medicine and Biology).

Conference Proceedings

- 1) **Vellavalapalli Satish**, Jatin Kumar, & Ramjee Repaka (2019). "Analysis of Ablation Volume Produced During Microwave Ablation of Breast Cancerous Lesion Using Fourier and Non-Fourier Models." Proceedings of the ASME 2019 International Mechanical Engineering Congress and Exposition. Volume 3: Biomedical and Biotechnology Engineering. Salt Lake City, Utah, USA. November 11–14. V003T04A038. ASME. <https://doi.org/10.1115/IMECE2019-10800>.

Patents

- 1) **Vellavalapalli Satish**, Ramjee Repaka (2023). "An applicator for treating biological tissue and a method thereof ". Published. Indian Patent and Trademark Office.

Table of Contents

Declaration	ii
Acknowledgement	iii
Certificate	iv
Lay Summary	v
Abstract	vii
List of Publications	ix
List of Figures	xi
List of Tables	xv
Notations and Abbreviations	xvi
1. Introduction	1
2. Literature Review/ Theoretical Framework	5
3. Research Design / Methodology	11
4. Results and Discussion	29
5. Summary / Conclusions	69
References/Bibliography	71

List of Figures

Figure 1.1 Estimated number of new cases in 2020, World, both sexes, all ages.....	1
Figure 1.2 Estimated number of deaths in 2020, World, both sexes, all age.....	2
Figure 1.3 Various Modalities in Cancer treatment.....	2
Figure 1.4 Cancer treatment planning system.....	3
Figure 3.1 3 – Dimensional two compartment tumor embedded organ.....	15
Figure 3.2 Mesh dependence study of the liver organ was conducted by considering variations in temperature with respect to the number of elements.....	16
Figure 3.3 Meshed computational domain of MWA comprising 1233150 tetrahedral elements.....	16
Figure 3.4 Schematic of the numerical model	18
Figure 3.5 The average FT-IR spectra of egg white in the mid-infrared region (4000 – 400 cm^{-1})	18
Figure 3.6 Meshed computational domain of MWA comprising 2197589 tetrahedral elements.....	19
Figure 3.7 In vitro experimental setup.....	20
Figure 3.8 Osensa optical temperature measuring device.....	20
Figure 3.9 post-ablation zones created in a hepatic gland at the end of 360 s with microwave power 140 W MWA procedure (a) numerical simulation, 3.1 cm \times 4.4 cm \times 4.7 cm and (b) experimental analysis on egg white, 2.9 cm \times 4.1 cm \times 4.5 cm.....	20
Figure 3.10 Schematic diagram of the trocar inserted into the tumor embedded biological tissue.....	21
Figure 3.11 Schematic of zero deployed, semi deployed, and fully deployed angular tine of trocar configurations. (All dimensions are in mm)	22
Figure 3.12 Fully deployed dual tine trocar (a) inserted into the hepatic gland embedded with 3 cm diameter tumor and (b) Enlarged view of the tines inside the tissue.....	22
Figure 3.13 Schematic view of trocar positioning relative to the tumour axis.....	22
Figure 3.14 The computed specific absorption rate (SAR) in KW/kg takes on its highest values near the tip and the slot with 15 W microwave power at a) 2.45 GHz, b) 6 GHz frequency on both the tines.....	23
Figure 3.15 Meshed 3 cm tumor embedded hepatic gland having 8127233 tetrahedral elements.....	24
Figure 3.16 Ablation zones created in hepatic gland at the end of 360 s MWA procedure with numerical simulation, 1.27 cm \times 2.4 cm.....	25
Figure 3.17 Meshed computational domain of MWA comprising 1,376,966 tetrahedral elements.....	26

Figure 3.18 The calculated specific absorption rate (SAR) in kW/kg for 15 W microwave power at a) 2.45 GHz and b) 6 GHz on both the tines.	26
Figure 3.19 Ablation regions obtained in hepatic gland by numerical simulation with 1.79 cm transverse ablation length.....	27
Figure 4.1 Thermal ablation of 3 cm tumor embedded various cancerous tissues at 2.45GHz frequency.....	29
Figure 4.2 Thermal ablation of 3 cm tumor embedded various cancerous tissues at 2.45 GHz frequency.....	31
Figure 4.3 Thermal ablation of 3 cm tumor embedded hepatic gland of various cancerous tissues at 2.45 GHz frequency.....	33
Figure 4.4 The temperature measuring points of the tissue.....	35
Figure 4.5 The time dependence of temperature at various points during MWA when the cancerous tumors in lung, breast, stomach/gastric, liver, colon liver metastatic, and kidney tissues are exposed to the microwave frequency of 2.45GHz and an input power of 100W for 4 minutes.....	35
Figure 4.6 The time dependence of fraction of tissue damage at various points during MWA when the cancerous tumors in lung, breast, stomach/gastric, liver, colon liver metastatic, and kidney tissues are exposed to the microwave frequency of 2.45GHz and an input power of 100W for 4 minutes.....	35
Figure 4.7 Tissue contraction obtained during MWA of different organs at microwave frequency of 2.45GHz and an input power of 100W for 4 minutes.....	36
Figure 4.8 Temperature measuring points and trocar positioning.....	37
Figure 4.9 Variation of temperature with the ablation time in the hepatic gland (a) in-vitro and numerical experiments at 2.45 GHz frequency, (b) numerical experiments at 2.45 GHz and (c) numerical experiments at 6 GHz.....	38
Figure 4.10 Temperature distribution in the hepatic gland tissue obtained during parallel insertion of water cooled MWA trocars: a) both trocars at 2.45 GHz, b) both trocars at 6 GHz and c) one trocar at 6 GHz and the other one at 2.45 GHz.....	39
Figure 4.11 Temperature distribution in the hepatic gland tissue obtained during non-parallel insertion of water cooled MWA trocars: a) 2.45 GHz on both trocars, b) 6 GHz on both trocars and c) 6 and 2.45 GHz on both trocars.....	40
Figure 4.12 Ablation zones in egg white obtained when trocars have been operated for 6 minutes at 140 W microwave power.....	42
Figure 4.13 Thermal Ablation of hepatic gland using the proposed novel trocar with a) 2.45 GHz frequency on longitudinal tine; b) 2.45 GHz frequency on curved tine; c) 6 GHz frequency on longitudinal tine and d) 6 GHz frequency on curved tine.....	44

Figure 4.14 Thermal ablation of 3 cm tumor embedded hepatic gland at a) 2.45 GHz frequency on both the tines; b) 6 GHz frequency on both the tines; c) 2.45 GHz frequency on longitudinal tine and 6 GHz on curved tine and d) 6 GHz frequency on longitudinal tine and 2.45 GHz on curved tine.....	47
Figure 4.15 Thermal ablation of 3 cm tumour embedded hepatic gland at 2.45 GHz.....	49
Figure 4.16 Thermal ablation of 3 cm tumour embedded hepatic gland at 6 GHz.....	49
Figure 4.17 Thermal ablation of 3 cm tumour embedded hepatic gland using multiple trocars operated at 2.45/6 GHz frequencies.....	50
Figure 4.18 Thermal ablation of 3 cm tumour embedded hepatic gland with inapt positioning of trocar operated at 2.45 GHz.....	50
Figure 4.19 Thermal ablation of 3 cm tumour embedded hepatic gland with inapt positioning of trocar operated at 6 GHz.....	51
Figure 4.20 Spatial locations of temperature and fraction of tissue damage monitoring points for longitudinal and curved tines.....	51
Figure 4.21 Variation of temperature and fraction of tissue damage with the treatment time when tines are maintained at different combinations of frequencies: a) 2.45 GHz frequency on both the tines; b) 2.45 GHz frequency on longitudinal tine and 6 GHz on curved tine; c) 6 GHz frequency on longitudinal tine and 2.45 GHz on curved tine and b) 6 GHz frequency on both the tines.....	53
Figure 4.22 Temperature distribution points at the radial edge of the tumor. (a) Positions of the temperature monitoring points (front view). (b) Positions of the temperature monitoring points (top view).....	55
Figure 4.23 Variation of temperature with time near the tumor edge for fully deployed tines: (a) At 2.45 GHz (both tines), (b) At 2.45 (left-side tine) and 6 GHz (right-side tine), (c) At 6 GHz (both tines) and (d) At point 1.....	55
Figure 4.24 Ablation regions (front view) obtained by MWA using first order Arrhenius rate equation for fully deployed tines operated at 2.45 and 6 GHz for 15 W microwave power....	56
Figure 4.25 Ablation regions (top view) obtained by MWA using first order Arrhenius rate equation for fully deployed tines operated at 2.45 and 6 GHz for 15 W microwave power....	57
Figure 4.26 Temperature distribution points at the radial edge of the tumor. (a) positions of the temperature monitoring points (front view). (b) positions of the temperature monitoring points (top view).....	59
Figure 4.27 Temperature rise with time near the edge of the tumor for semi and fully deployed tines operated at: (a) 2.45 GHz (both tines), (b) 2.45 GHz (left-side tine) and 6 GHz (right-side tine), (c) 6 GHz (left-side tine) and 2.45 GHz (right-side tine), (d) 6 GHz (both tines) and (e) At point 1.....	60
Figure 4.28 Ablation regions (front view) obtained by MWA using first order Arrhenius rate equation for fully (1 st) deployed and semi (2 nd) deployed tines operated at 2.45 and 6 GHz for 15 W microwave power.....	61

Figure 4.29 Ablation regions (top view) obtained by MWA using first order Arrhenius rate equation for fully (1st) deployed and semi (2nd) deployed tines operated at 2.45 and 6 GHz for 15 W microwave power.....	63
Figure 4.30 Temperature distribution points on the radial edge of the tumor. (a) positions of the temperature monitoring points (front view). (b) positions of the temperature monitoring points (top view).....	63
Figure 4.31 Temperature rise with time at four points near the edge of the tumor for semi deployed tines operated at: (a) 2.45 GHz (both tines), (b) 2.45 GHz (left-side tine) and 6 GHz (right-side tine), (c) 6 GHz (both tines) and (d) At point 1.....	63
Figure 4.32 Ablation regions (front view) obtained by MWA using first order Arrhenius rate equation for semi deployed tines operated at 2.45 and 6 GHz for 15 W microwave power....	65
Figure 4.33 Ablation regions (top view) obtained by MWA using first order Arrhenius rate equation for semi deployed tines operated at 2.45 and 6 GHz for 15 W microwave power.....	66
Figure 4.34 Tissue contraction obtained during MWA for three deploying conditions of the tine operated at a) 2.45 and b) 6 GHz for 15 W microwave power.....	66

List of Tables

Table 3.1 Dimensions of microwave coaxial antenna.....	14
Table 3.2: Material properties of microwave coaxial antenna.....	15
Table 3.3: Properties of different cancer tissue used in numerical simulation	15
Table 3.4: Comparison of major absorptions in IR spectra of egg white and hepatic gland tissue.....	19
Table 3.5: Properties of tissue/gland.....	23
Table 3.6: Material properties of microwave coaxial antenna (tine).....	27
Table 3.7: Validation of ablation region in hepatic gland against the experimental results by Saito et al. during MWA at 2.45 GHz.....	27
Table 4.1: Microwave ablation of six major organs operated at 100 W for 4 treatment minutes.....	30
Table 4.2: Ablation zone dimensions following 6 min of MWA at 140 W with trocars inserted non-parallelly and operated at 2.45 GHz and 6 GHz frequencies.....	40
Table 4.3: Ablation zone dimensions following 6 min of MWA at 140 W with non-parallel insertion of trocars and operated at 2.45 GHz and 6 GHz frequencies.....	41
Table 4.4: Dimensions of the generated ablation zones in egg white using Solero MWA antenna operated for 6 min at 140 W microwave power.....	43
Table 4.5: Specifications of Antenna.....	45
Table 4.6: Comparison of antenna performance of various combinations obtained numerically.....	46
Table 4.7: Comparison of the simulated ablation results with the novel microwave antenna at various frequency combinations.....	48
Table 4.8: Minimum diameter of the tumor to be ablated during MWA using fully deployed tines.....	58
Table 4.9: Minimum diameter of the tumor to be ablated during MWA of semi and fully deployed tines.....	62
Table 4.10: Minimum diameter of the tumor to be ablated during MWA using semi deployed tines.....	65

Notations and Abbreviations

E	Electric field vector (V/m)	ε_r'	Dielectric constant
E	Electrical field strength (V/m)	f	Frequency (Hz)
K	Thermal conductivity (W/(m·K))	ω	Angular frequency (Hz)
P	Power density (W/m ³)	ω	Curved frequency (Hz)
Q_m	Metabolic heat generation (W/m ³)	ω_b	Blood perfusion rate (1/s)
Q_p	Power disipation (W/m ³)	μ_r	Relative permeability
T	Temperature (K)	σ	Electrical conductivity (S/m)
T_b	Baseline physiological temperature (K)	ρ	Density (kg/m ³)
c	Specific heat (J/(kg·K))	k_0	Free space wavenumber (cm ⁻¹)
ε_0	Permittivity of free space (F/m)	n	Unit vector
ε_r	Relative permittivity		

Subscripts t and b referring to the tissue and the blood domain, respectively

Chapter 1

Introduction

The introduction of thesis provides a comprehensive overview of the research topic and establishes the context of the study. It begins by highlighting the significance and relevance of the subject matter in the field of cancer treatment. The introduction discussed the current state of knowledge, identify gaps or limitations in existing research, and articulate the research objectives and aims.

While there are several chronic diseases more destructive to life than cancer, none is more feared. Cancer is a group of diseases characterized by the uncontrolled growth and spread of abnormal cells owing to internal factors (inherited mutations, immune system, hormonal or genetics) and/or external factors (food habits, lifestyle, radiations, chemicals known as carcinogens, tobacco or certain viral infections). Despite significant progress in understanding, diagnosing, treating, and preventing the disease in the past decades, cancer still remains the major threat to human beings [1]. Cancer is the second most commonly diagnosed disease in the world. According to the World Health Organization, Cancer is the most commonly diagnosed and accounts for the death globally, with one in six deaths, in 2020 (*refer Fig. 1.1*)[2].

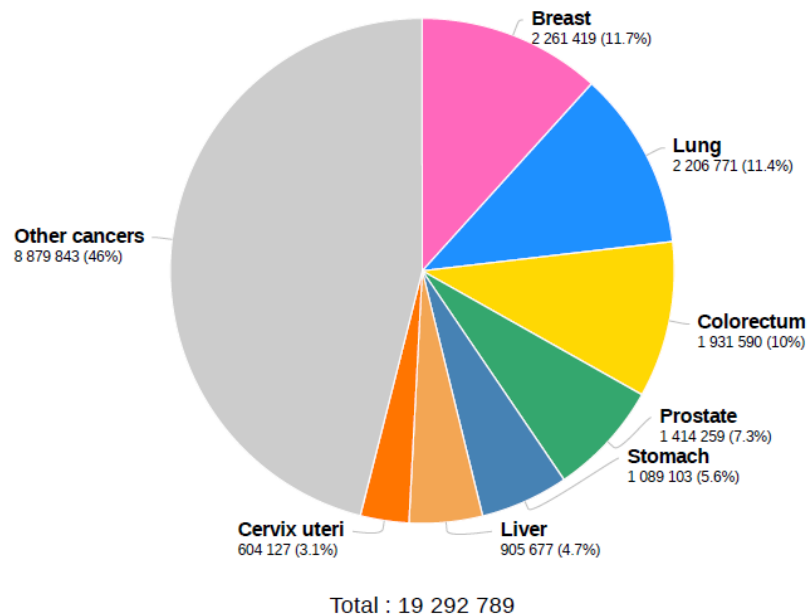


Figure 1.1 Estimated number of new cases in 2020, World, both sexes, all ages

As per International Agency for Research on Cancer (IARC), 1 in 5 people develop cancer during their lifetime. The most commonly diagnosed types of cancer deaths worldwide are lung, breast, stomach/gastric, liver, colon liver metastatic, and kidney. Among the leading cancer diseases, Hepatocellular carcinoma (HCC) ranks sixth in most commonly diagnosed

cancer and fourth in mortality rate caused due to cancer worldwide in 2020 (*refer Fig. 1.2*)[2]. In the case of males, HCC ranks fifth in global cases and third in terms of death. Hepatocellular carcinoma diagnosis often occurs at the advanced stage, making it challenging to treat with the existing curative therapies [3]. Moreover, regular chemotherapy is less effective and leads to a low survival rate [4,5]. Various modalities available for treating cancer are chemotherapy, surgery, resection, organ transplantation, radiation, minimally invasive thermal therapies, and trans-arterial chemoembolization [6] (*refer Fig. 1.3*). Amongst the treatment modalities surgical resection is the most common modality used to treat hepatocellular carcinoma. However, it is only suitable for only a small group of patients with no medical history and good hepatic gland functioning [7]. Localized tumor ablation therapies gain their importance more than surgical resection with more satisfactory results with less recurrence rate. It can overcome various problems associated with conventional treatment procedures, viz., morbidity, complications and chances of recurrence [8].

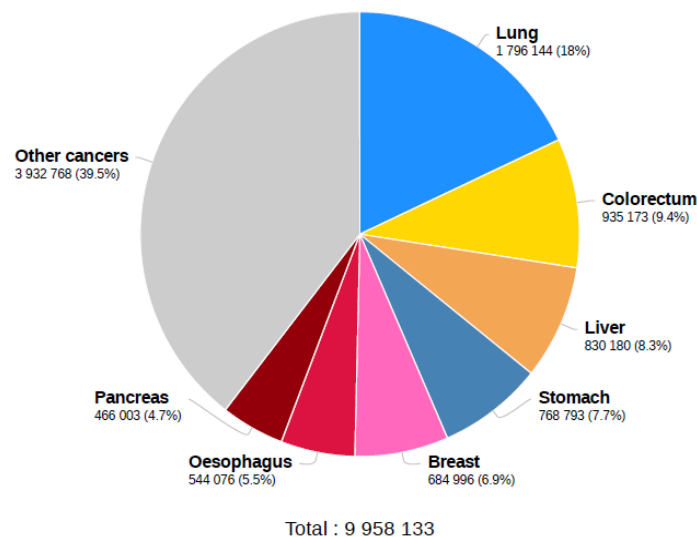


Figure 1.2 Estimated number of deaths in 2020, World, both sexes, all ages

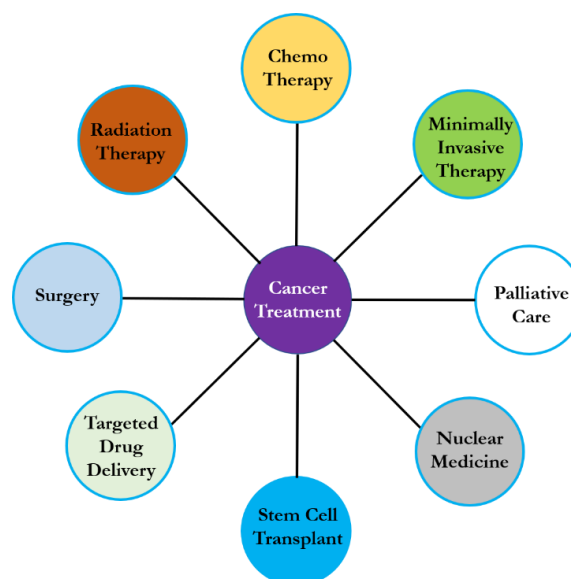


Figure 1.3 Various Modalities in Cancer Treatment

Based on the energy source, the minimally invasive therapies (localized tumor ablation therapies) are classified into laser, radiofrequency, microwave, high intensity focused ultrasound, cryoablation, irreversible electroporation and nanosecond pulsed electric fields [9–11]. These techniques are primarily used by clinicians to treat cancerous and benign tumors. Apart from other treatment modalities, microwave ablation modality is a newly emerged minimally invasive thermal therapy technique for the treatment of various malignant tumors of 3 cm in diameter[12]. So far, there is no practically available medical device that can ablate tumors having diameter greater than 4 cm using a single applicator. Large tumors can be treated efficiently by MWA technique using multiple trocars (two or three) or by repositioning a single trocar[13]. Multiple trocars must be inserted simultaneously in clinical practices to achieve a large ablation zone [14].

MWA procedure is carried out by inserting the medical applicator into the tissue through the surgical opening, laparoscopy, or percutaneously using medical image guidance (*refer* Fig. 1.4). The three major components of the MWA device are the microwave generator, power distribution system, and trocar. The trocar plays an important role in the MWA system, which transfers energy from the generator to the biological tissue.

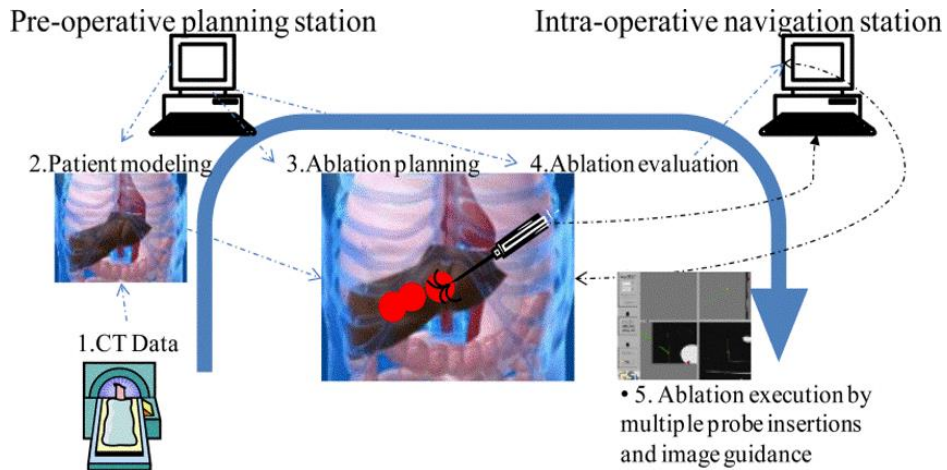


Figure 1.4: Cancer treatment planning system [15]

The microwave energy from the trocar to the tissue at 2.45 GHz frequency agitates the water molecules in the tissue, generating friction and heat and leading to coagulative tissue necrosis [16]. Among the range of frequencies available for microwave ablation, only microwaves with 2.5 GHz, 5.89 GHz and 24 GHz can be used in medical applications as per (ISM) Radio Band guidelines [17,18]. Use of further higher frequencies in MWA apart from the available conventional frequencies show a better radiation efficiency with high energy absorption by the tissue and low power requirement[19].

Numerical modelling of treatment modalities for curing cancerous tumors helps to understand the effect of varying parameters on ablation volume in a unique environment [20].

It plays a major role in overcoming drawbacks of existing treatment modalities, thereby establishing a better treatment planning system (TPS).

1.1 Significance, Scope and Definitions

The present study analyzed the microwave ablation of cancerous tumors located in six major cancer-prone organs and estimated the significance of input power and treatment time parameters in the apt positioning of the trocar. The six major organs are lungs, breast, stomach/gastric, liver, liver (with colon metastasis), and kidney. The input power (100 W) and ablation times (4 minutes) with apt and inapt positioning of the trocar have been considered to compare the ablation volume of various cancerous tissues. The present study addresses one of the major problems clinicians face: the improper placement of the trocar due to poor imaging techniques and human error, resulting in incomplete tumor removal and increased surgical procedures. In addition, the present work also consists of a novel trocar design that has been proposed to overcome the above-mentioned issues. A numerical analysis of MWA using the novel medical applicator (also referred to as trocar or antenna) in L and U shapes has been presented in this chapter. The novel microwave applicator consists of a flexible dual tine trocar, with each tine supplied with energy at equal and/or different frequencies, 2.45/6 GHz. Once the trocar is inserted into the tumor, the flexible tines can be deployed independently with varying lengths. With the proposed trocar design, large size ablation zones can be obtained by varying the frequency of the supplied energy and the deployment length of the tines. The use of high-frequency energy in MWA (6 GHz) further addresses the issue of collateral damage to the tissue and the low spherical shaped ablation region associated with the MWA procedure at 2.45 GHz frequency.

The present study has been designed to assess the ablation region obtained using multiple MWA trocars both numerically and experimentally. Further, multiple trocars have been inserted into the tissue in parallel and non-parallel positions operating at 2.45 GHz and 6 GHz frequencies. Internal trocar cooling mechanism has been considered in this study. Experimental analysis has been performed on egg white with added albumin protein.

In conclusion, the introduction to this thesis has successfully laid the groundwork for the cancer research endeavour. By emphasizing the significance and relevance of the high frequency MWA as cancer treatment modalities, it has provided a clear rationale for the study. Furthermore, the introduction effectively outlined the current state of knowledge, identified existing gaps and limitations in research, and precisely articulated the research objectives and aims.

Literature Review/Theoretical Framework

The literature survey of the thesis provides a comprehensive and critical analysis of existing intellectual works relevant to present research topic. It establishes a solid foundation for the study by facilitating the positioning of the research within the broader academic discourse. Through the establishment of the theoretical and conceptual framework, research lay a groundwork, showcasing its significance and relevance.

Microwave ablation (MWA) is a newly evolving field in minimally invasive thermal therapy techniques. It uses electromagnetic waves at frequencies ranging from 300 MHz to 300 GHz. Electromagnetic waves have wide medical research applications in diagnoses and therapies. Medical practitioners primarily use microwave ablation (MWA) in the field of oncology, i.e., to raise the cancerous tumour's temperature above 52°C, in order to achieve its necrosis state. The electromagnetic waves generated in the magnetron travel via coaxial cable/waveguide and penetrate the biological tissue through the applicator slot. The irradiated region and penetration of the electromagnetic waves during microwave ablation depend upon the type of tissue and energy (i.e., frequency). The penetration depth of electromagnetic waves is inversely proportional to their frequencies. As the frequencies increase, the penetration depth of the microwaves decreases, leading to higher energy density accumulation within a smaller region.

Based on the mortality rates caused by cancer, the present study considers six major organs affected by cancer: lung, breast, stomach/gastric, liver, liver (with colon metastasis), and kidney for MWA analysis. Various parameters (input power, treatment time) influencing the outcome of microwave ablation in the apt positioning of the trocar into the tissue during microwave ablation have been presented in this paper. The present numerical study helps in predicting the actual ablation volume by taking tissue contraction parameters also into consideration. The main focus would be to report the impact of individual variations in the model outcomes in terms of treatment time, damage volume and temperature distribution. Different correlations can be developed, highlighting the relationship between the input properties and the model outcomes. Based on the performed sensitivity analysis, dielectric parameters, thermal parameters, and the temperature interval across which the tissue changes phase have been the most significant aspects which impact the MWA model outputs. Further, the thermal contraction of tissue significantly affects the MWA techniques. Most of the studies available are on the liver and kidneys, and a few are on lung tissue.

The available microwave ablation applicators at 2.45 GHz are used for heating the tissue during treatment. The energy density is considered to be low for biological tissue at this particular frequency, leading to a teardrop-shaped ablation region of less sphericity index. The

low-frequency ablation region further leads to collateral damage to the tissue along its length and affects the applicator efficiency in ablating the tissue. Additionally, healthy tissue ablation is also attributed to uncontrolled energy deposition mechanism in the biological tissue. Further, the applicators available in the market are limited to treat low ablation regions only. Also, multiple and parallel insertions of applicators are required to obtain larger ablation region. Multiple applicators lead to increased insertion of applicators into the biological tissue and lead to a sizeable unwanted ablation region. The addition of a sleeve mechanism to the applicator modifies the ablation pattern of various sizes. Further, the addition of cooling to the applicator increases its efficiency as well. Therefore, a need exists in developing MWA applicators for better treatment planning in the biological tissues. The use of high-frequency MWA applicator results in more concentrated energy with a larger ablation region. Currently available applicators having coaxial cable (TEM mode) are based on available conventional frequencies. These applicators are limited to achieving low ablation region with less sphericity index. The use of higher frequency in the coaxial cable (TEM mode) increases the applicator's diameter, which is unsuitable for treating biological tissue. As frequency increases, the width of the waveguide decreases, making it apt for minimally invasive treatment. Using a high-frequency MWA (using waveguides) applicator for minimally invasive ablation procedures with a cooling system and sleeve mechanism is a novel idea. The novel trocar design in the present thesis overcomes the problem associated with collateral damage to the tissue along its length. The problem in using a higher frequency in the MWA can be rectified with the proposed applicator. This applicator solves the issue of obtaining a sphericity index in ablating the tissue. A single high-frequency MWA applicator shows better efficiency than combining two existing applicators, and eliminated the need of deploying multiple applicators. During the ablation procedure the problems that generally occur are backward heating of the applicator's shaft, skin injury at the point of insertion of the applicator and the power loss in the energy transmission line of the system. In order to overcome the above-mentioned problems, shaft temperature has to be maintained low by cooling the applicator. The cooling mechanism in the microwave applicator is disclosed in the article [21] which is an internally cooled applicator for the coaxial antenna at 2.45 GHz. It utilizes the space between the outer and inner conductor of the applicator for water passage. The present invention consists of an external cooling system to the applicator, which circulates the water on the extreme outer layer to increase its efficiency. It can also reduce backward heating of the applicator due to radiated microwave energy and shows a better temperature distribution with a large ablation region.

2.1 Literature Survey:

Several ablation techniques are currently available. Apart from various existing conventional cancer treatment procedures (viz., surgery, radiation therapy, and chemotherapy), minimally invasive thermal ablation procedures show better results in treating focal cancerous

tumors. Commonly used minimally invasive ablation techniques include radiofrequency ablation (RFA), microwave ablation (MWA), high-intensity focused ultrasound (HIFU) ablation, cryoablation and chemical ablation. Seror et al. [22] compared different types of ablation techniques stated advantages and disadvantages of radiofrequency ablation, cryotherapy, microwave ablation and electroporation methods. Understanding the differences in different treatment modalities is crucial since they impact the benefits and constraints associated with each technique. In the treatment of cancer, the selection of an appropriate method should be based on the individual patient. Florida et al. [23] described the importance of microwave ablation procedure in renal tumors and stated various advantages and development trends in it. To achieve the most comprehensive ablation possible, it is imperative to enhance the technique of ablation and further refine imaging guidance. MWA is a technology that can consistently and repeatedly generate a substantial ablative lesion in solid renal neoplasms, ensuring uniform tissue necrosis without any skipped areas. Ge et al. [5] investigated on a multi-slot coaxial antenna designed for achieving near-spherical ablation zones during MWA of hepatic gland by ensuring there was proper impedance matching to the treated tissue. The proposed antenna offers superior heating efficiency of tissues and produces more near-spherical ablation zones compared to the available antennas. Xi et al. [24] compared the various types of available frequencies for microwave ablation technique. Which states that high-frequency microwave ablation (MWA) causes less damage to normal tissue, creates a more concentrated ablation region, and elicits a better material response compared to conventional MWA. Kuang et al. [25] investigated the use of a cooled-shaft antenna in MWA techniques. The study concluded that use of cooling shaft trocar could increase the size of the ablation zone induced by microwaves at higher energy levels and further reduces the risk of skin burn in ablation therapies. Ibitoye et al. [26] analysed the efficiency of different antennas proposed for microwave ablation (MWA) using both numerical and experimental approaches. The proposed antenna models consist of monopole, single slot, dual slot, and sleeved trocars. The results stated that the sleeved antenna demonstrates the highest ability to concentrate microwave energy into tissues, resulting in highest sphericity. Audit et al. [27] proposed the importance of waveguide applicator in medical applications microwave radiometry. Furthermore, the results indicate that waveguide applicators, as a replacement for coaxial cable antennas, can be utilized for various applications including thermography cancer detection, thermoregulatory investigation, and microwave-induced hyperthermia. Stuchly et al. [28] proposed the idea of multimode square waveguide applicators for medical applications of microwave power and stated Microwave diathermy applicators. The results showed that uniform heating of a specified volume can be achieved using waveguide microwave applicator. Izzo et al. [29] compared the microwave ablation procedure with RFA and stated that microwaves create larger ablations than radiofrequency when controlled for power in ex vitro tissue. Brace et al. [30] developed a finite element model to study tissue contraction of the liver. The study proposed importance of tissue

contraction on microwave ablation procedure.

2.2 Summary and Implications

In addition to the past treatment modalities used for cancer, ablation modalities are increasingly being utilized in all patients due to their numerous benefits compared to other treatment options. Ablation techniques, such as radiofrequency ablation, microwave ablation, electroporation, HIFU and cryoablation, offer several advantages that make them highly beneficial for cancer patients [9,31]. Except for electroporation, all of these methods cause fatal damage at a cellular level and irreversible architectural deconstruction at a tissue level by the thermal effect. Minimally-invasive thermal ablation techniques provide an effective approach for local destruction of solid tumor. Theoretical models of the ablation process are a powerful tool for predicting the temperature profile in tissue and resultant tissue damage created by ablation devices. These models play an important role in the design and optimization of devices for microwave tissue ablation. They are useful tools for exploring and planning treatment delivery strategies. However, the Pennes model has been widely used for studying heat transport and temperature distribution in numerous biological and medical applications due to its simplicity, computational efficiency, and effectiveness. Microwave ablation is known to produce an oval-shaped ablation zone. However, spherical ablation is more beneficial because it may improve the achievement of large ablation zone, sufficient margins and further the effectiveness of treating lesions that are more than 3 cm in diameter. Additionally, spherical ablation zones may minimize the risk of complications associated with the thermal damage of adjacent normal liver tissue, compared to elongated ablation zones. As antennas are generally constructed using coaxial cable, smaller-diameter antennas can have trouble handling higher power levels without unwanted thermal damage to tissues around the proximal antenna shaft. Circulation of chilled saline solution or water is the most commonly used method for cooling the antenna shaft, and the addition of active cooling has enabled delivery of higher powers for longer times, and in turn, production of larger ablation zones.

2.3 Drawbacks: Microwave Ablation (MWA)

Microwave ablation is recognized for generating an ablation zone with a teardrop shape. In spite of various advantages among other treatment modalities, MWA still suffers from drawbacks and one out of them is non-spherical ablation zone. Apart from the ablation of the tumour, normal tissue is being damaged more. Since spherical ablation is considered more advantageous as it has the potential to enhance the attainment of large and adequate margins [32,33]. Tumors greater than 3 cm in size have historically been difficult to treat with percutaneous ablation. Multiple Trocars are to be inserted parallelly to ablate the tumor of more than 3 cm in diameters [13]. Large tumours can be treated efficiently by MWA technique using multiple trocars (two or three) or by repositioning a single trocar. Multiple trocars must be inserted simultaneously in clinical practices to achieve a large ablation zone. Further, microwave power is inherently more

difficult to generate and deliver safely and efficiently to the tissue. This is primarily because microwave energy must be carried in coaxial cables since there are larger in diameter, more cumbersome and prone to heating. Decreased cable surface area leads to more power loss and increased cable heating [33]. The next major problem faced by the MWA technique is the development of a cooling system for the trocar. A robust active shaft cooling mechanism can mitigate many of these risks and is imperative to high power delivery. Currently, available microwave systems have technical limitations of underpowered systems, shaft heating, large-diameter probes, long and relatively thin ablation zones, unpredictable size and shape of the ablation region. The major limitations with existing systems: inability to treat tumors having diameter more than 3 cm and ablation time limited to 10 minutes [33]. Even though multiple trocars increase ablation volume, inapt positioning leads to ablate healthy tissue. It has been found that even a slight error in positioning the electrode would result in a significant mismatch in the shape of ablation volume produced during ablation. Multiple overlapping ablations or simultaneous use of multiple applicators may be required to successfully treat the entire tumor along with safety margin, though accurate targeting and placement of applicator can often be technically challenging [34].

Lacunae: Microwave Ablation (MWA)

Most of the studies on microwave ablation are of limited to treating tumors having diameter less than 3 cm. Limited number of studies use multiple probes with parallel insertion to treat the tumor with more than 3 cm in diameter. No study is available on the delivery of microwave power at higher frequency to avoid difficulties in constructing coaxial cables. No studies are available on optimizing the diameter of the trocar wherein the requirement of inherent cooling mechanism for better ablation outcome is necessary. Precise position of trocar into the tissue is one of the major problems clinicians faces during thermal ablation procedure. Inadequate position of trocar leads to incomplete tumor ablation and further increases the operational procedure.

Objectives:

1. Understanding the impact of microwave ablation parameters on vital cancerous organs.
2. MWA of HCC using parallel and non-parallel insertion of trocars.
3. MWA of HCC Tumors using novel design L shaped dual tine dual frequency trocar: One fixed and one flexible tine.
4. MWA of HCC Tumors using novel design U shaped dual tine dual frequency trocar: Both are flexible tines.

The methodology section of the thesis provides a comprehensive outline of the systematic approach that are employed to conduct the research. This section details the specific procedures, tools, and techniques utilized to develop numerical model and perform experimental analysis.

3.1 Numerical Modelling of MWA

Numerical analysis of internally cooled coaxial microwave ablation trocar for microwave ablation therapies comprises the following physical processes.

- (1) The transverse electric and magnetic (TEM) waves are emitted from a microwave coaxial antenna through the slot at an operating frequency of 2.45 GHz.
- (2) The absorption of TEM waves by the biological tissue produces heating due to dielectric hysteresis or rotating dipoles (continuous realignment of polar molecules), leading to the ablation of the tissue.
- (3) The thermal energy (heat) is carried within the tissue by conduction.
- (4) Due to the supplied energy, the change in temperature causes tissue contraction (i.e., change in its volume).

The electromagnetic waves and bioheat transfer physics model have been coupled to produce electromagnetic heating and heat transfer in solids and fluids and laminar flow physics models to produce an internal cooling system for trocar using COMSOL Multiphysics software.

The Helmholtz harmonic wave equation has been considered to calculate the electrical energy at all the mesh points of the biological tissue [18].

$$\nabla \times \mu_r^{-1}(\nabla \times E) - k_0^2(\epsilon_r - \frac{j\sigma}{\omega\epsilon_0})E = 0 \quad (1)$$

where E , μ_r , ϵ_r , σ , ϵ_0 , ω and k_0 represent the electric field vector (V/m), relative permeability, relative permittivity, electrical conductivity (S/m) of the material, the permittivity of free space, angular frequency (Hz) and free space wavenumber, respectively.

The amount of power absorbed (Q_p (W/m³)) from the electrical field by the tissue during microwave ablation has been expressed as

$$Q_p = \frac{\sigma E^2}{2} \quad (2)$$

which also serves as the heat source for Pennes bioheat transfer equation.

The Pennes bio-heat transfer equation has been used to compute the temperature distribution in the biological tissue during the microwave ablation procedure [35].

$$\rho_t c_t \frac{\partial T}{\partial t} = \nabla \cdot (k_t \nabla T) - \omega_b \rho_b c_b (T - T_b) + Q_m + Q_p \quad (3)$$

where ρ_i , k , Q_m and Q_p represents the time-scaling coefficient, thermal conductivity (W/(m·K)), metabolic heat generation (W/m³) and microwave power deposited (W/m³), respectively. Also, ρ_b , c , c_b , ω_b and T_b represent blood density (kg/m³), specific heat (J/(kg·K)), blood specific heat (J/(kg·K)), blood perfusion rate (1/s) and baseline physiological temperature (K), respectively.

The Arrhenius first-order equation has been used to compute the damage integral of the biological tissue during the microwave ablation procedure [36].

$$\Omega(t) = \ln \left(\frac{c_o}{c_{UD}(t)} \right) = \int_0^t A \exp \left[-\frac{E_a}{RT(t)} \right] dt \quad (4)$$

where c_o , $c_{UD}(t)$ and R represents an initial concentration of living cells, the concentration of remaining cells after time t and the universal gas constant, respectively. A is a frequency factor and E_a is the irreversible destructive reaction activation energy [37]. A damage integral of $\Omega = 1$ corresponds to a 63% percent probability of cell death at a specific point. A damage integral of $\Omega = 4.6$, corresponds to 99% percent probability of cell death at a point in the model. It shows a larger ablation volume, as it accounts for the fact that 63% of the destroyed cells cannot be restrained to their original position.

The boundary conditions considered in the modelling of the 3-D homogeneous triangular hepatic gland are

- (5) The initial temperature of the 3-D hepatic gland has been considered to be at room temperature

$$T_b = 37^\circ\text{C} \quad (5)$$

- (6) The entire periphery region of the domain has been considered to be a perfect thermal insulator,

$$\vec{n} \cdot \mathbf{k} (\nabla T) = 0 \quad (6)$$

where \mathbf{n} , \mathbf{k} and T represent the unit vector at the computational domain boundary, thermal conductivity and temperature, respectively.

- (7) In order to overcome the reflection of electromagnetic waves at the edges of the numerical domain, the Sommerfeld radiation condition has been considered at all boundary regions [38]

$$\vec{n} \times (\nabla \times \vec{E}) - jk\vec{n} \times (\vec{E} \times \vec{n}) = 0 \quad (7)$$

where \mathbf{n} , \vec{E} and k represent the normal unit vector at the computational domain boundary, electric field vector and the wavenumber, respectively.

- (8) The walls of the conductors have been considered to be perfect electric conductors [22]

$$\vec{n} \times \vec{E} = 0 \quad (8)$$

(9) The liver's thermal conductivity (k_{liver}), density (ρ_{liver}), and specific heat (c_{liver}) are dependent on temperature [39].

$$k_{liver}(T) = 4190 [0.133 + 1.36 W_a(T)] \quad (9)$$

$$\rho_{liver}(T) = 1300 - 300 W_a(T) \quad (10)$$

$$c_{liver}(T) = 0.419 [0.37 + 0.63 W_a(T)] \quad (11)$$

(10) The parameter $W_a(T)$ is the measured remaining tissue water content versus the liver tissue temperature [40,41].

$$W_a(T) = \begin{cases} 0.778 - 0.779 \times \exp\left(\frac{T-106}{3.42}\right) & T \leq 103^\circ\text{C} \\ -0.03924 (T - 103) + 0.454392 & 103^\circ\text{C} < T \leq 104^\circ\text{C} \\ 0.778 \times \exp\left(-\frac{T-80}{34.37}\right) & T > 104^\circ\text{C} \end{cases} \quad (12)$$

(11) The loss tangent ($\tan \delta$) denotes the loss in a dielectric, at a particular frequency and is defined as [42]

$$\tan \delta = \varepsilon_r'' / \varepsilon_r', \quad (13)$$

$$\varepsilon_r = \varepsilon_r' - j\varepsilon_r'', \quad (14)$$

where, $\varepsilon_r'' = \frac{\sigma}{2\pi f \varepsilon_0}$ is characterizes the resistance and denotes the absorption or loss of energy, σ is the AC conductivity, f denotes the frequency, ε_r' is called the dielectric constant, ε_r denotes the complex relative permittivity, and ε_0 denotes the permittivity of vacuum.

$$\tan \delta = \frac{\sigma}{2\pi f \varepsilon_0 \varepsilon_r} \quad (15)$$

The initial value of the electric field for the whole domain has been considered to be 0 V/m. The cooling mechanism of the trocar, which uses water as the coolant, has been incorporated into the numerical analysis. The boundary conditions considered in modelling the cooling system are as follows:

(12) The convective heat transfer coefficient of the water has been considered to be [43]

$$h = 1000 \text{ W m}^{-2} \text{ }^\circ\text{C}^{-1} \quad (16)$$

(13) The initial temperature of the cooling water entering into the feeding cable of the trocar has been considered [43] to be

$$T_i = 10^\circ\text{C} \quad (17)$$

(14) The maximum temperature of the cooling water that the tissue can heat is limited to [43]

$$T_f = 18.6^\circ\text{C} \quad (18)$$

(15) The ablation has been considered in the region where the temperature exceeds 60 °C.

(16) The non-isothermal flow through the rectangular channel embedded by the screen boundary conditions with the slip walls has been considered.

$$\rho(U \cdot \nabla) \cdot U = \nabla[-pI + K] + F \quad (19)$$

$$\rho(\nabla \cdot U) = 0 \quad (20)$$

where ρ density of the fluid is, p denotes pressure, K is the stress tensor and U denotes the velocity field.

Coupling between bioheat transfer and solid mechanics physics is given by the equation.

$$\epsilon_{th} = \alpha(T)(\nabla T) \quad (21)$$

$$\epsilon_{th} = \alpha(T)(T - T_b) \quad (22)$$

where ϵ_{th} is the strain due to thermal expansion, α is the coefficient of thermal expansion, T_b is the baseline physiological temperature.

(17) Solid mechanics behaviour of the tissue is given by

$$\epsilon_{el} = \epsilon_t - \epsilon_{th} \quad (23)$$

where ϵ_{el} – elastic strain, ϵ_t – total strain

(18) For a linear elastic material, Hooke's law relates the stress tensor to the elastic strain Tensor as

$$S = S_{ad} + C : \epsilon_{el} \quad (24)$$

where C is the 4th order elasticity tensor, “:” stands for the double-dot tensor product (or double contraction)

$$C = c(E, \vartheta) \quad (25)$$

$$\nabla \cdot S + F \cdot v = 0 \quad (26)$$

$$\epsilon_t = \frac{1}{2} [(\nabla u) T + (\nabla u)] \quad (27)$$

where S – stress, S_{ad} – additional stress, C – Constitutive tensor, F – body force, v – volume, u – displacement, E – Young's modulus, ϑ – Poisson's ratio.

The dimensions and material properties of the microwave coaxial antenna have been provided in Tables 3.1 and 3.2 respectively.

Table 3.1: Dimensions of microwave coaxial antenna [44]

Property	Value
Diameter of the central conductor	0.29 mm
The inner diameter of the outer conductor	0.94 mm
The outer diameter of the outer conductor	1.19 mm
Diameter of catheter	1.79 mm

Table 3.2: *Material properties of microwave coaxial antenna [44]*

Parameters	Dielectric	Slot	Catheter
Relative Permittivity	2.03	1	2.6
Electrical Conductivity (S/m)	0	0	0
Relative Permeability	1	1	1

3.2 Understanding the impact of microwave ablation parameters on vital cancerous organs.

A two-compartment tumour (3 cm in diameter) hepatic gland has been considered in the present study. The tumour is located at a distance of 4 cm from the bottom of the tissue, as shown in Fig. 3.1. A microwave coaxial antenna of 1.79 mm diameter and 80 mm height has been inserted into the tumour with the tip lying 1 mm below the centre of the tumour [45]. The antenna consists of a circular hollow slot of 1 mm cut with an outer layer made of Polytetrafluoroethylene (PTFE). The microwave antenna operates at a frequency of 2.45 GHz with different powers, viz., 60W, 100W and 120W.

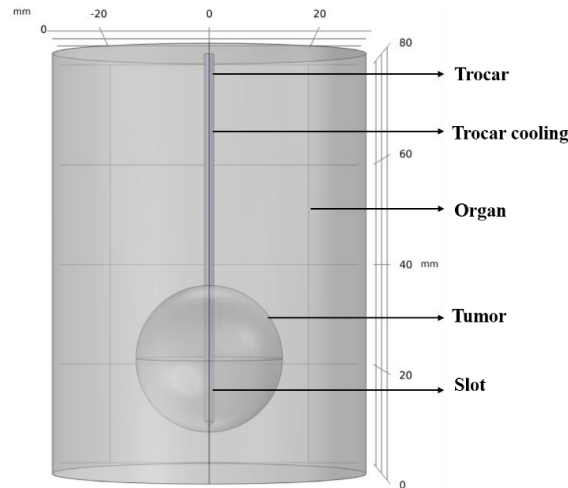


Figure 3.1 3 – Dimensional two compartment tumor embedded organ

Table 3.3: *Properties of different cancer tissue used in numerical simulation [12,46–57]*

Material (Tissue / Electrode)	Electrical conductivity (S/m)	Specific heat capacity c_p (J/(kg·K))	Thermal Conductivity (W/(m·K))	Density (kg/m ³)	Relative Permittivity	Young's Modulus
Lung	0.80	2500	0.30	260	20.5	5000
Breast[12]	1.97	2960	0.33	1041	57.2	25500
Stomach/Gastric	2.21	3690	0.53	1088	62.2	42500
Liver	1.69	3540	0.52	1079	43.0	38183
Colon Liver Metastatic	2.04	3655	0.54	1088	53.9	3170000
Kidney	2.43	3890	0.54	1050	52.8	48560

Numerical simulation setup

Grid Independence Test:

In the present study, numerical simulations have been carried out using COMSOL Multiphysics (COMSOL Inc., AB, Stockholm, Sweden) with inbuilt electromagnetic heating and thermal expansion Multiphysics. The maximum size of the element grid for computational modelling with electromagnetic radiation should be less than or equal to the wavelength of the EM radiation [58]. In the present study the maximum element size of 2 mm has been considered for the entire domain. The minimum size of the element in the dielectric region of the trocar has been set to 0.1 mm, which is smaller than the wavelength of the electromagnetic waves at 2.45 GHz frequency (approximately 18 mm). Custom data is generated by giving specific element sizes to the geometry during meshing. In our model, the trocar size was customized with a maximum element size of 2 mm and a minimum element size of 0.01 mm, while the remaining domain was given a maximum element size of 2 mm. By using customized data, we were able to generate a finite mesh from Mesh dependence study (Fig. 3.2) only the complicated regions, thus reducing the number of elements. The final computational domain consists of 1,233,150 elements as shown in Figure 3.3.

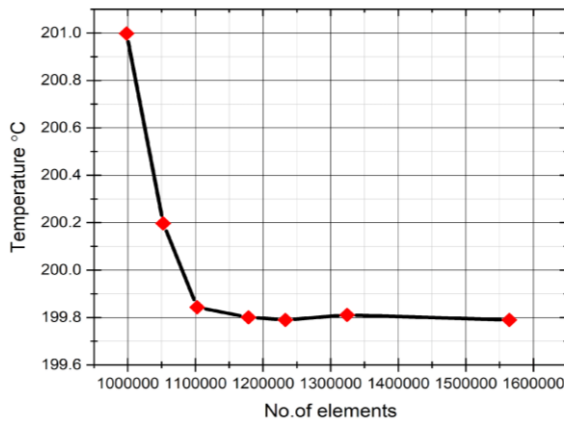


Figure 3.2 Mesh dependence study of the liver organ was conducted by considering variations in temperature with respect to the number of elements

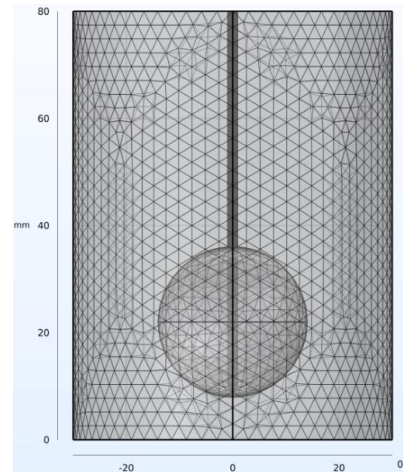
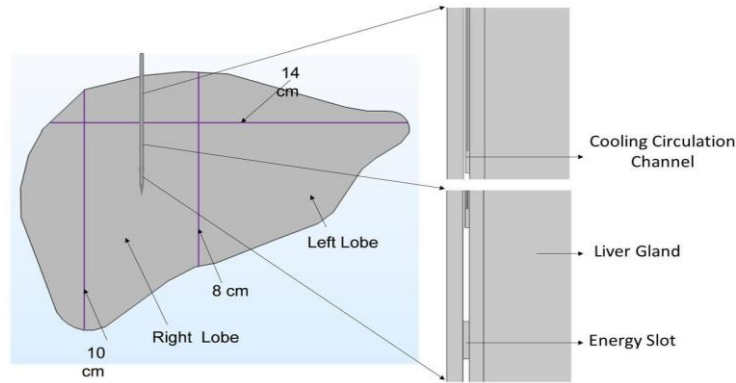


Figure 3.3 Meshed computational domain of MWA comprising 1233150 tetrahedral elements

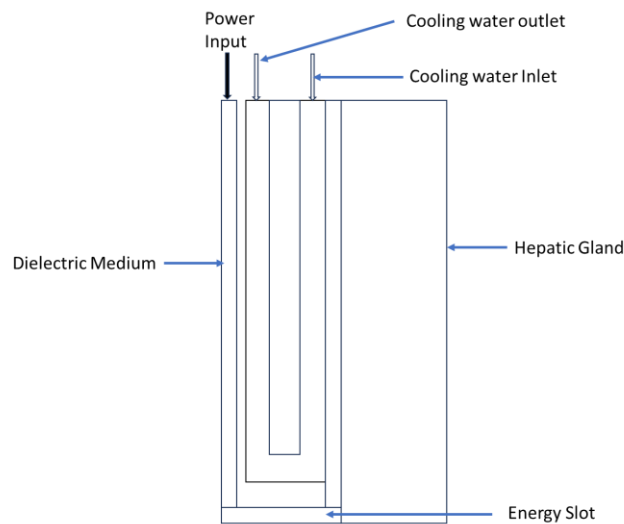
3.3. MWA of HCC using parallel and non-parallel insertion of trocars:

In the present study, an internally cooled coaxial microwave ablation trocar has been inserted into a homogeneous triangular hepatic gland (14 cm width and 10 cm height), as shown in Fig. 3.4 a. The Trocar comprises a dielectric medium (0.67 mm in diameter) sandwiched between the inner conductor (0.27 mm diameter) and the outer conductor (0.92 mm diameter). A ring-shaped slot, 1 mm wide, has been cut off from the outer conductor at a distance of 5.5

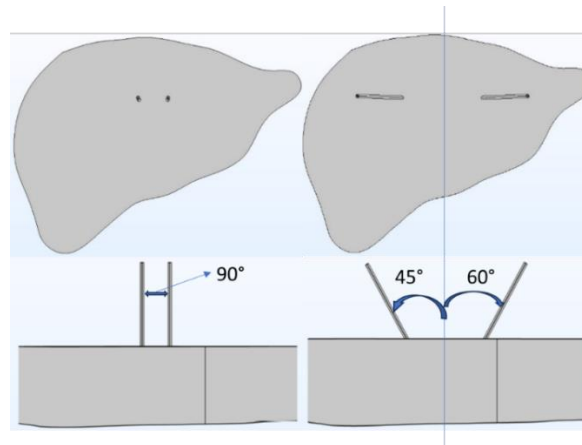
mm length from the short-circuited tip. The entire applicator has been housed in a cylindrical catheter (1.79 mm in diameter) covered with Polytetrafluoroethylene (PTFE) for hygiene and guidance purposes, as shown in Fig. 3.4 a and 3.4 b. The microwave trocar operates at a frequency of 2.45 GHz with different powers, viz., 60W, 100W and 140W. Further ablation times of 2 min, 4 min and 6 min have been considered along with the varied power values to achieve the required ablation region. The trocars have been inserted in parallel and non-parallel arrangements, as shown in Fig. 3.4 c.



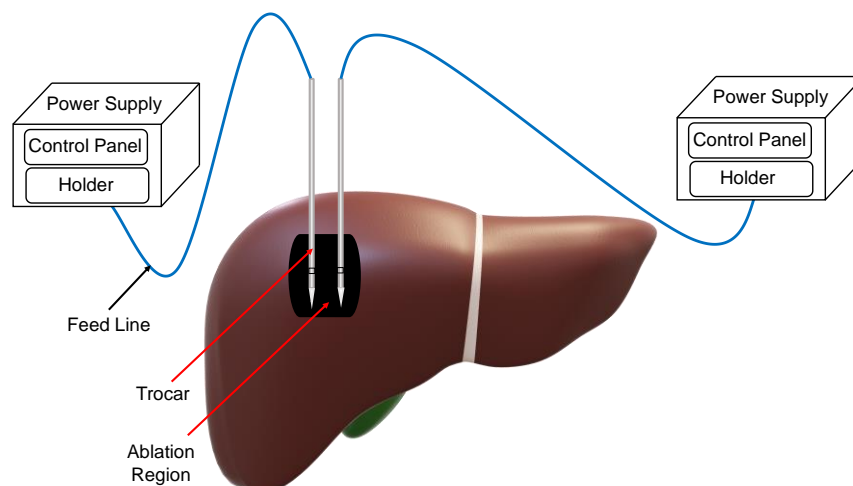
a) 2 – D schematic view of internally cooled MWA trocar inserted into the hepatic gland



b) Enlarged view (Detail A) illustrating the cooling system of the trocar



c) 3-D schematic view of parallel and non-parallel insertion of multiple trocars into the hepatic gland



c) Trocar Operation Procedure in Clinical Practice

Figure 3.4 Visualization of Trocar Operation Procedure in Clinical Practice

Fourier transform infrared spectroscopy (FTIR) on Egg white:

The Fourier-transform infrared spectroscopy (FTIR) has been used to identify the organic and inorganic compounds of egg white gel and compare it with the human liver. The data has been collected by Windows-based OPUS spectroscopy software connected to the FTIR (TENSOR II FTIR Spectrometer, Bruker Optics, Billerica, MA). Figure 3.5 illustrates the FTIR fields of egg white in $4000\text{--}400\text{ cm}^{-1}$ region. The spectral band assignment of egg white has been presented in Table 3.4.

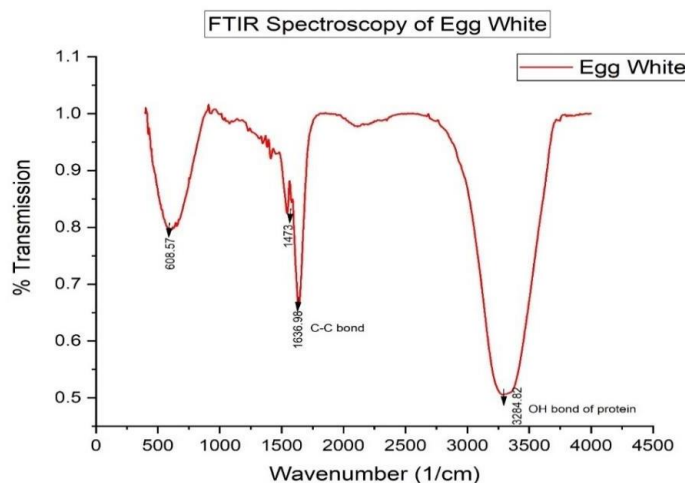


Figure 3.5 The average FT-IR spectra of egg white in the mid-infrared region ($4000\text{--}400\text{ cm}^{-1}$)

A band peak absorption in IR spectra of egg white and hepatic gland tissue has been presented in Table 3.4. The projecting peak at 3282 cm^{-1} is assigned to non-parallel O – H stretching of proteins and intermolecular H bonding. The O – H bond results in molecular friction and collision (continuous realignment) of polar molecules, resulting in dielectric hysteresis of the egg white when exposed to microwave waves at 2.45 GHz frequency. Similarly, the absorption peaks of 1636.9 cm^{-1} ($\approx 1650\text{ cm}^{-1}$ for the hepatic gland) and 1473 cm^{-1} ($\approx 1452\text{ cm}^{-1}$ for the hepatic gland) show the organic compound of protein C = O stretch, and

CH₂ (methylene) bending of the lipids and proteins. Both the proteins and lipids are the primary essential components for human functioning. All of these characteristic bonds cause the egg white to be a successful model mimicking the hepatic gland for use in microwave ablation procedure.

Table 3.4: Comparison of major absorptions in IR spectra of egg white and hepatic gland tissue

Peak No	Wavenumber (cm ⁻¹)		Definition of the spectral assignment
	Egg White	Hepatic gland tissue [38]	
1	3284.82	3300	O–H stretching of proteins and intermolecular H bonding.
2	1636.9	1650	Protein C=O stretch
3	1473	1452	CH ₂ bending: mainly lipids, with a little contribution from proteins
4	> 1500	>1500	Fingerprint region

Numerical Simulation Setup

The present study used COMSOL Multiphysics (COMSOL Inc., AB, Stockholm, Sweden) software with inbuilt bioheat transfer, electromagnetic waves and laminar flow interfaces to obtain the numerical results. The present study uses an 'extra fine mesh' of tetrahedral shape with a minimum element size of 0.0001, as shown in Fig. 3.6.

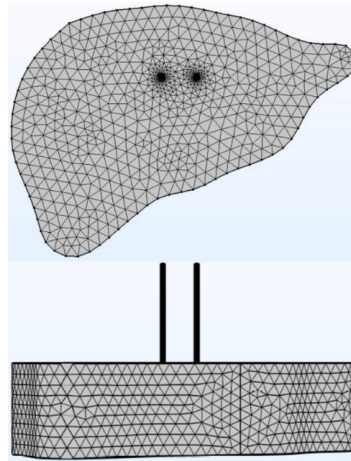


Figure 3.6 Meshed computational domain of MWA comprising 2197589 tetrahedral elements

Experimental procedure

The experimental process has been followed and mentioned below:

Step 1: After separating the egg white from the eggs, they are filled in the 3D printed hepatic gland shape on the microwavable plate. Trocar and thermocouple have been inserted into the egg white (*refer* Figs. 3.7 and 3.8).

Step 2: Start the temperature data acquisition instrument (Osensa) and the microwave ablation experiment.

Step 3: After completing the in-vitro experiment, turn off the data acquisition system and the saline water-cooling system of the trocar, followed by the microwave ablation device.

Step 4: The transverse and longitudinal diameters of the ablation region of egg white have been measured at the end of the experiment, and the aspect ratio of the ablation area has been calculated.

Step 5: Experiments have been repeated three times under the same conditions to achieve the most accurate and valid results.

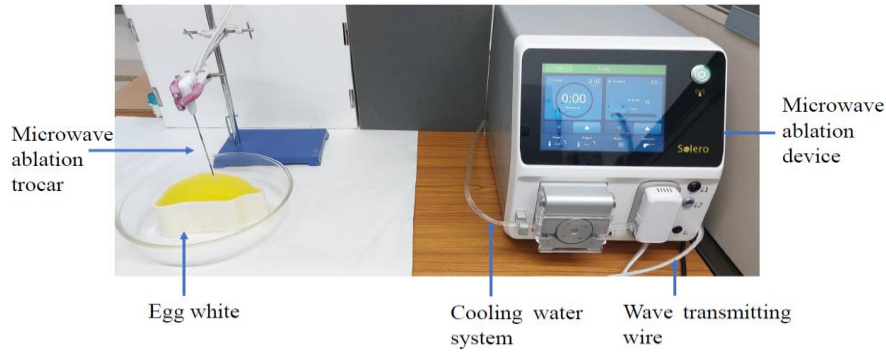


Figure 3.7 In vitro experimental setup



Figure 3.8 Osensa optical temperature measuring device

Experimental Validations

Both numerical and in vitro models have been validated by comparing the results provided by Makovich et al. [59], as shown in Fig. 3.9. Makovich et al. performed the ablation of tumour located in segment 8 of the hepatic gland in human patient using Solero MWA device operated at 140 W microwave power for 6 minutes.

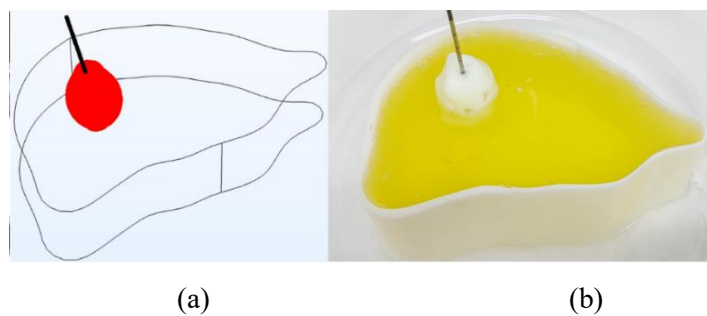


Figure 3.9 post-ablation zones created in a hepatic gland at the end of 360 s with microwave power 140 W MWA procedure (a) numerical simulation, 3.1 cm × 4.4 cm × 4.7 cm and (b) experimental analysis on egg white, 2.9 cm × 4.1 cm × 4.5 cm.

A good agreement has been obtained in terms of ablation region between the numerical analysis of $3.1 \text{ cm} \times 4.4 \text{ cm} \times 4.7 \text{ cm}$ (TR \times AP \times CC) and the in vitro studies of $2.9 \text{ cm} \times 4.1 \text{ cm} \times 4.5 \text{ cm}$ (TR \times AP \times CC) with the human trials of $3.2 \times 4.3 \times 4.7 \text{ cm}$ (TR \times AP \times CC) (Figs. 3.9 (a), and 3.9 (b)). A minor difference has been observed due to the model's uncertain properties.

3.4 MWA of HCC Tumors using novel design L shaped dual tine dual frequency trocar: One fixed and one flexible tine.

A two-compartment tumor (3 cm diameter) embedded liver gland has been considered in the present study. The liver gland's physical domain is considered to be of cylinder having 85 mm length and 30 mm radius. The tumor is located at the centre and at a distance of 15.5 cm from the bottom of the liver gland (see Fig. 3.10). The 3-Dimensional dual tine coaxial antenna, with both tines (straight and curved) having 1.79 mm in diameter and 70 mm in length, has been inserted into the tissue (see Fig. 3.11). Further, the straight tine is having a ring-shaped slot of 1 mm in length and the curved tine is having a ring-shaped slot of 1.3 mm in length, both on the outer conductor side of the tines and 5 mm from the short-circuited tip (refer to the enlarged view of tines in Fig. 3.12). The tines are enclosed with individual sleeves (catheters) made of PTFE (polytetrafluoroethylene) [45]. The dimensions of microwave coaxial antenna have been provided in Table 3.5. The dual tine antenna operates at 2.45 GHz (straight/curved/both) and 6 GHz (curved/straight/both) at 15 W. The material properties of microwave coaxial antenna considered in the present numerical study has been provided in Table 3.5. Once the trocar is inserted into the tissue, the flexible tine can be deployed as per the requirement of the ablation region. Figure 3.11 illustrate various combinations that arise due to varying deploying lengths of the tine used in the present article. In the present study a MWA of fully deployed dual tine trocar inserted into the hepatic gland embedded with 3 cm diameter tumor has been considered.

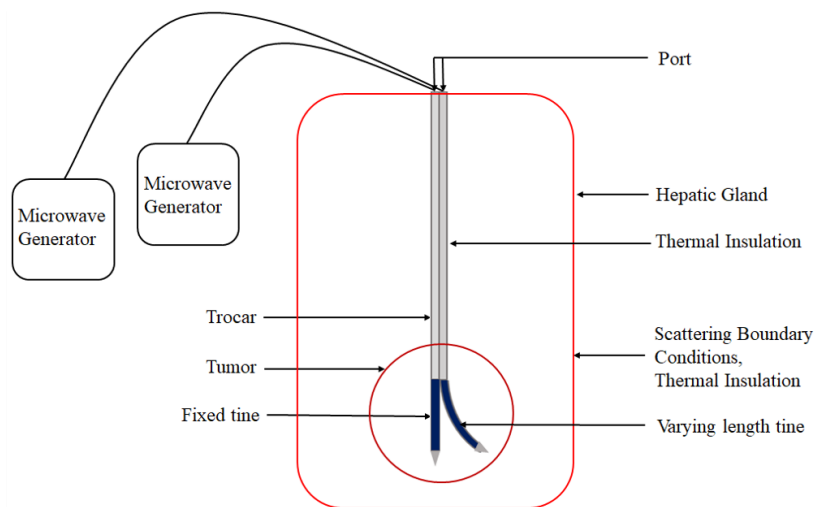


Figure 3.10 Schematic diagram of the trocar inserted into the tumor embedded biological tissue.

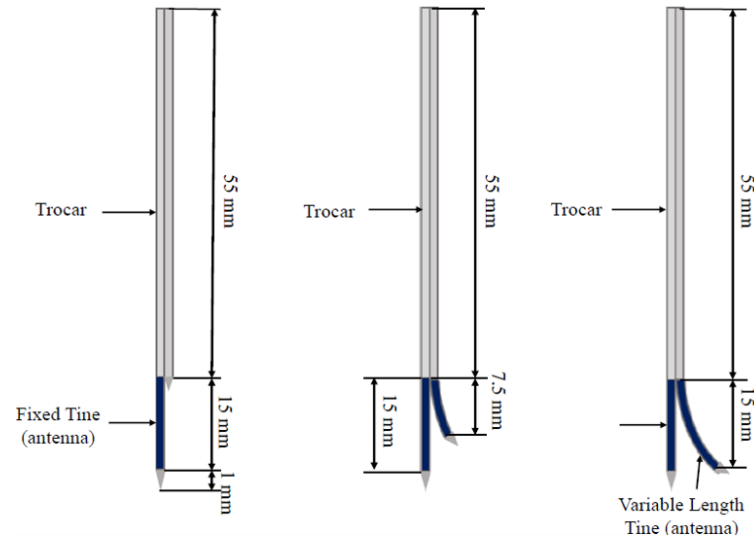


Figure 3.11 Schematic of zero deployed, semi deployed, and fully deployed angular tine of trocar configurations. (All dimensions are in mm)

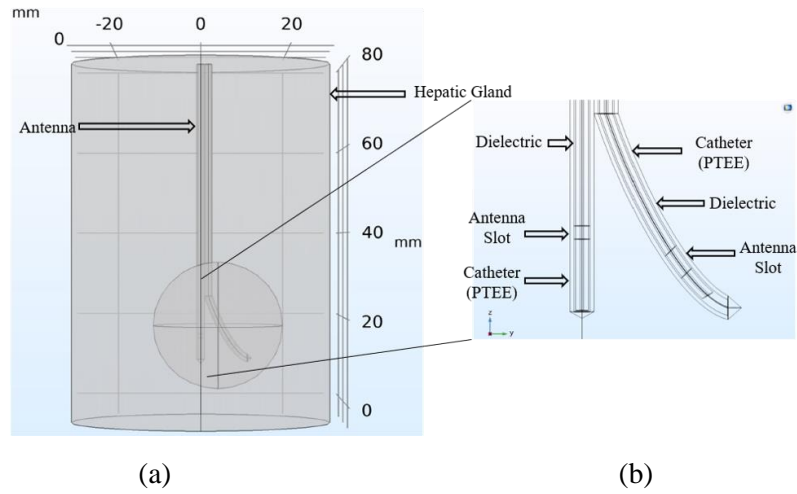


Figure 3.12 Fully deployed dual tine trocar (a) inserted into the hepatic gland embedded with 3 cm diameter tumor and (b) Enlarged view of the tines inside the tissue.

From the proposed trocar, deploying length of the flexible tine will be varied as per the requirement of the ablation region. Further, it overcomes the problem associated with the inapt positioning of the trocar. Figure 3.13 below shows the flexible tine with various positionings to achieve the required ablation region.

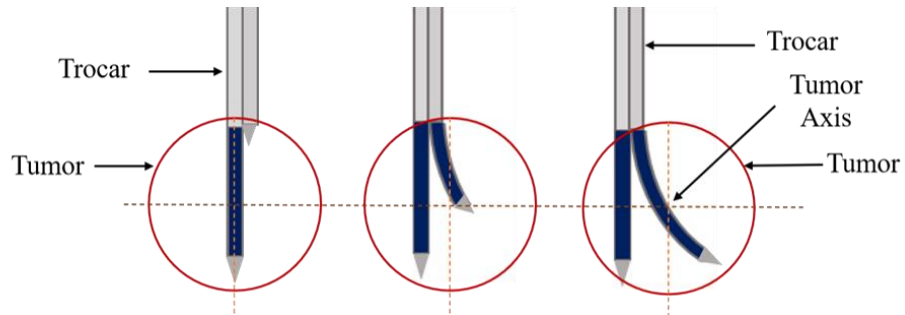


Figure 3.13 Schematic view of trocar positioning relative to the tumour axis.

The specific absorption rate of microwave energy of the biological tissue when it is being exposed to electromagnetic waves has been shown in Fig. 3.14. A good agreement has been obtained between the present results (35 kW/kg) and the data available in the literature [60], i.e., 34.5 kW/kg of specific absorption rate, when the antenna has been operated at 2.45 GHz.

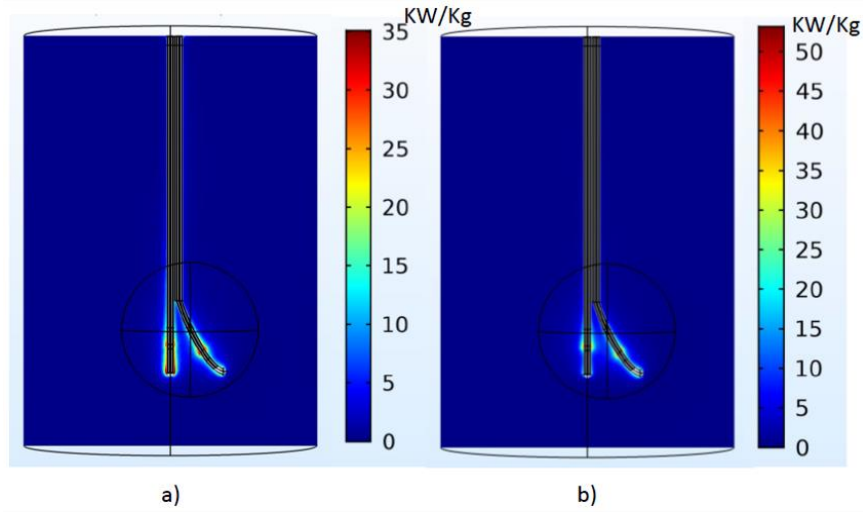


Figure 3.14 The computed specific absorption rate (SAR) in KW/kg takes on its highest values near the tip and the slot with 15 W microwave power at a) 2.45 GHz, b) 6 GHz frequency on both the tines.

The thermo-physical properties of tissue/gland considered in the present numerical study have been provided in Table 3.5.

Table 3.5: *Properties of tissue/gland* [17,24,26,44,61]

Material (Tissue/Gland)	Liver Tissue	Liver Tumor	Blood
Electrical conductivity (S/m)	1.69	2	2.58
Specific heat capacity c (J/(kg·K))	3540	3960	3600
Thermal Conductivity k (W/m·K)	0.52	0.57	0.5
Density ρ (Kg/m ³)	1079	1040	1060
Blood perfusion ω_b (s ⁻¹)	0.0155	0.0155	—
Relative Permittivity at 2.45 GHz	43.035	17.529	68.5
Tangent Delta at 2.45 GHz	0.288	0.837	0.276
Relative Permittivity at 6 GHz	37.849	16.927	58.5
Tangent Delta at 6 GHz	0.133	0.353	0.132
Relative Permeability	1	1	1

Numerical simulation setup

A Finite element analysis has been carried out using COMSOL-Multiphysics software (COMSOL Inc., AB, Stockholm, Sweden) with coupled bioheat and electromagnetic physics interfaces. The physical domain has been discretized using tetrahedral extra fine mesh elements. For the computational modelling of electromagnetic radiation, the maximum size mesh element should be less than or equal to the EM radiation wavelength. A study of the variation of wavelength with frequency for the hepatic gland states that at 6 GHz frequency the maximum wavelength of electromagnetic waves is 7 mm [58]. In the present study, the maximum element size of 2 mm has been considered for the entire domain.

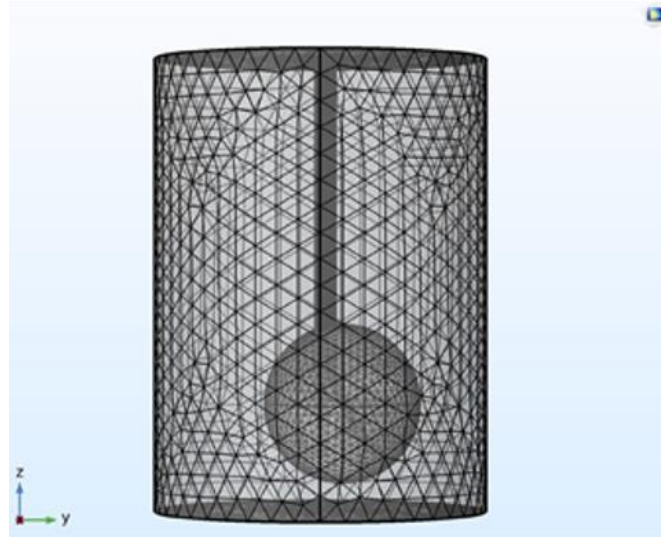


Figure 3.15 Meshed 3 cm tumor embedded hepatic gland having 8127233 tetrahedral elements

The minimum size of the element has been taken to be 0.1 mm for the entire domain, which is lesser in size than the wavelength of the electromagnetic waves at 6 GHz frequency (i.e., nearly 7 mm). The sensible part of the computational domain (i.e., trocar) has been studied using extremely fine tetrahedral mesh (i.e., minimum mesh element size of 0.001647 mm) elements using independent grid study. The total mesh elements for the entire computational domain are 8127233 (Fig. 3.15). The computer simulation has been performed on Dell Precision Tower 7810 workstation with eight Core 3.1 GHz Xeon processors and 64 GB RAM.

Model analysis

The numerical model integrity and accuracy have been validated by comparing the simulation result at 2.45 GHz frequency and 15 W microwave power with the experimental results obtained by Deshazer et al., [62] as shown in Fig. 3.16. Deshazer et al. conducted MWA procedure on an ex vitro liver sample using a single slot microwave antenna at 2.45 GHz frequency and 15 W microwave power. A good agreement has been obtained in terms of the ablation region between the present numerical results (1.27 cm in the transverse direction and 2.4 cm in the axial direction) and the experimental results (1.30 ± 0.3 cm in the transverse direction and 2.66

± 0.22 cm in the axial direction) available in the literature [62], (Fig. 3.16). A minor difference of less than 0.3 cm has been observed which is attributed to the model's uncertain properties. Table 3.6 shows the numerical and experimental values obtained for MWA for hepatic gland.

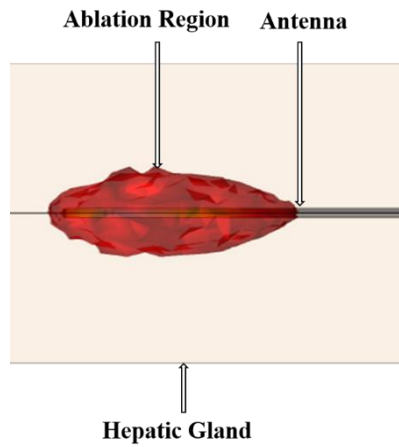


Figure 3.16 Ablation zones created in hepatic gland at the end of 360 s MWA procedure with numerical simulation, $1.27 \text{ cm} \times 2.4 \text{ cm}$.

Table 3.6: Comparison of ablation volume obtained among experimental and numerical values

Ablation Dimensions	Experimental Values	Numerical Values
Transverse Direction (cm)	1.27	1.30 ± 0.3
Axial Direction (cm)	2.4	2.66 ± 0.22

3.5 MWA of HCC Tumors using novel design U shaped dual tine dual frequency trocar: Both are flexible tine.

Numerical simulation setup

Numerical simulations have been carried out using COMSOL Multiphysics (COMSOL Inc., AB, Stockholm, Sweden) with inbuilt electromagnetic heating and bioheat transfer physics. The present study has been carried out using an 'extra fine mesh' of tetrahedral shape with a minimum element size of 0.0001 mm. The total number of mesh elements generated have been 1,376,966. The maximum element sizes in hepatic gland and tumor domains have been considered to be 2.98 mm and 1.7 mm, respectively. Similarly, the maximum element size in the trocar domain has been considered to be 1.7 mm. The above configurations of the mesh sizes are determined by grid independence study by varying the element size with their temperature variation properties. A relative tolerance of 0.0001 has been considered for the electromagnetic and bio heat interface. The simulations have been carried out using COMSOL Multiphysics 5.4 version software on a Dell Precision Tower 7810 workstation with eight Core 3.1 GHz Xeon processors and 64 GB RAM. The average computational time for each set of

simulation is around 1 hour 30 minutes. Figure 3.17 indicates the meshed computational domain of MWA comprising 1,376,966 tetrahedral elements.

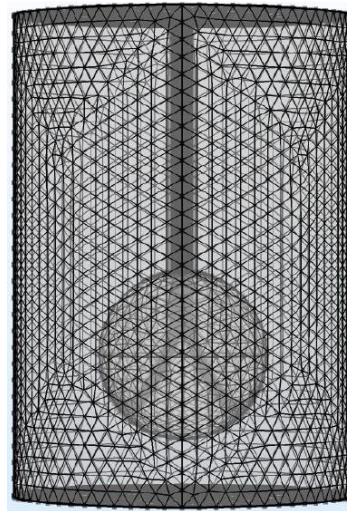


Figure 3.17 Meshed computational domain of MWA comprising 1,376,966 tetrahedral elements.

Antenna Specifications

Table 3.9 shows the computed specifications of the antenna operated at 2.45 and 6 GHz obtained numerically for 15W with 10 minutes treatment time. The MWA procedure performed at 2.45 GHz frequency for fully deployed tines generates a Reflection Coefficient (dB) of -16.119 (< -10 dB) indicates low power loss for the given power input [63]. Similarly, MWA procedure performed at 6 GHz frequency shows a Reflection Coefficient (dB) of -9.34 (≥ -10 dB) which can be considered to be within the acceptable range for the given power input. Further, optimizing the antenna with a large slot area [64] and adding a choke will overcome the problem of return power losses at the given load conditions. The proposed trocar's specific absorption rate (SAR) has been analyzed at a) 2.45 GHz and b) 6 GHz and has been presented in Fig. 3.18. Figure 3.18 (a) shows the energy deposition along the tine length is 47 kW/kg with a maximum power deliverance of 14.02 W into the tissue. Further, for the case of 6 GHz frequency it can be seen from Fig. 3.18 (b) that, the energy deposition of 53 kW/kg is more concentrated at the slot area than along the tine length, leading to high energy density within a smaller region. Table 3.6 indicates the material properties of microwave coaxial antenna.

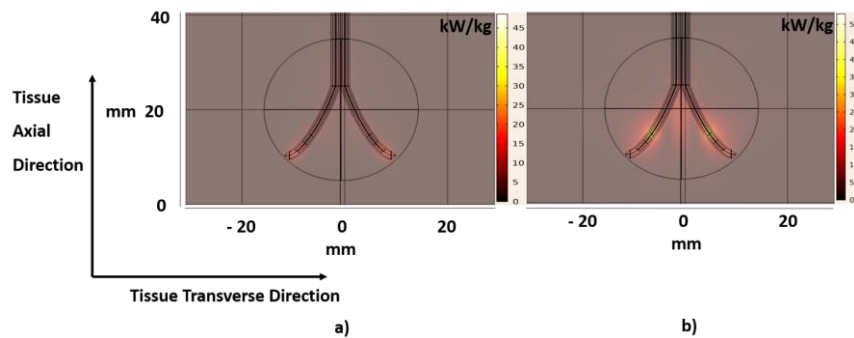


Figure 3.18 The calculated specific absorption rate (SAR) in kW/kg for 15 W microwave power at a) 2.45 GHz and b) 6 GHz on both the tines.

Table 3.6: Material properties of microwave coaxial antenna (tine)

Frequency of the tines (GHz)	Reflection Coefficient	SAR (kW/kg)	Power (W)
2.45	- 16.119	47	14.02
6	- 9.34	53	10.23

Experimental Validations

The novel MWA tine design's integrity and precision have been validated by comparing the ablation volume obtained using the present numerical simulations with the available experimental results [65] for the non-cooled monopolar electrode. Figure 3.19 shows the ablation region obtained using numerical simulation of MWA at 2.45 GHz. A good agreement in transverse ablation length has been seen between the numerical (1.79 cm) and experimental analysis (*refer* Table 3.7). A difference of nearly ± 0.1 cm in the ablation length is attributed to the inexactness of the material properties in the design model with the ex-vitro organs. Hence, all the parameters and equations used in the present study have been considered to be appropriate.

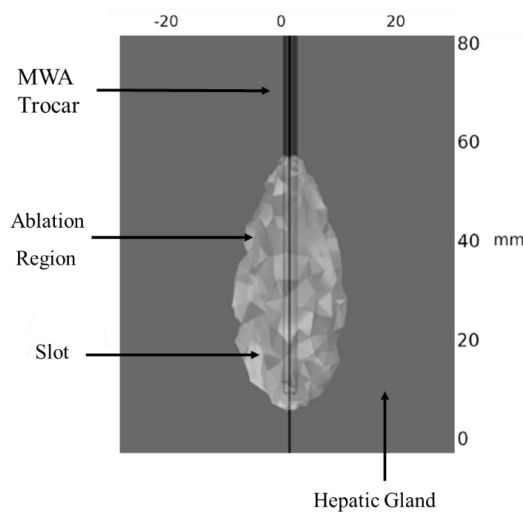


Figure 3.19 Ablation regions obtained in hepatic gland by numerical simulation with 1.79 cm transverse ablation length.

Table 3.7: Validation of ablation region in hepatic gland against the experimental results by Saito *et al.*[65] during MWA at 2.45 GHz.

Dimensions	Numerical Simulation	Pig Liver
Lateral Dimension	1.79 cm	1.85 cm
Longitudinal Dimension	4.8 cm	4.5 cm

Results and Discussion

The results and discussion section within the thesis showcases the research findings and offers a comprehensive analysis and interpretation of these results. This section assumes a critical role in the thesis as it effectively demonstrates the study's contribution and significance.

4.1 Understanding the impact of microwave ablation parameters on vital cancerous organs.

Ablation region obtained by various organs at fixed power and time:

Each type of tissue differs from one another in terms of structure and properties. The application of MWA medical technique varies depending on the characteristics of the tissue. The principle of microwave ablation (MWA) involves the use of microwave waves emitted by the trocar to heat tissue. The absorption of waves by the biological tissue produces heating due to dielectric hysteresis or rotating dipoles (continuous realignment of polar molecules), leading to ablation of the tissue. The temperature distributions of breast, colon, liver, kidney, lung, and stomach cancer tissues that have been exposed to the microwaves of frequency 2.45GHz at 100 W microwave power for a duration of 4 minutes have been shown in Fig. 4.1.

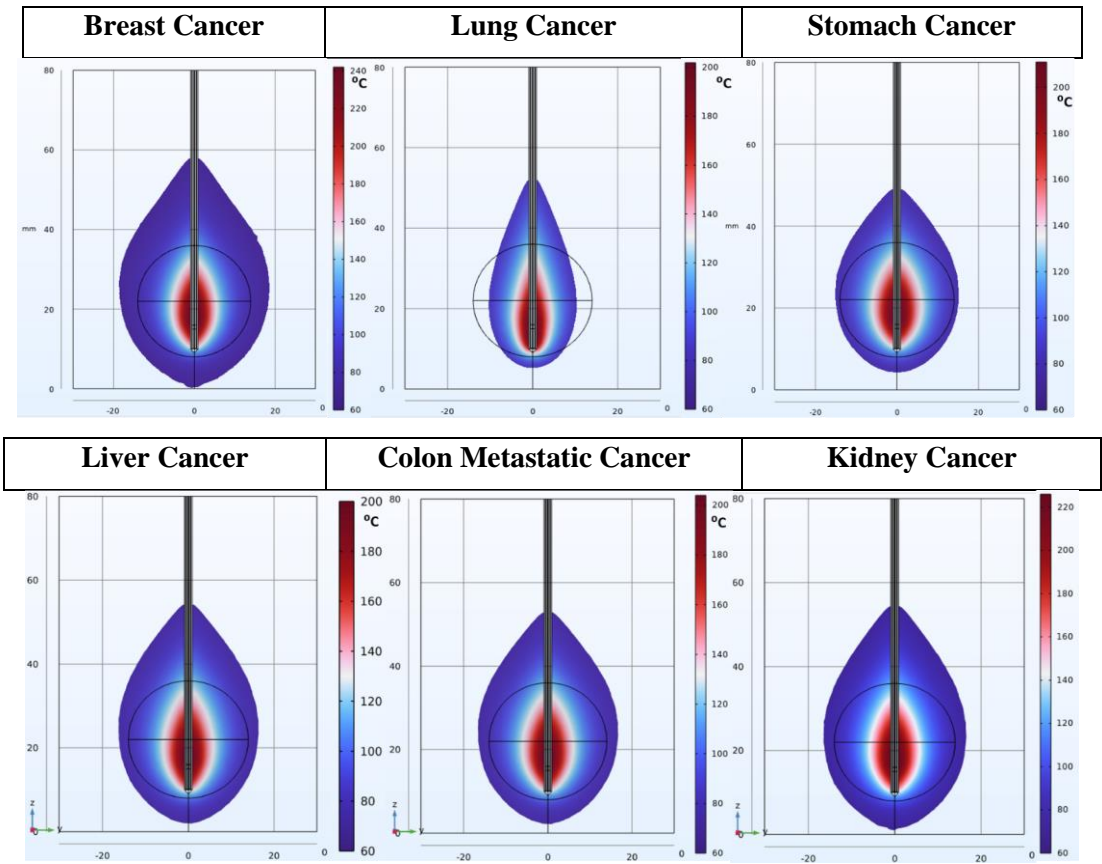


Figure 4.1 Thermal ablation of 3 cm tumor embedded hepatic gland of various cancerous tissues at 2.45 GHz frequency.

The isothermal plots greater than 60°C are used to measure the zone of complete thermal damage induced by an ablation procedure. As shown in the figure, healthy tissue located at the periphery of the tumor also experiences heating under the same operating conditions, except for cases of lung cancer. Table 4.1 shows the maximum diameter of the tissue ablated for different organs under the same operating conditions. The maximum amount of ablation region has been observed for the breast tissue and hepatic gland for a treatment time of 4 minutes. With low specific heat capacity and density parameters, microwave ablation of breast and hepatic glands leads to a larger diameter of the ablation region compared to other organs at 100 W microwave power with treatment time of 4 minutes.

Experimental Validation:

The ablation of liver cancer resulted in a size of 3.4 cm × 4.5 cm (Fig. 4.1), which is almost similar to the size obtained using the Solero microwave ablation device. This is also in consistent with the results of human trials, which showed an average size of 3.7 cm [66]. A good agreement has been obtained in terms of ablation region between the numerical analysis of 2 cm × 3.3 cm (Fig. 4.1) with the human trails [67] with slight difference of nearly 0.1 cm attributed to slight change in properties. Furthermore, the ablation of kidney cancer resulted in a size of 3.3 cm × 4.6 cm (Fig. 4.1), which is nearly identical to the size obtained using the Solero microwave ablation device, which was 3.4 cm × 4.5 cm [68].

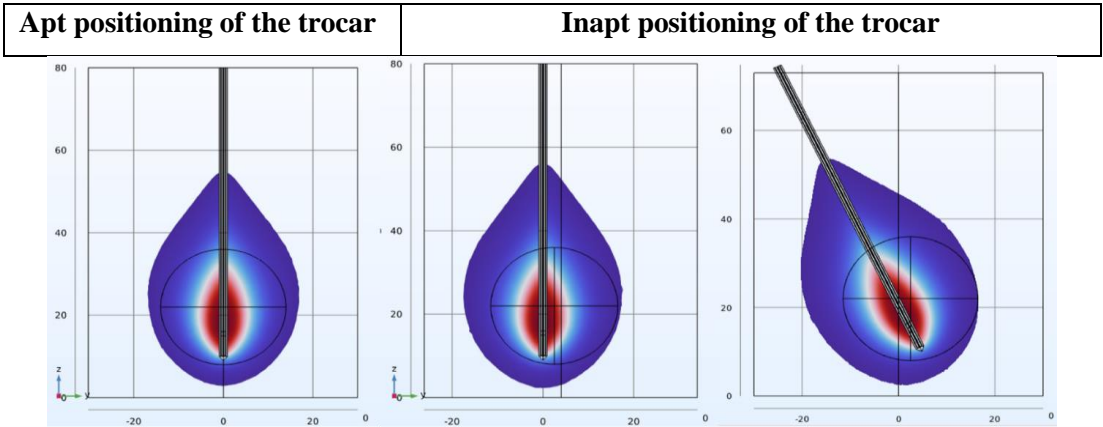
The dimensions of the ablation margins obtained from the numerical simulations of a 3 cm in diameter tumour embedded in different organs have been tabulated in Table 4.1. The MWA of breast cancer and liver cancer indicates the largest lateral diameters of 3.9 and 3.4 cm in the ablation region, compared to other organs. The smallest dimensions of the ablation region have been observed for the lung organ, at 2 cm in diameter. Further ablation along the trocar, resulting in more damage to the healthy tissue, has been observed in cases of lung and breast tumors. The optimal ablation characteristics for stomach cancer have been observed to be 3.1 cm × 4.2 cm, followed by 3.4 cm × 4.5 cm for liver cancer. MWA of cancerous organs such as the liver and breast become more complex with larger ablation margins, as it requires precise positioning of the trocar within the tissue.

Table 4.1: *Microwave ablation of six major organs operated at 100 W for 4 treatment minutes.*

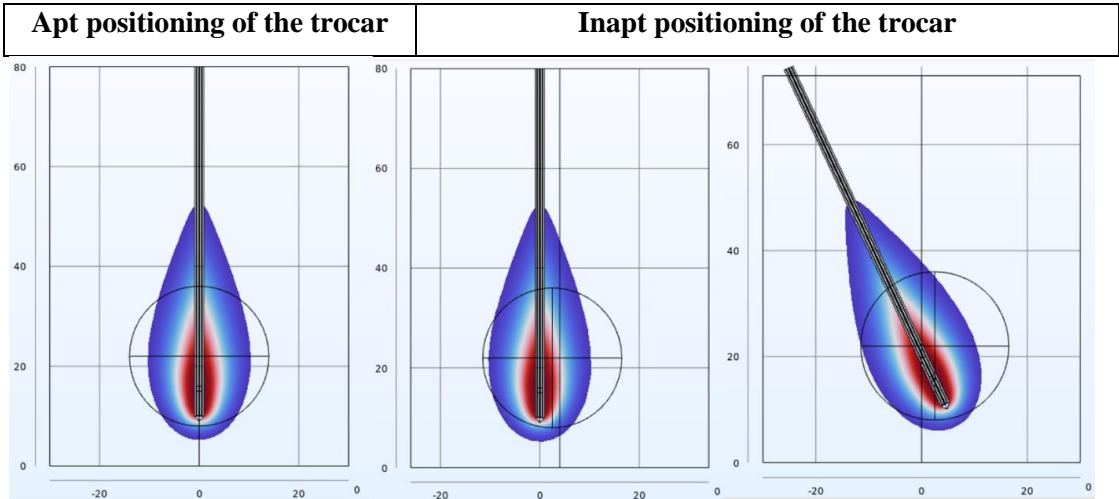
Organs	Lateral Diameter of the tumor ablated (cm)	Longitudinal Diameter of the tumor ablated (cm)
Breast Cancer	3.9	5.9
Colon Liver Metastatic	3.25	4.4
Kidney Cancer	3.3	4.6
Liver Cancer	3.4	4.5
Lung Cancer	2	3.5
Stomach Cancer	3.1	4.2

Stating the importance of apt positioning of trocar into the tissue:

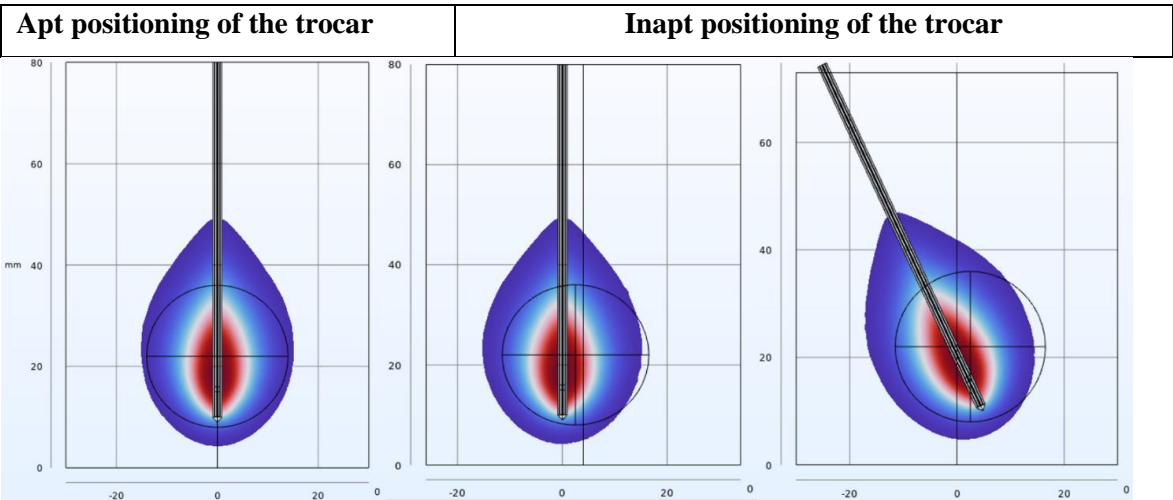
Poor medical imaging techniques or human error in the positioning of the trocar can result in incomplete tumor ablation and damage to surrounding normal tissue [57,69,70]. It further increases the number of multiple trocars for complete ablation of the tumor.



a) Microwave ablation Breast Cancer



b) Microwave ablation Lung Cancer

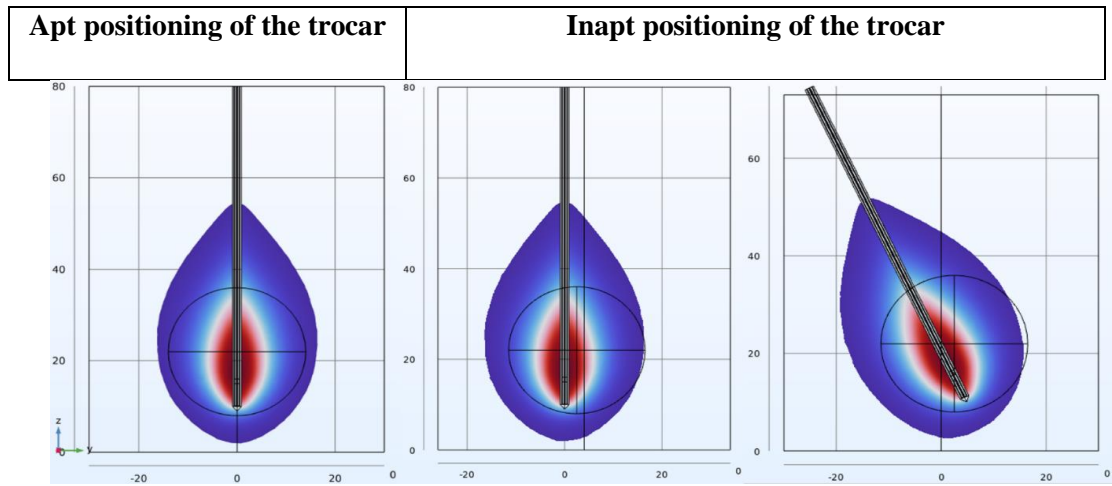


c) Microwave ablation stomach/gastric cancer

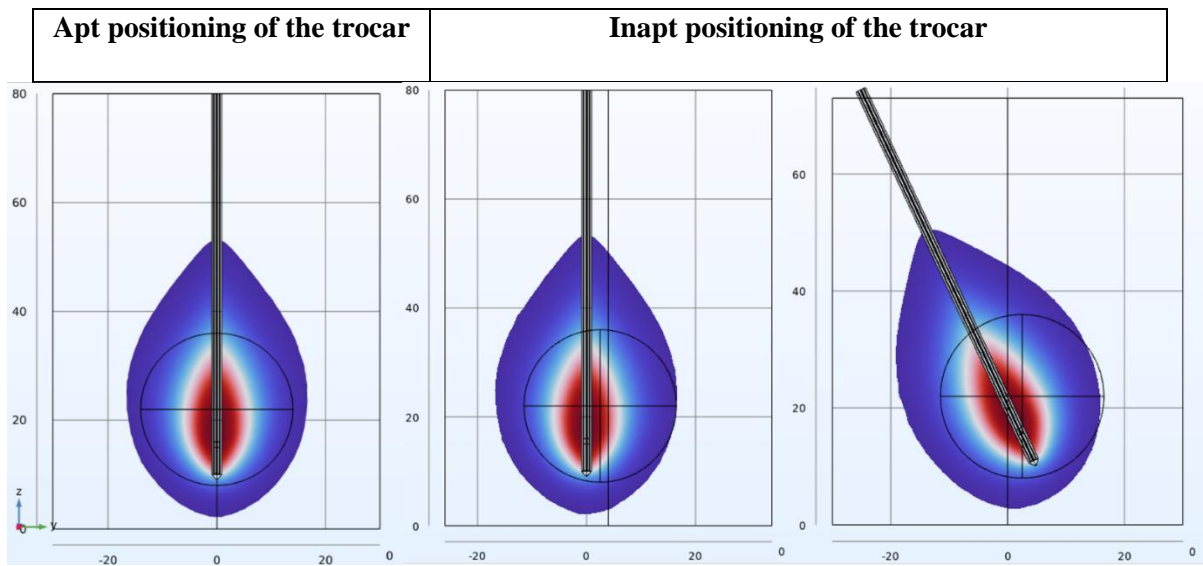
Figure 4.2 Thermal ablation of 3 cm tumor embedded cancerous tissues at 2.45 GHz frequency.

Due to its high relative permittivity and electrical conductance, microwave ablation of breast cancer results in a larger volume of ablation compared to the other organs. The results demonstrate that proper placement of the trocar results in complete tumor ablation, with an additional 1 cm margin of ablated tissue around the periphery of the targeted region (Fig. 4.2 (a)). A slight inapt positioning of trocar (either linearly and angular insertion) results in ablation of a large volume of healthy tissue. Despite the comparatively lower permittivity and conductivity of the lung tissue, microwave penetration depth is greater in the lung compared to other organs. Due to poor thermal conductivity, heat carried by lung tissue is limited, resulting in a smaller margin of tissue ablation. Due to the small ablation margin, complete ablation of lung tissue requires the use of multiple trocar microwave ablation (MWA) procedures (Fig. 4.2 (b)). Further, incorrect positioning of the trocar may result in the need for an increased number of trocars to achieve complete tissue ablation. Microwave ablation (MWA) of kidney tissue results in an ablation margin smaller than that of breast tissue and slightly larger than that of lung tissue (Fig. 4.2 (c)). With high electrical conductivity and more density results in less penetration depth of the microwave. Inapt positioning of the trocar in kidney tissue results in incomplete tumor ablation and causing damage to the healthy tissue.

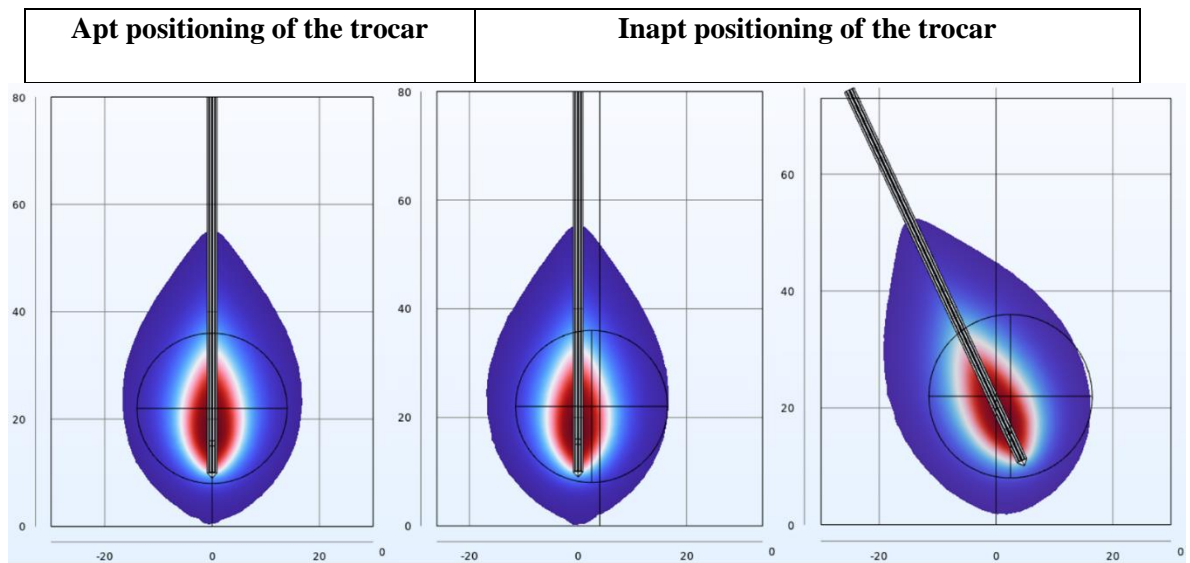
The microwave ablation of liver and liver with colon metastatic cancer has been shown in Figs. 4.3 (a) and (b). With low electrical conductivity and density, microwave ablation of the hepatic gland produces a slightly larger ablation margin compared to that of the liver with colon metastatic cancer. Incorrect trocar placement during MWA in the hepatic gland may result in the ablation of a large volume of healthy tissue. Due to its high-water content, the depth of electromagnetic field penetration in kidney tissue is relatively low. However, the presence of a large amount of water molecules also results in high heat generation rate during microwave ablation. The advantage of rapid heating in microwave ablation can compensate for the issue of heat being carried away by perfusion. For MWA of kidney tissue, the length of the ablation zone is generally along the length of the trocar (Fig. 4.3 (c)). Improper positioning of the trocar can result in the ablation of a significant amount of healthy tissue.



a) Microwave ablation Hepatic Gland Cancer



b) Microwave ablation of liver (colon metastatic) cancer



c) Microwave ablation Kidney Cancer

Figure 4.3 Thermal ablation of 3 cm tumor embedded various cancerous tissues at 2.45 GHz frequency.

Temperature distribution:

The ablation and temperature profiles are two major criteria used to analyze the performance of the MWA. Figure 4.4 shows the temperature measuring points on the tissue. The temperature distributions of various cancerous organs have been shown in Fig. 4.5. The temperature rise is highest near the trocar and decreases as you move away from it. This is because the waves transmitted from the trocar generate heat, which leads to a sharp increase in temperature near the antenna. As we move away from the trocar, the heat energy is being transmitted by conduction, resulting in a gradual rise in the temperature plot. The highest temperatures are reached in the breast and kidney tissues as compared to the other organs. The tissue is ablated at temperatures greater than 60°C . The isothermal plots greater than 60°C are used to measure the zone of complete thermal damage induced by an ablation procedure. During the first minute of MWA, there is a rapid rise in temperature and then it slowly grows to reach maximum temperatures of 240°C , 225°C , 210°C , 205°C , 201°C , and 195°C within the breast, kidney, stomach/gastric, colon metastatic liver, lung, and liver cancerous tissues, respectively.

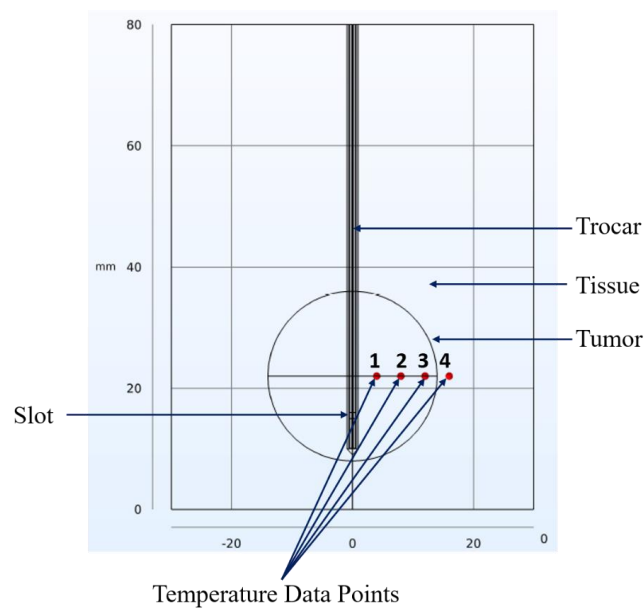
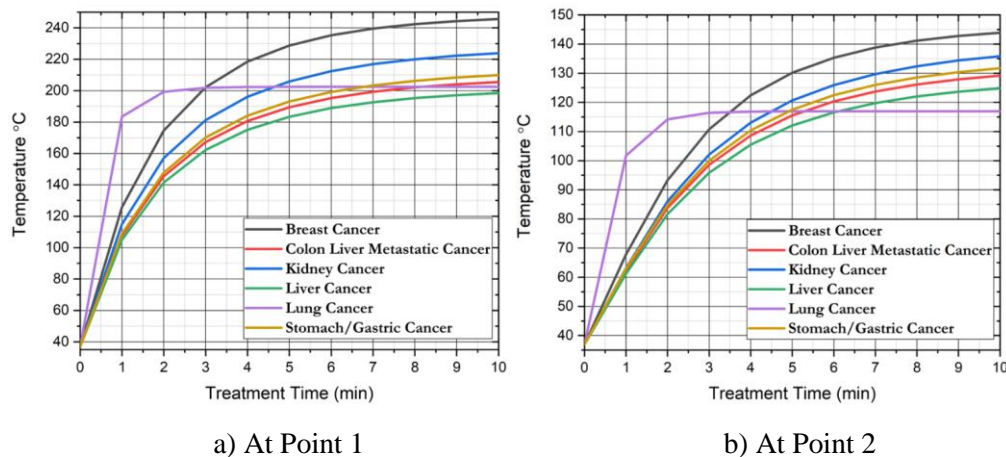


Figure 4.4 The temperature measuring points of the tissue



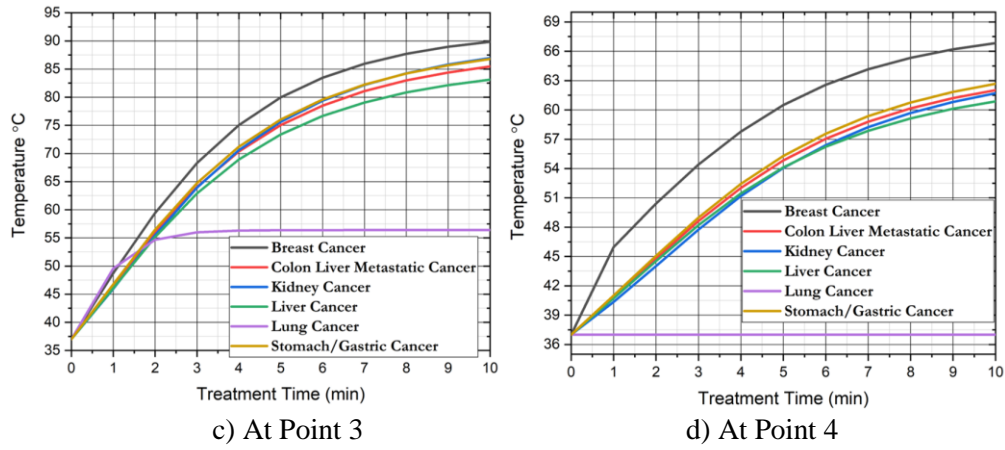


Figure 4.5 The time dependence of temperature at various points during MWA when the cancerous tumors in lung, breast, stomach/gastric, liver, colon liver metastatic, and kidney tissues are exposed to the microwave frequency of 2.45GHz and an input power of 100W for 4 minutes.

Fraction of tissue damage:

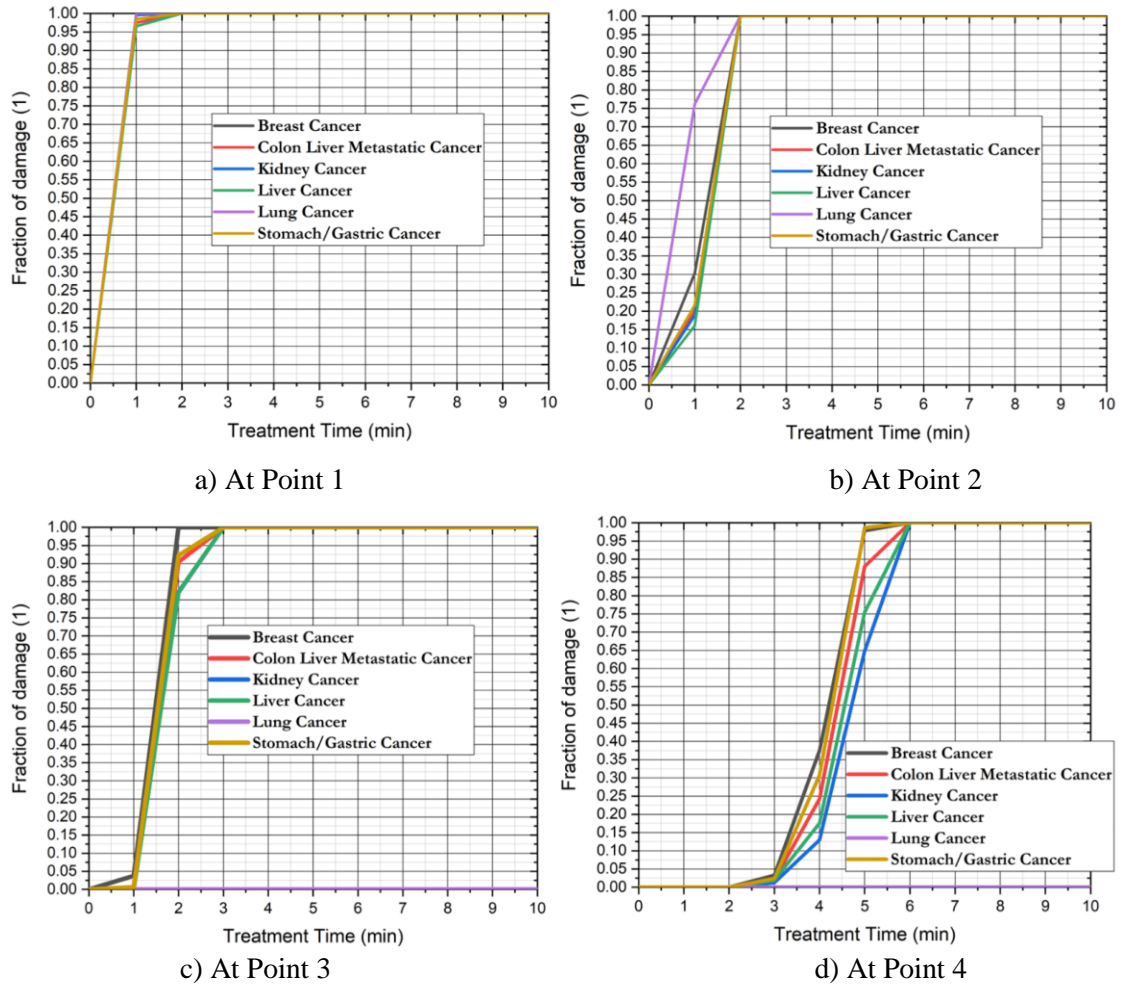
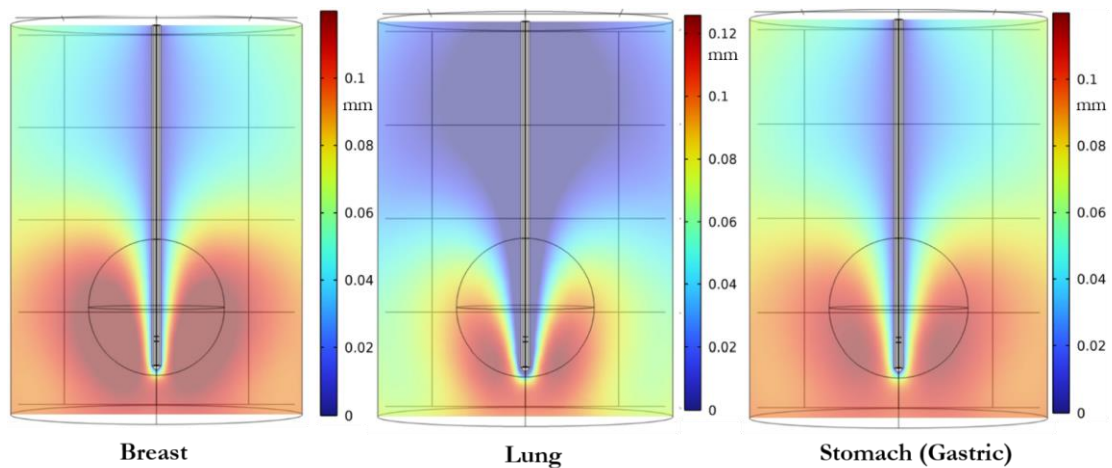


Figure 4.6 The time dependence of fraction of tissue damage at various points during MWA when the cancerous tumors in lung, breast, stomach/gastric, liver, colon liver metastatic, and kidney tissues are exposed to the microwave frequency of 2.45GHz and an input power of 100W for 4 minutes.

Tissue damage integral is also one of the major criteria in the analysis of the ablation region. The Arrhenius rate equation has been used to calculate the tissue damage integral, which was then used to plot the fraction of tissue damage as a function of treatment time. All the graphs of different organs follow the similar trend with the treatment time (Fig. 4.6). The tissue damage integral ($\Omega=1$) corresponds to 100% complete tissue ablation at that point. The tissue damage integral is highest near the trocar (Fig. 4.6 (a)) and decreases as the distance from the trocar increases (Fig. 4.6 (d)). It can be seen from graphs c) and d) that the tissue damage integral of lung tissue ($\Omega = 0$) which indicates the ablation of tissue is limited up to point 2.

Tissue Contraction:

The tissue contraction is directly proportional to the increase in the temperature resulting in the maximum amount of tissue displacement (contraction) occurring near the trocar. It can be seen from Fig. 4.7 that the lung, stomach, and kidney organs exhibit lesser deformations, with low volumetric tissue contractions of 0.14 mm, 0.11 mm, and 0.8 mm, respectively, as compared to the deformation values of other organs. This is due to the fact that the coefficient of thermal expansion value is less for organs as compared to the other tissues. Similarly, the organs, liver, colon metastatic and breast organs show larger deformations, 0.23 mm, 0.115 mm and 0.18 mm, respectively, as compared to the other organs. It is evident from the figures that the liver and breast tissues exhibit greater deformation and contraction during microwave ablation as compared to the other organs. The amount of tissue contraction helps in predicting the actual ablation region and also helps to overcome the heat sink effect due to blood vessels.



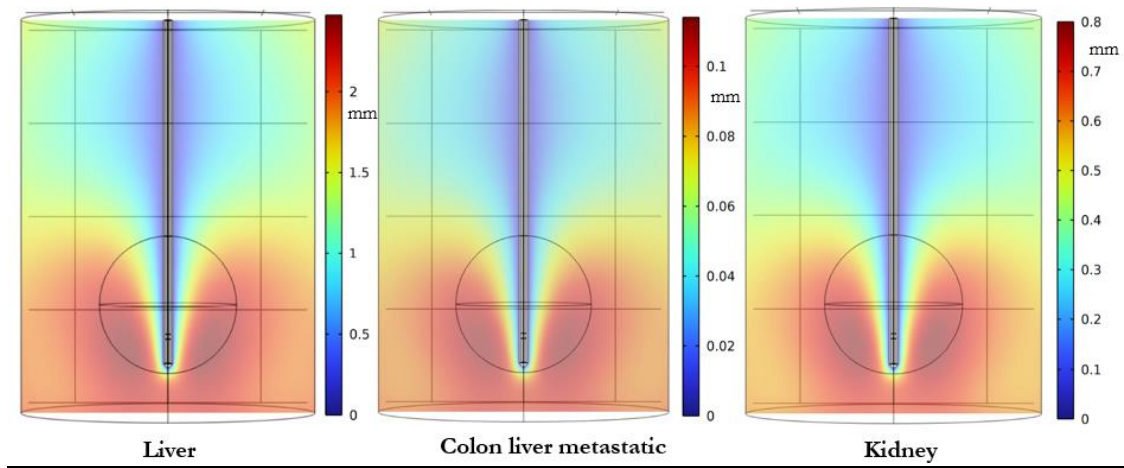


Figure 4.7 Tissue contraction obtained during MWA of different organs at microwave frequency of 2.45GHz and an input power of 100W for 4 minutes.

4.2 MWA of HCC using parallel and non-parallel insertion of trocars:

The present objective has been designed to assess the ablation region obtained using multiple MWA trocars both numerically and experimentally. Further, multiple trocars have been inserted into the tissue in parallel and non-parallel positions operating at 2.45 GHz and 6 GHz frequencies. Internal trocar cooling mechanism has been considered in this study. Experimental analysis has been performed on egg white with added albumin protein.

Numerical Simulations

Temperature distribution

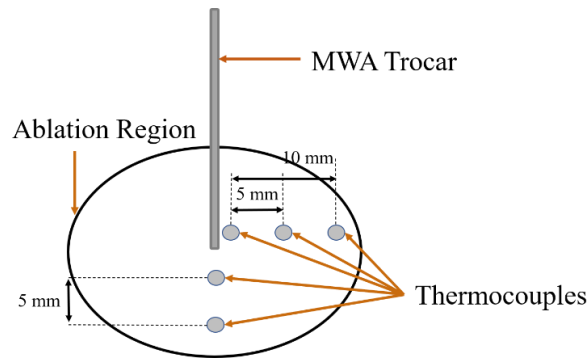


Figure 4.8 Temperature measuring points and trocar positioning

Temperature measurements at 0 mm, 5 mm and 10 mm distances from the microwave trocar slot for microwave power of 140 W for 6 minutes have been shown in Fig. 4.8. The temperature data obtained for both numerical and experimental (using thermocouples) studies have been presented in Fig. 4.9 (a). It can be seen from Fig. 4.9 (a), (b) and (c) that there is a rapid raise in the temperature values near to the slot area, followed by the points away from

it. Initially the temperature rises rapidly and slows down after 50 s. The temperature variation of the tissue rises slowly as we move away from the slot and tends to be linear.

The temperature variations with the ablation time obtained from the numerical and in vitro studies have been compared and presented in Fig. 4.9 (a). It can be seen from Fig. 4.9 (a) that, there is a minor variation in temperature vs ablation time plots obtained from numerical and in vitro studies performed at 2.45 GHz frequency. Both the numerical and in vitro studies follow similar trend in temperature variation with respect to time.

The temperature variations with the ablation time obtained from numerical studies at various frequencies have been shown in Figs. 4.9 (b) and 4.9 (c). It can be seen from the graphs that the temperature variations exhibit a similar trend. Since the tissue shows better energy absorption properties at a higher frequency (6 GHz), more rapid heating with a temperature of more than 10°C is observed compared to conventional frequencies (2.45 GHz).

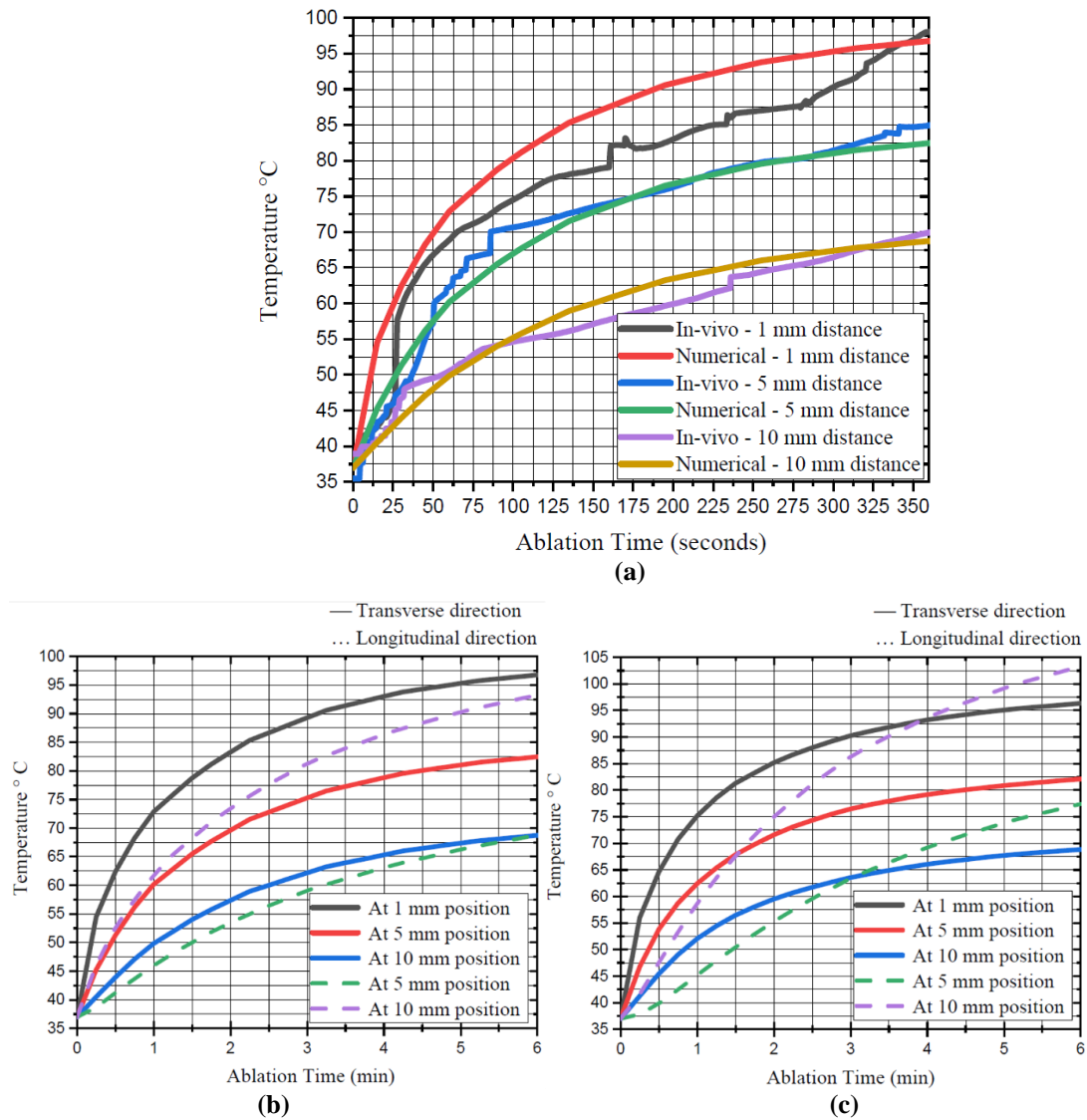


Figure 4.9 Variation of temperature with the ablation time in the hepatic gland (a) in-vitro and numerical experiments at 2.45 GHz frequency, (b) numerical experiments at 2.45 GHz and (c) numerical experiments at 6 GHz.

Microwave ablation of hepatic gland tissue during parallel insertion of trocars

The predicted ablation zones in the triangular hepatic tissue when two trocars have been inserted parallelly and operated for 6 min, 140 W power at 2.45 and 6 GHz frequencies have been shown in Fig. 4.10. The two internally cooled trocars have been spaced at a distance of 10 mm apart. Table 4.2 lists the dimensions of simulated and measured ablation zones for two-trocar MWA. Simulation results indicate that MWA at 6 GHz frequencies yields larger ablation region than with 2.45 GHz systems. Moreover, simulation results demonstrate that 6 GHz (Fig. 4.10 (b)) yields more spherical ablation zones in a coronal or frontal plane perpendicular to the trocar's axis compared to MWA at 2.45 GHz, making it suitable for treating large spherical tumours. The teardrop shape ablation has been obtained by two trocar MWA operated at 2.45 GHz (Fig. 4.10 (a)). However, when two trocars are operated at combined frequencies of 2.45/6 GHz; an irregularly-shaped ablation region has been achieved (Fig. 4.10 (c))[71].

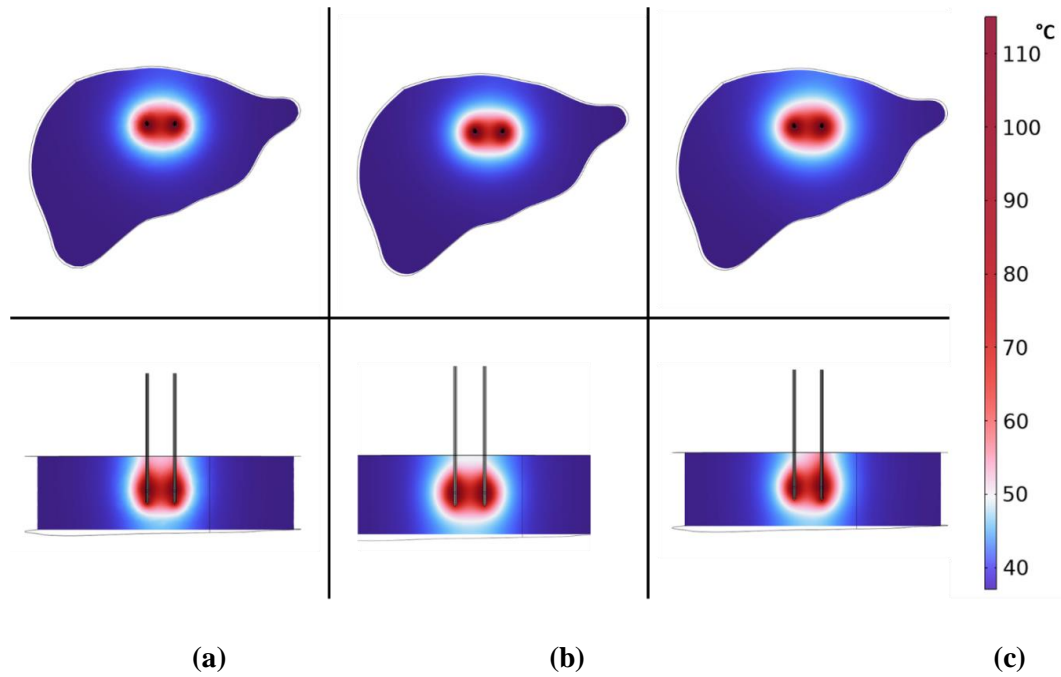


Figure 4.10 Temperature distribution in the hepatic gland tissue obtained during parallel insertion of water cooled MWA trocars: a) both trocars at 2.45 GHz, b) both trocars at 6 GHz and c) one trocar at 6 GHz and the other one at 2.45 GHz.

The dimensions, d_1 (mm) the diameter of the ablation zone aligned with both the trocars, d_2 (mm) the diameter of the ablation zone perpendicular to both the trocars and the volume of the ablation region have been tabulated in Table 4.2. The dual-trocar ablation at 6 GHz shows the optimal ablation characteristics of 63 mm (d_1) \times 60 mm (d_2) diameter of the ablation boundary compared to 50 mm (d_1) \times 63 mm (d_2) at 2.45 GHz and 55 mm (d_1) \times 63 mm (d_2) for the case when the trocars are operated at 2.45 and 6 GHz frequencies. Multiple trocar tumour ablations at 6 GHz show a spherical ablation volume.

Table 4.2: Ablation zone dimensions following 6 min of MWA at 140 W with trocars inserted non-parallelly and operated at 2.45 GHz and 6 GHz frequencies (see Fig. 4.10).

S.No.	Frequency Combination	d_1 (mm)	d_2 (mm)	Volume (cm ³)
1	2.45 GHz	50	63	85
2	6 GHz	63	60	95
3	2.45 and 6 GHz	55	63	93.5

d_1 is the diameter of the ablation zone aligned with the two trocars and d_2 is the diameter of the ablation zone perpendicular to the two trocars.

Microwave ablation of hepatic gland tissue during non-parallel insertion of two trocars

The predicted ablation zones in the triangular hepatic tissue using two trocars inserted non-parallelly and operated for 6 min with a power input of 140 W at 2.45 GHz and 6 GHz frequencies have been shown in Fig. 4.11. The dimensions, the radial diameter d_1 (mm), the transverse diameter d_2 (mm), and the ablation volume obtained during non-parallel insertion of two trocars MWA have been detailed in Table 4.3.

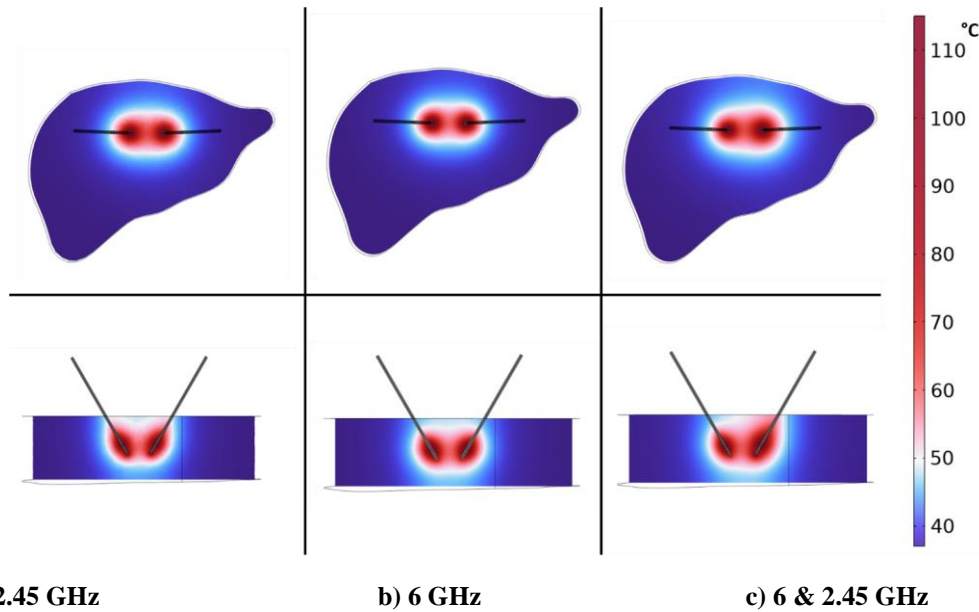


Figure 4.11 Temperature distribution in the hepatic gland tissue obtained during non-parallel insertion of water cooled MWA trocars: a) 2.45 GHz on both trocars, b) 6 GHz on both trocars and c) 6 and 2.45 GHz on both trocars.

The simulated results show that MWA with non-parallel trocar positioning leads to larger ablation volume than parallel trocar positioning. Moreover, simulation results show that MWA at 6 GHz (Fig. 4.11 (b)) yields a uniform-shaped ablation region of 65 mm (d_1) \times 60 mm (d_2) with less backward heating of the trocar compared to MWA at 2.45 GHz. The rectangular shaped ablation region of 55 mm (d_1) \times 63 mm (d_2) has been obtained by two trocars operated at 2.45 GHz (Fig. 4.11 (a)). Further, an irregular shaped ablation region has been achieved by trocars operated at 2.45 and 6 GHz (Fig. 4.11 (c)) frequencies. This

configuration can be used to treat tumours of irregular shapes. Even though multiple trocars increase ablation volume, inapt positioning leads to the ablation of healthy tissue [53]. The problem, as mentioned, can be overcome by using non-parallel trocar positioning. Further, the angle of the trocar insertion and the energy among the trocars (frequency, time and power) will be decided based on the tumour's precise location in the tissue.

Table 4.3: *Ablation zone dimensions following 6 min of MWA at 140 W with non-parallel insertion of trocars and operated at 2.45 GHz and 6 GHz frequencies (see Fig. 4.11).*

S.No.	Frequency Combination	d1 (mm)	d2 (mm)	Volume (cm ³)
1	2.45 GHz	55	63	88.7
2	6 GHz	65	60	95
3	2.45 and 6 GHz	58	63	87

d_1 is the diameter of the ablation zone aligned with the trocars and d_2 is the diameter of the ablation zone perpendicular to the trocars.

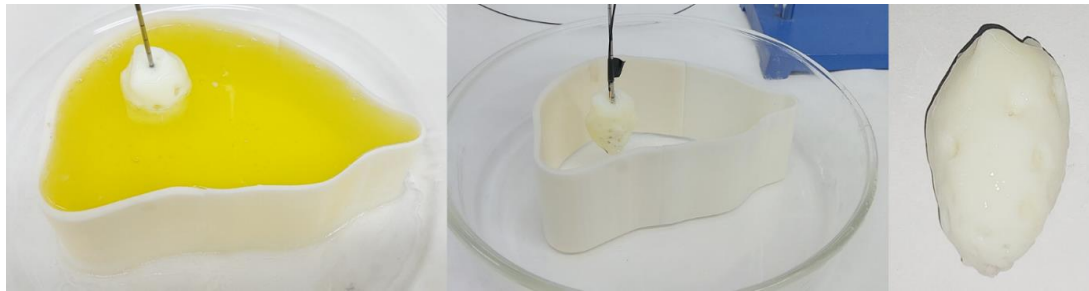
Ablation Experiments on Egg White

Even though simultaneous activation of multiple trocars is more advantageous in producing larger lesion volume, sequential probe ablation is more additive in clinical operations. Apt positioning, thermal protection and space between the trocars make sequential activation of the trocar more advantageous than the ablation obtained using simultaneous insertions of multiple trocars.

The ablation volume generated by MWA using parallel and non-parallel insertion of single, dual and triple trocars into the tissue has been shown in Fig.4.12. The present in vitro analysis has been performed wherein sequential insertion of trocars into the tissue has been performed. The experiments have been performed on egg white in 3D Printed periphery regions operated for 6 min, 140 W power at 2.45 frequency (shown in Fig. 4.12): a) single trocar; b) parallel positioned two trocars; c) non-parallel positioned two trocars; d) parallel positioned three trocars and e) non-parallel positioned three trocar during microwave ablation. The dimensions of the combined ablation region, width (mm) and length (mm), have been tabulated in Table 4.4.

The egg white changes from a transparent state to an opaque white as the temperature rises above 50°C due to coagulation of albumin due to denaturation. A teardrop-shaped ablation region of 29 mm (radial) × 45 mm (axial) has been obtained by deploying a single trocar (Fig. 4.12 (a)). Dual trocar microwave ablation creates lesions almost twice in size as those generated by the single trocar, followed by the triple-trocar tumour ablation. Ablation during

simultaneous insertion of trocars leads to approximately spherical lesions, with a uniform coagulation region compared to the sequential insertion of trocars.



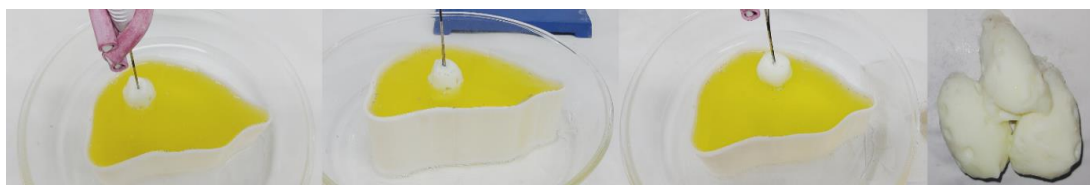
a) single trocar



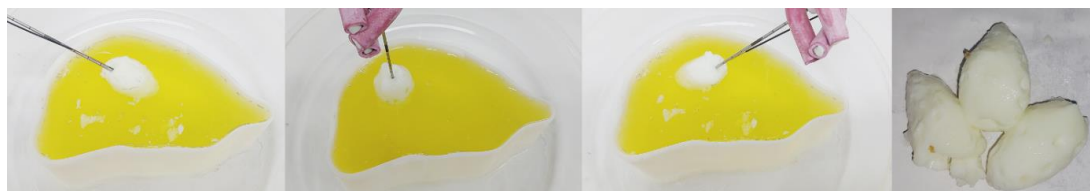
b) parallel insertion of two trocars



c) non-parallel insertion of two trocars



d) parallel insertion of three trocars



e) non-parallel insertion of three trocars

Figure 4.12 Ablation zones in egg white obtained when trocars have been operated for 6 minutes at 140 W microwave power.

Parallel position of two trocars operated sequentially has been shown in Fig. 4.12 (b). Nearly teared shaped ablation region (having square shaped cross-section) with dimensions of 54 mm (radial) \times 45 mm (axial) has been achieved in two parallel ablations. Further, it can be seen from Fig. 4.12 (c) that the non-parallel trocar insertion ablation region of irregular shape has been achieved. Figures 4.12 (d) and (e) show parallel and non-parallel insertion of three trocars. The results show that trocar insertion and operation can vary based for required ablation region, and its parameters (power, time) can be altered based on the tumour volume.

Table 4.4: *Dimensions of the generated ablation zones in egg white using Solero MWA antenna operated for 6 min at 140 W microwave power.*

S.No	No. of trocars and its positing into the tissue	Longitudinal measurement (mm)	Lateral measurement (mm)
1	Single Trocar	29	45
2	Two trocars (parallel insertion)	54	45
3	Two trocars (non-parallel insertion)	58	42
4	Three trocars (parallel insertion)	54	51
5	Three trocars (non-parallel insertion)	58	51

4.3. MWA of HCC Tumors using novel design L shaped dual tine dual frequency trocar: One fixed and one flexible tine.

A novel microwave trocar design has been proposed and considered in the present study wherein single antenna is being replaced with multiple tines supplied with energy at available conventional and high frequencies. A dual tine MWA trocar with each tine supplied with energy at different frequencies (2.45 GHz and 6 GHz) has been considered to ablate the hepatic tumor.

Ablation Region at different frequencies

Considering the influence of microwave power and frequency on the ablation region, the present numerical model evaluates the ablation characteristics with a microwave power of 15 W at two microwave frequencies, 2.45 and 6 GHz. The performance of the proposed novel MWA antenna has been analyzed by performing different combinations of simulations with tines individually maintained at different frequencies. They are a) longitudinal tine at 2.45 GHz frequency; b) curved tine at 2.45 GHz frequency; c) longitudinal tine at 6 GHz frequency and d) curved tine at 6 GHz frequency. In this numerical analysis a tumor of 3 cm in diameter has been embedded into the hepatic gland tissue. The obtained zones at various frequencies have been shown in Fig. 4.13.

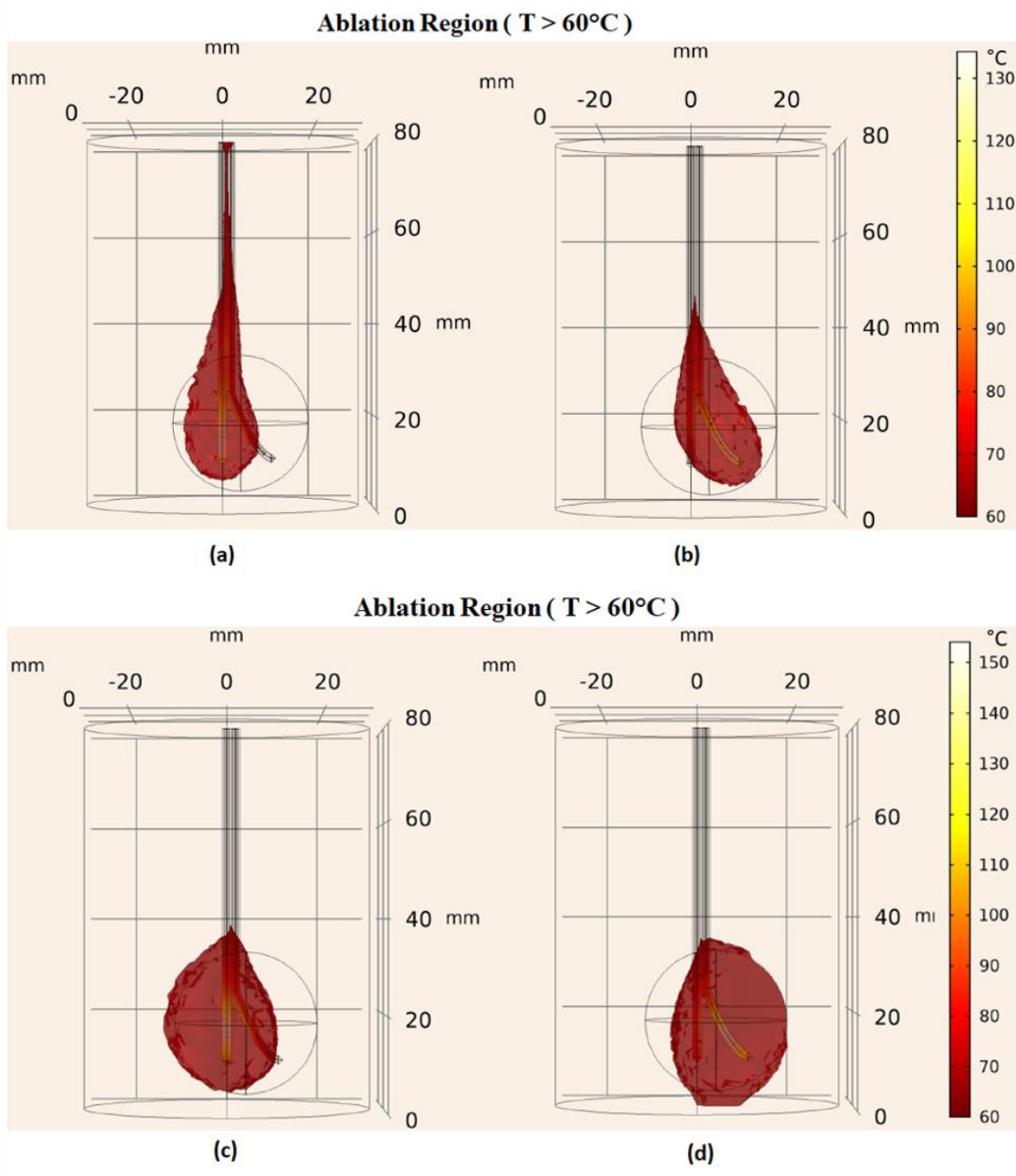


Figure 4.13 Thermal Ablation of hepatic gland using the proposed novel trocar with a) 2.45 GHz frequency on longitudinal tine; b) 2.45 GHz frequency on curved tine; c) 6 GHz frequency on longitudinal tine and d) 6 GHz frequency on curved tine.

It can be seen from Figs. 4.13 (a) and (b) that a teardrop-shaped ablation region along the trocar length has been obtained. Further, it can be seen From Fig. 4.13 (a) that, indiscriminate damage to the healthy tissue along the trocar length is evident. The obtained ablation zones when both the tines are maintained at 6 GHz have been shown in Figs. 4.13 (c) and (d) for longitudinal and curved tines, respectively. It is apparent from the presented results that a more concentrated spherical ablation region has been obtained when the tines are supplied with energy at a high frequency, i.e., 6 GHz. This is due to the fact that the biological tissue shows a better microwave energy absorption rate at higher frequencies [19].

Antenna Specifications

In the design of a novel microwave antenna, the minimum criteria that an antenna has to meet for its efficient working is to have a Reflection Coefficient (dB) / Return Loss less than -10 dB, VSWR (Voltage Standing Wave Ratio) should be less than 2.0 with less power losses at the load conditions [72]. Table 4.5 shows the comparison of the required specifications and achieved specifications of antenna operated at 2.45 and 6 GHz frequencies which have been obtained numerically. From Table 4.5, it can be seen that a good agreement in Reflection Coefficient (dB) / Return Loss and VSWR between the required and achieved specifications has been obtained at 2.45 GHz frequency. The low Reflection Coefficient (dB) / Return Loss and VSWR signifies less energy losses at the load conditions. It can also be seen from Table 4.5 that the Reflection Coefficient (dB) / Return Loss at 6 GHz frequency is slightly greater than -10 dB. However, VSWR is within the acceptable range. Further optimizing the antenna with a large slot area [64], and reflector design [73] will help the antenna overcome high Reflection Coefficient (dB), VSWR with less power losses at the load conditions.

Table 4.5: *Specifications of Antenna*

Parameter	Required Specifications at 2.45/6 GHz	Achieved Specifications at 2.45 GHz	Achieved Specifications at 6 GHz
Reflection Coefficient (dB)/Return Loss	< -10 dB	-18.119	-9.568
Power dissipation	15 W	14.030	10.208
VSWR	< 2.0	1.2834	1.995

Antenna Performance Characteristics

The major parameters required to analyse the efficiency of novel MWA antenna are the reflection coefficient, power dissipation, maximum power dissipation density, Specific Absorption Rate (SAR), maximum temperature, ablation diameters, ablation lengths for microwave ablation therapy [26]. A parametric comparison of the proposed trocar at various combinations of energy frequencies (for 15 W and 10 Min) has been tabulated in Table 4.6. It is evident from Table 4.6 that, the trocar operated at 2.45 GHz frequency shows low reflection coefficient (-18.119 dB) with large power dissipation (14.030 W) and less power loss at the load in comparison to the tines operated at 6 GHz and a combination of 2.45/6 GHz frequencies. Apart from a high reflection coefficient (-9.6 dB) with low power dissipation (10.208 W), the tines operated at high-frequency microwave energy (6 GHz) show a better specific absorption rate of energy into the tissue than the tine operated at available conventional frequency (2.45 GHz). As the frequency increases, the depth of penetration of

the wave decreases, making it high energy density within a smaller region. Similarly, a trocar operated at 2.45/6 frequency combination shows more SAR compared to the tines operated at same frequencies. A good aspect ratio in terms of ablation length to the diameter (of 1.3) is obtained at high-frequency microwave energy (6 GHz) in comparison to the trocar operated at low frequency (2.45 GHz) (of 1.8), and combination of low (2.45 GHz) and high frequency (6 GHz) microwave energy (of 1.5).

Table 4.6: *Comparison of antenna performance of various combinations obtained numerically*

Parameter	At 2.45 GHz frequency on both the tines	At 6 GHz frequency on both the tines	At 2.45 GHz frequency on longitudinal tine and 6 GHz on curved tine	At 6 GHz frequency on longitudinal tine and 2.45 GHz on curved tine
Reflection Coefficient (dB)	-18.119	-9.6	-18.119 & -9.6	-9.6 & -18.119
Power Dissipation (W)	14.030	10.208	14.38	14.38
Maximum Power Dissipation Density (MW/m ³)	35.1	52.9	62.9	62.9
Specific Absorption Rate (SAR) (KW/Kg) (At 15 W, 10 Min)	35	53.18	63	63
Maximum Temperature (°C) (At 15 W, 10 Min)	123°C	140°C	142°C	139°C
Ablation Diameter (cm)	4.5	4.0	4.1	4.1
Ablation Length (cm)	2.5	3.0	2.7	2.7

Irregular ablation region using dual tine multiple frequency trocar with temperature distribution

The efficacy of proposed novel microwave antenna design has been analyzed by performing MWA on hepatic gland. The simulated ablation region ($T > 60^{\circ}\text{C}$) of the hepatic gland embedded with 3 cm tumor has been shown in Fig. 4.14. The lethal temperature in the present study has been considered to be 60°C . Figure 4.15 shows ablation region obtained at a) 2.45 GHz frequency on both the tines; b) 6 GHz frequency on both the tines; c) 2.45 GHz frequency on longitudinal tine and 6 GHz on curved tine and d) 6 GHz frequency on longitudinal tine and 2.45 GHz on curved tine.

A teardrop-shaped ablation region of less than 30 mm (more than 25 mm) in diameter with more backward heating along the trocar's length can be seen from Fig. 4.14 (a). There is an indiscriminate and collateral damage occurred to the healthy tissue along the trocar length. It helps to treat the teardrop-shaped tumor of above 27 mm in diameter. In this case, an additional trocar cooling system is required to overcome the collateral damage to the healthy

tissue. It will also increase trocar efficiency with more ablation region in the lateral direction [74]. Figure 4.14 (b) shows a spherical shaped ablation region (greater than 30 mm) with a more sphericity index of complete tumor ablation. It can be seen from the simulation results that, a concentrated ablation region with less collateral damage is occurred to the healthy tissue. This is due to the fact that high-frequency MWA shows a better material response rate with more concentrated energy within the tissue [19]. High-frequency MWA can reduce the backward heating and minimize the collateral damage to the healthy tissue. It is evident from Figs. 4.14 (c) and (d) that, a combination of teardrop and spherical shaped ablation region has been obtained. It helps to treat the irregular shaped tumors having diameter greater than 27 mm.

One of the significant limitations of the present computational studies is the lack of a trocar cooling system, which helps in cooling the trocar and tissue, resulting in more concentrated ablation regions. It will also increase the sphericity index of the ablation region. The frequency combination of trocars will influence the shape and size of the ablation zone.

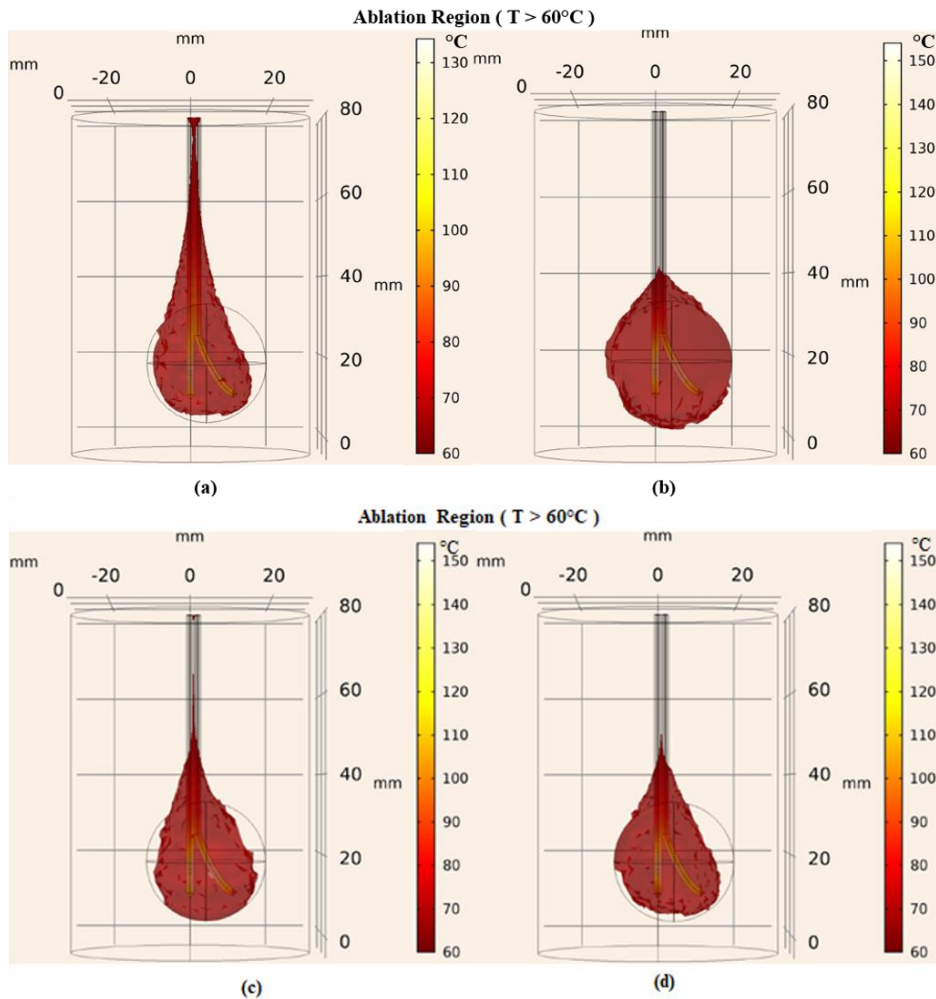


Figure 4.14 Thermal ablation of 3 cm tumor embedded hepatic gland at a) 2.45 GHz frequency on both the tines; b) 6 GHz frequency on both the tines; c) 2.45 GHz frequency on longitudinal tine and 6 GHz on curved tine and d) 6 GHz frequency on longitudinal tine and 2.45 GHz on curved tine.

The diameter of the tumor ablated and ablation volume obtained for the simulated antenna models have been shown in Table 4.7. It can be seen from Table 4.7 that the novel microwave antenna at high-frequency combination results in a larger diameter tumor ablation zone as compared to the ablation zone obtained using the trocar maintained at conventional frequencies. The ablation volume for all the configurations presented here seems to be almost the same. However, it is essential to note that the ablation region's extent for 2.45 GHz case is different, extending along the trocar's length. In contrast, at 6 GHz, a more concentrated spherical ablation region has been observed. Further, deployment of the curved tine and treatment time can be varied to obtain various ablation regions. A decrease in tine deployment will further decrease the ablation volume and makes it suitable for ablating small size tumors.

Table 4.7: *Comparison of the simulated ablation results with the novel microwave antenna at various frequency combinations*

S. No	Novel microwave antenna at various frequency combinations	The diameter of the tumor ablated (mm)	Ablation volume (cm ³)
1	2.45 GHz frequency on both longitudinal and curved tines	25	22.4776
2	2.45 GHz frequency on longitudinal tine and 6 GHz on curved tines	27	22.567
3	6 GHz frequency on longitudinal tine and 2.45 GHz on curved tines	27	22.571
4	6 GHz frequency on both longitudinal and curved tines	30	22.576

Comparison of the ablation volume obtained using the existing MWA trocars/modalities with the proposed trocar

Comparison of the ablation volume obtained using the existing MWA trocars/modalities with the proposed trocar has been presented in Fig. 4.15, wherein a 3 cm tumour embedded in the hepatic gland has been ablated. Figures 4.15 (a) to 4.15 (c) and 4.16 (a) to 4.16 (c) present MWA of 3 cm tumour embedded in the hepatic gland using the trocar operated at 2.45 GHz and 6 GHz frequencies, respectively. Figures 4.17 (a) to 4.17 (c) present the thermal ablation of a 3 cm tumour embedded in the hepatic gland using multiple trocars operated at 2.45/6 GHz frequencies.

It can be seen from Figs. 4.15 (a) and 4.16 (a) that the existing MWA trocars are limited to treat tumours having a diameter range of 2 cm to 2.5 cm when the trocars are operated at 2.45/6 GHz frequencies. Further, multiple and parallel trocars are required for treating nearly 2.5 cm tumours, resulting in an increase in the number of insertions into the

biological tissue and uncontrolled ablation region (i.e., results in ablating the healthy tissue) (Figs. 4.15 (b), 4.16 (b), 4.17 (a), and 4.17 (b)). Parallel insertion of multiple trocars requires ideal spacing in between the trocars to obtain maximum ablation region without indentations since indentations would result in incomplete tumour ablation (as shown in Figs. 4.15 (b), 4.16 (b), 4.17 (a), and 4.17 (b)). It is evident from Figs. 4.15 (c), 4.16 (c) and 4.17 (c) that the proposed trocar can overcome the problems associated in using multiple and parallel trocars in ablating large size tumors of symmetric and axisymmetric shapes, restrict the damage to the healthy tissues and achieve more concentrated ablation regions.

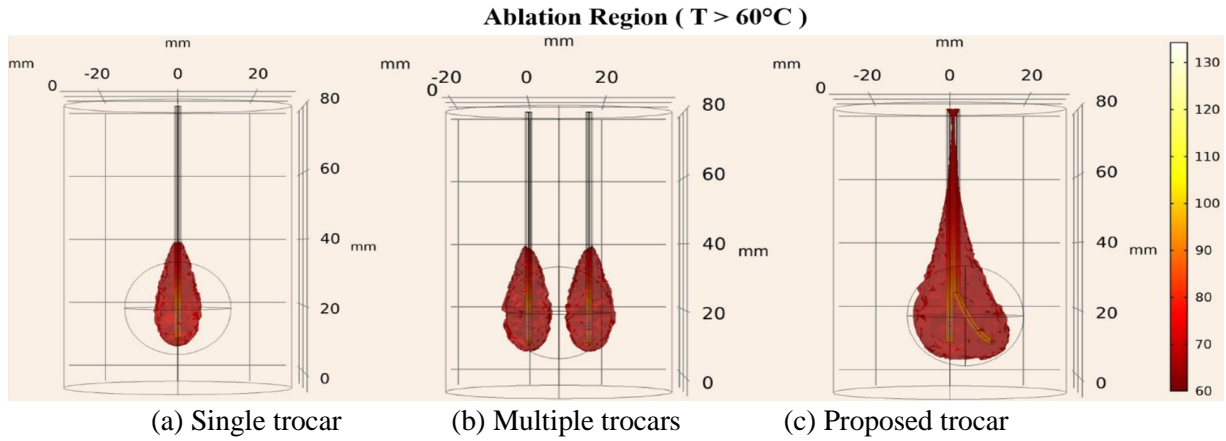


Figure 4.15 Thermal ablation of 3 cm tumour embedded hepatic gland at 2.45 GHz

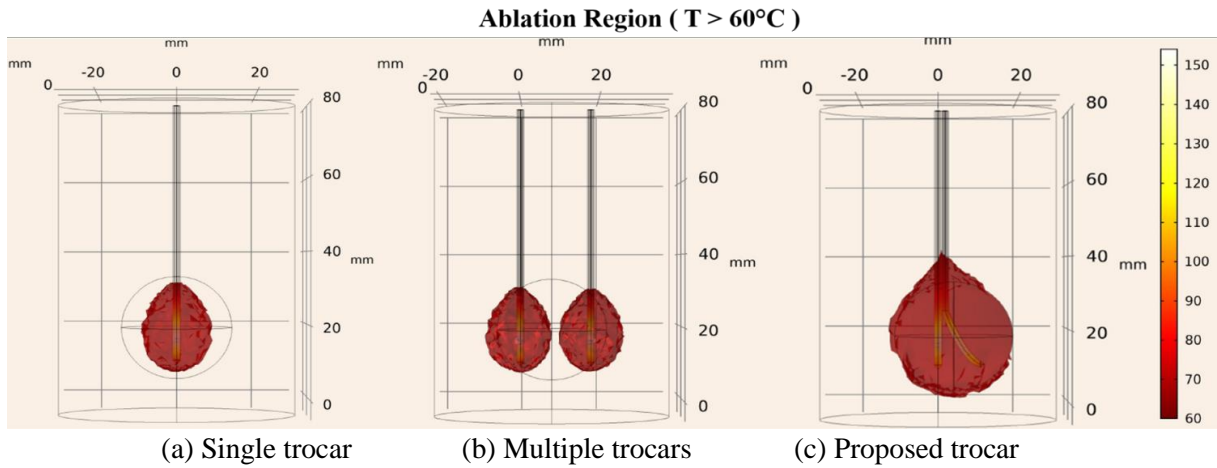
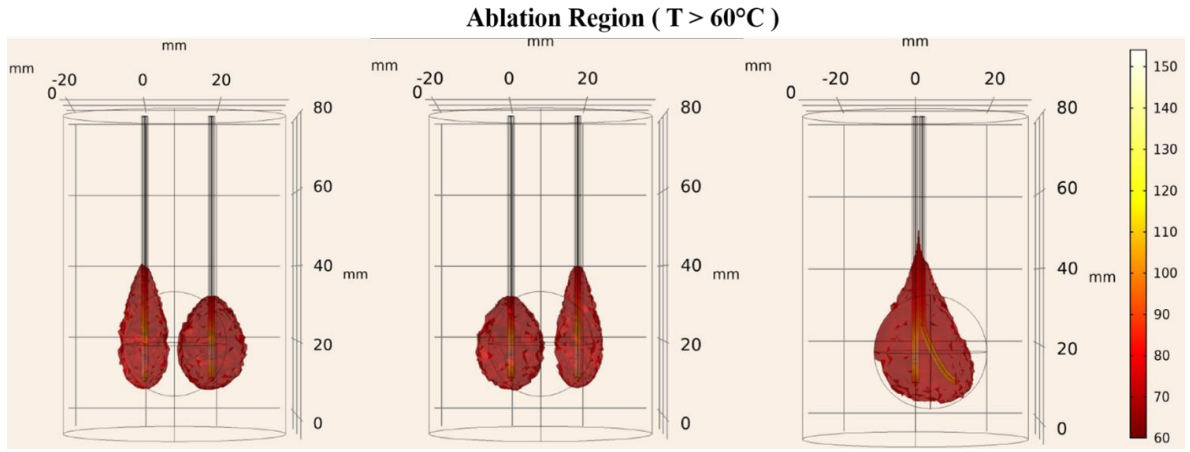


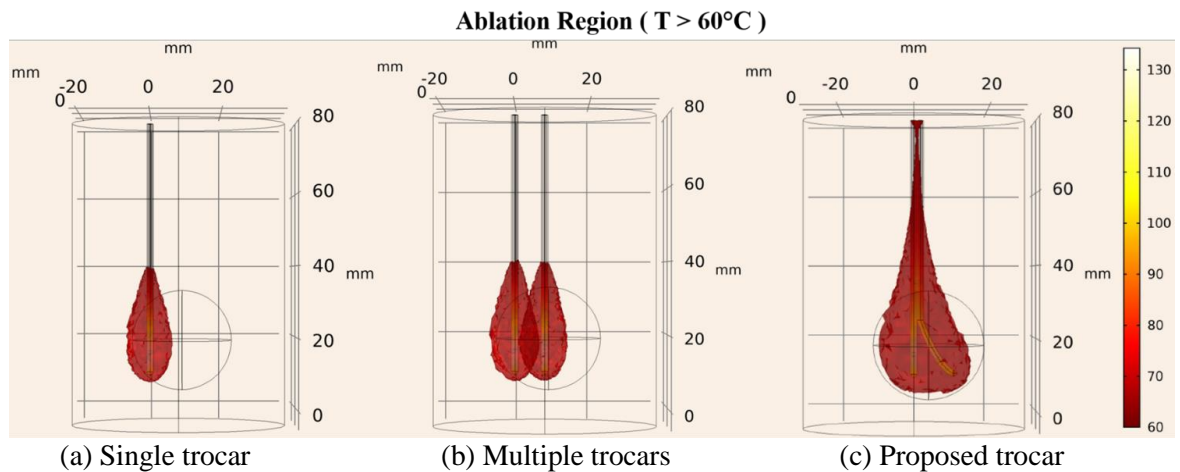
Figure 4.16 Thermal ablation of 3 cm tumour embedded hepatic gland at 6 GHz



(a) Multiple trocars (2.45/6 GHz) (b) Multiple trocars (6/2.45 GHz) (c) Proposed trocar (2.45/6 GHz)

Figure 4.17 Thermal ablation of 3 cm tumour embedded hepatic gland using multiple trocars operated at 2.45/6 GHz frequencies

Inapt trocar positioning leads to incomplete tumour ablation and leads to damage of nearby healthy tissues. Further, multiple parallel trocars are required to treat large size tumours, increasing the number of precise trocar insertions into the tissue and leading to uncontrolled ablation regions (i.e., results in ablating the healthy tissue). It can be seen from Figs. 4.18 (a), 4.18 (b), 4.19 (a) and 4.19 (b) that inapt position of the trocar leads to incomplete tumour ablation and further increases the requirement for multiple parallel insertions of trocars for complete tumour ablation. One of the major contributions of the present study is that a single trocar has been replaced with multiple tines supplied with energy at available conventional and high frequencies. The proposed design is expected to overcome multiple and parallel insertion of trocars required for treating large-size tumours. Once the trocar is inserted into the tissue, the flexible tine can be deployed as per the requirement of the ablation region. It can overcome the problem associated with the trocar's precise insertion, irregularly shaped ablation region by sparing healthy tissue and nearby blood vessels.



(a) Single trocar (b) Multiple trocars (c) Proposed trocar

Figure 4.18 Thermal ablation of 3 cm tumour embedded hepatic gland with inapt positioning of trocar operated at 2.45 GHz

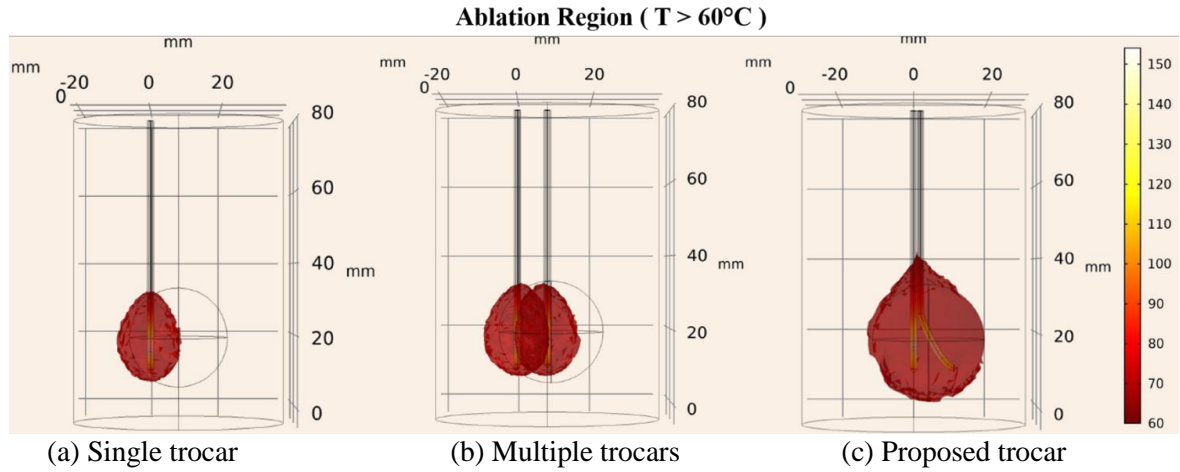


Figure 4.19 Thermal ablation of 3 cm tumour embedded hepatic gland with inapt positioning of trocar operated at 6 GHz

Temperature and tissue damage integral characteristics during MWA

Temperature distribution and tissue damage integral (obtained from Arrhenius rate equation) are the two major parameters to predict tumor necrosis. Figure 4.20 shows the geometry of tumor embedded liver gland with temperature and tissue damage monitoring points. Five radial temperature values and tissue damage monitoring points have been considered for each tine near the antenna slot.

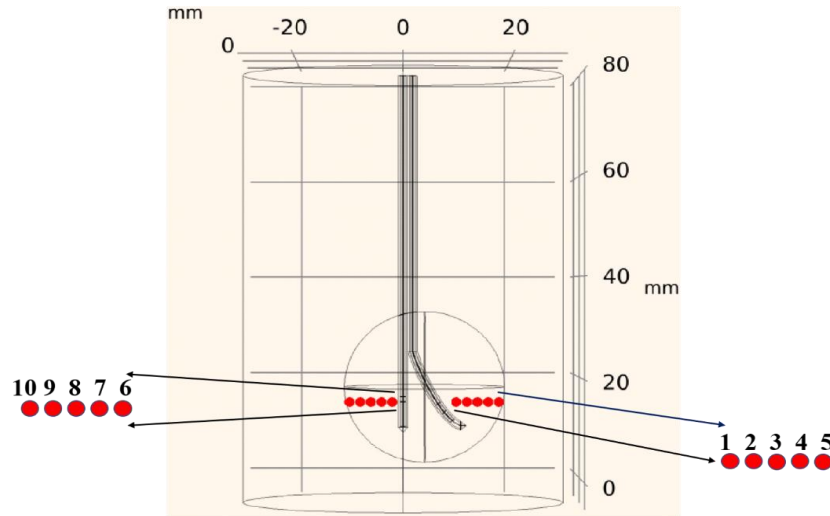
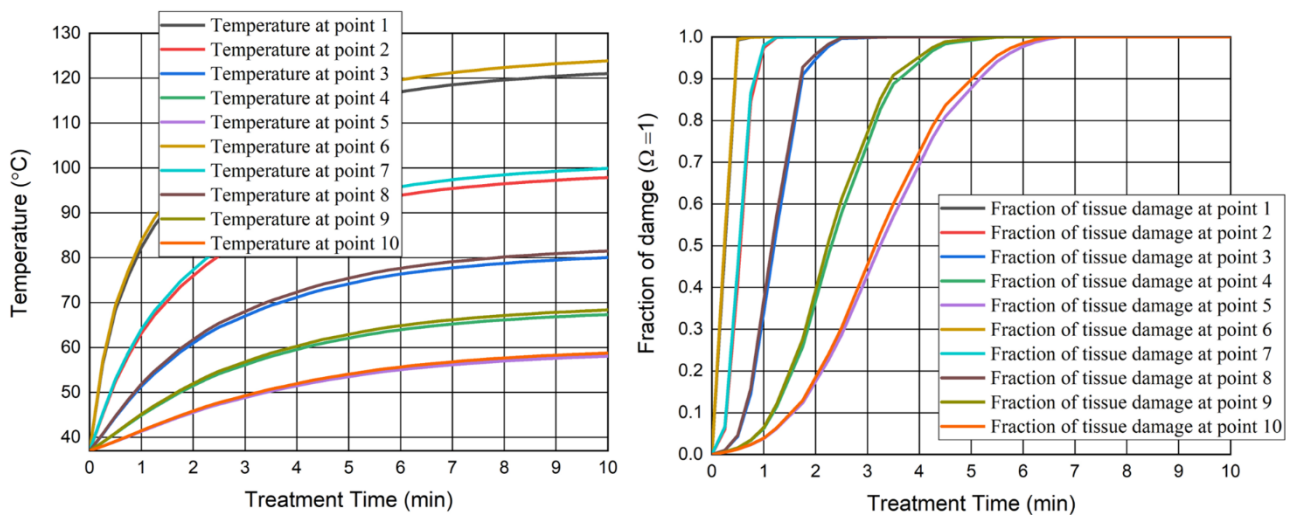


Figure 4.20 Spatial locations of temperature and fraction of tissue damage monitoring points for longitudinal and curved tines.

Figure 4.21 shows the variation of temperature and tissue necrosis (corresponding to $\Omega = 1$) with time during MWA at a) 2.45 GHz frequency on both the tines; b) 2.45 GHz frequency on longitudinal tine and 6 GHz on curved tine; c) 6 GHz frequency on longitudinal tine and 2.45 GHz on curved tine and d) 6 GHz frequency on both the tines. All the graphs show a similar trend of temperature rise with the treatment time. The point near to the antenna

slot shows more rise in the temperature followed by the last point. The tissue damage integral $\Omega = 1$ corresponds to 100 % complete tissue ablation at that point. It is evident from Fig. 4.21 that, there is a linear variation in the tissue damage at all monitoring points of the novel antenna at various frequencies. The results show that the ablation temperature has been achieved within one minute of the treatment time. The treatment time required for tissue necrosis during high-frequency MWA is less as compared to the treatment time required when conventional frequency is used.

When tines (longitudinal and curved) are maintained at the same frequency, the temperature profiles are similar at both the tines (*refer* Figs. 4.21 (a) and (d)). A slight increase in curved tine temperature variation has been observed as there is a minor enlargement in the antenna slot, resulting in more energy distribution. Similarly, the variation of tissue damage integral with time at tines follows a similar trend when both tines are maintained at the same frequency. It can be seen from Fig. 4.21 (a) that, the minimum time required for tumor necrosis ($\Omega = 1$) is 6 minutes. Figures 4.21 (b) and (c) show the optimal time of 6 min required for tumor necrosis ($\Omega = 1$). Since the tumor shows better energy absorption properties at a higher frequency, a temperature of more than 15°C is observed as compared to the case where conventional frequencies have been used. It can be seen from the results that tumor necrosis with the tine maintaining at a higher frequency (6 GHz) is achieved in 4 minutes, followed by the tine maintained at a conventional frequency (2.45 GHz) in 6 minutes. Further, it can be seen from Fig. 4.21 (d) that a higher temperature of 141°C at 2 mm away from the antenna slot has been observed since the tumor shows better heating rate at a higher frequency [19]. The optimal time required for the complete tumor necrosis has been achieved within 4 minutes of the ablation time.



(a)

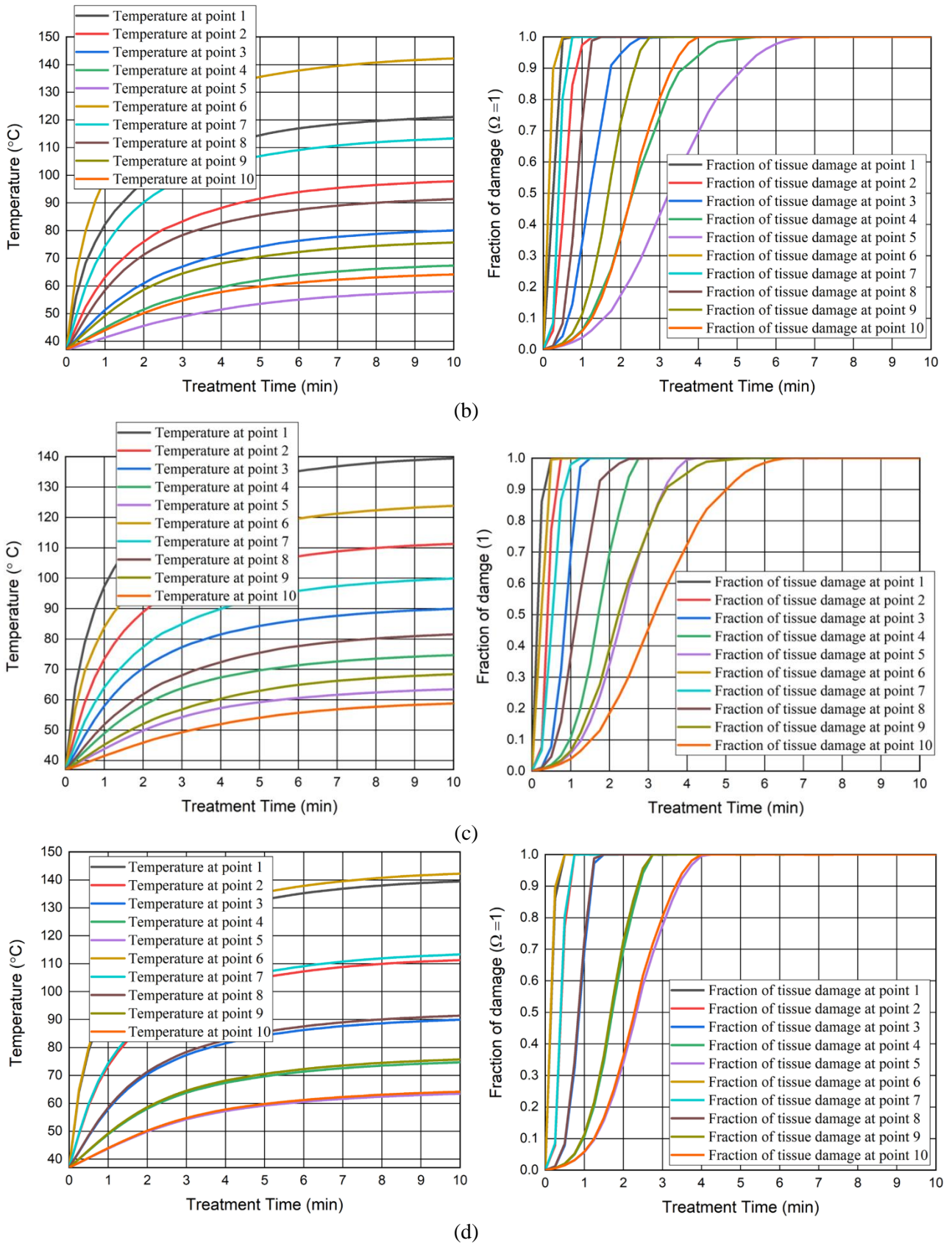


Figure 4.21 Variation of temperature and fraction of tissue damage with the treatment time when tines are maintained at different combinations of frequencies: a) 2.45 GHz frequency on both the tines; b) 2.45 GHz frequency on longitudinal tine and 6 GHz on curved tine; c) 6 GHz frequency on longitudinal tine and 2.45 GHz on curved tine and b) 6 GHz frequency on both the tines.

4.4 MWA of HCC Tumors using novel design U shaped dual tine dual frequency trocar: Both are flexible tine.

The ablation region obtained during MWA of hepatic gland using the novel medical applicator, the effect of change in deploying length of the trocar and supplied energy, have been presented in the following sections. In all these cases a tumor of 3-cm in diameter has been embedded into the hepatic gland. Further, the ablation regions presented in all the below cases are for a power input of 15 W for 10 min.

Case study 1: MWA of HCC using the novel trocar with fully deployed tines

The MWA results in a sharp rise in the tissue temperature, above 60 °C, even for a shorter exposure time, and causes irreversible cell damage [75]. Figures 4.22 (a) (front view) and 4.22 (b) (top view) show the geometry of the temperature notation points along the edge of the tumor with a microwave power of 15 W. The temperature rise curve in all the cases follows a similar trend with high value near the slot and gradually reduces as the distance from the slot increases. Figure 4.23 (a) shows the temperature rise at points 1, 2, 3 and 4 along the circular edge of the tumor for the fully deployed tine at 2.45 GHz. The temperature rise at points 1 and 2 is higher than at points 3 and 4, which indicates that the oval shaped ablation (tumor necrosis) region has occurred at points 1 and 2 only. Further, Fig. 4.23 (b) shows the temperature rise at points 1, 2, 3 and 4 along the circular edge of the tumor at 2.45 and 6 GHz. The temperature rises at point 1 near the tine at high-frequency (6 GHz) shows more than at point 2 near the tine at conventional frequency (2.45 GHz). High-frequency MWA leads to a large ablation region with more concentrated energy as compared to the tines operated with the conventional frequency. Lastly, Fig. 4.23 (c) describes the temperature rise at points 1, 2, 3 and 4 along the circular edge of the tumor for the fully deployed tines at 6 GHz. The temperature rise at all the points is higher as compared to the other two cases and additionally temperatures at points 1 and 2 are slightly higher due to the orientation of tine tips towards these points. Figure 4.23 (d) shows the variation in temperature over time for the tissue at point 1, when the trocar is operated at 2.45 and 6 GHz. The temperature rise is higher for the trocar operated at 6 GHz than the trocar operated at 2.45 GHz.

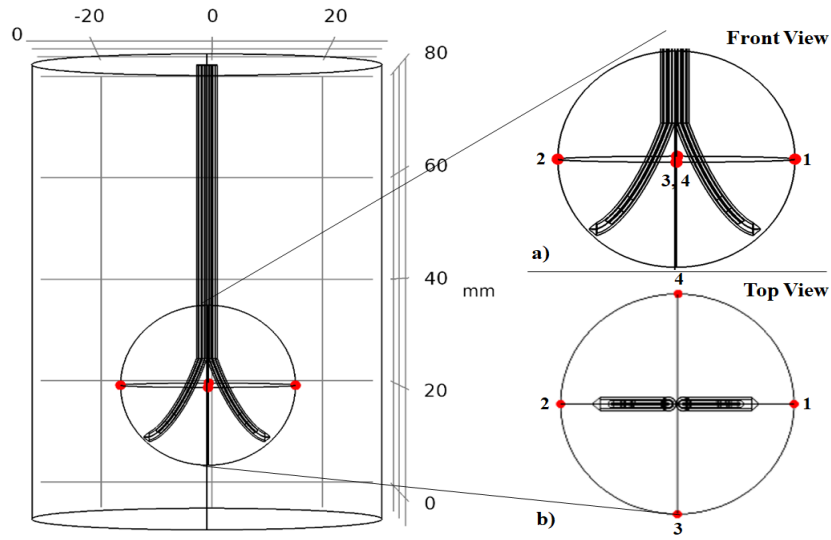


Figure 4.22 Temperature distribution points at the radial edge of the tumor. (a) Positions of the temperature monitoring points (front view). (b) Positions of the temperature monitoring points (top view).

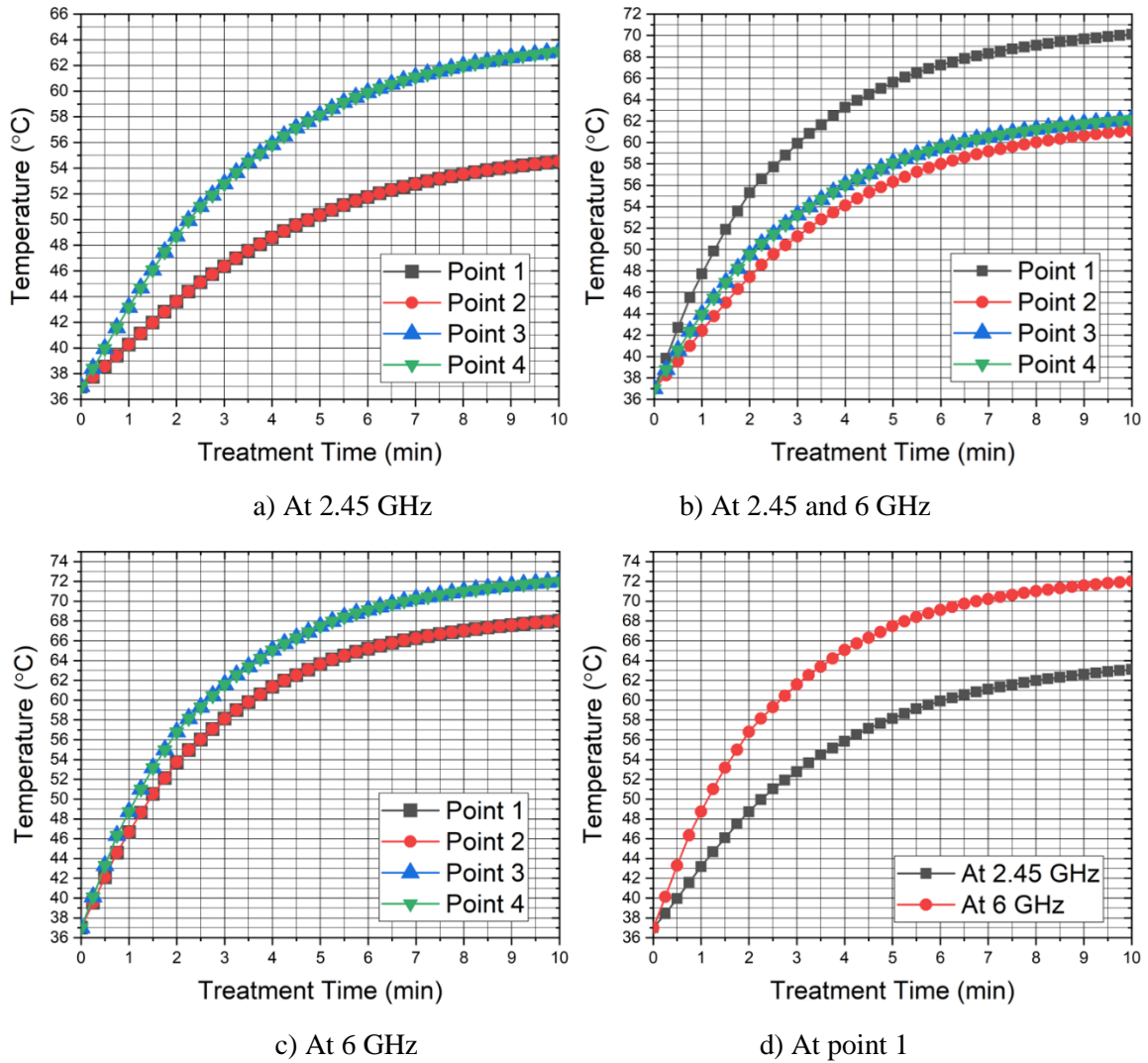


Figure 4.23 Variation of temperature with time near the tumor edge for fully deployed tines: (a) At 2.45 GHz (both tines), (b) At 2.45 (left-side tine) and 6 GHz (right-side tine), (c) At 6 GHz (both tines) and (d) At point 1.

The potential to develop unique medical applicators based on the precise target margin or specific ablation region will help in better curative treatment modalities. Figures 4.24 and 4.25 illustrate the simulation results of the ablation regions (using the first order Arrhenius rate equation) obtained during MWA on the tumor embedded in the hepatic gland. The Arrhenius rate equation will consider a damage integral of $\Omega = 1$ corresponds to 63% percent probability of cell death. Once the trocar is duly inserted into the tumor, both the tines can be fully deployed, as illustrated in Figs. 4.24 and 4.25. Further, Fig. 4.24 (front view) and Fig. 4.25 (top view) demonstrate the extent of ablation region obtained during MWA of hepatocellular carcinoma. The frequency of the supplied energy has been varied among the tines to obtain various ablation regions. Figures 4.24 and 4.25 represent the ablation region obtained by a fully deployed trocar supplied with energy at different combinations of frequencies at 15 W for 10 minutes: (a) 2.45 GHz (both tines), (b) 2.45 GHz (left-side tine) and 6 GHz (right-side tine), (c) 6 GHz (both tines).

It can be seen from Fig. 4.24 that, the ablation region obtained by the novel MWA trocar with energy supplied at 2.45 GHz frequency is of a teardrop shape and caused more collateral damage to the tissue indiscriminately. The addition of cooling system to the trocar, for this case, reduces the collateral damage occurring due to backward heating. Additionally, cooling system improves the efficiency in terms of obtaining a spherical ablation region [74]. It can be seen from Fig. 4.24 (b) that, an irregular shaped ablation region has been obtained for case (b). The irregularity in the ablation region is attributed to variation in the frequencies at which the energy is supplied to both the tines. The ablation region is a combination of spherical and teardrop shaped ablation regions. Further, it can be seen from Fig. 4.24 (c) that a spherical shaped ablation region with larger ablation volume has been obtained.

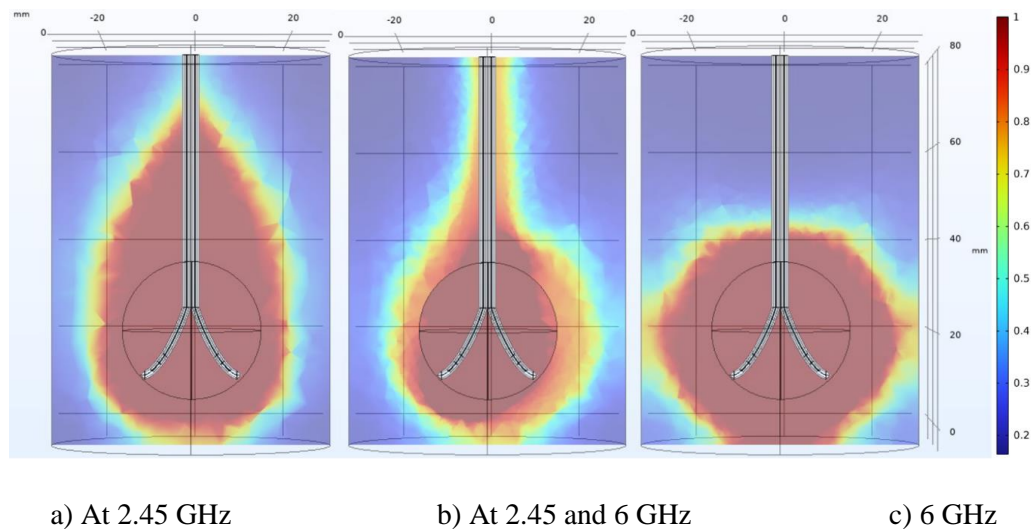


Figure 4.24 Ablation regions (front view) obtained by MWA using first order Arrhenius rate equation for fully deployed tines operated at 2.45 and 6 GHz for 15 W microwave power.

Therefore, it can be construed that the present trocar is 2-3 times more efficient in obtaining the extent of ablation of 3.5 cm than the existing non-cooled trocars with the extent of ablation of 1.85 cm [65] in terms of obtaining larger ablation volumes. Additionally, backward heating problem has been minimized with time at high-frequency time (6 GHz) as compared to the existing conventional frequency time (2.45 GHz).

By developing novel trocars and treatment planning system with better optimization characteristics, larger size tumors (> 4 cm) can also be effectively treated by MWA techniques. The top view of the ablation margin obtained during MWA of HCC using novel trocar has been shown in Fig. 4.25. An incomplete ablation of tumor (oculiform) has been achieved with the novel trocar operated at 2.45 GHz on both the tines. An asymmetric ablation region of the broad ovate shaped ablation region has been achieved when the trocar is supplied with energy at 2.45 GHz and 6 GHz on first and second tines, respectively. The tines supplied with energy at high frequency leads to an increase in the ablation region as compared to the tines operated at conventional frequencies (915 MHz or 2.45 GHz). Further, the high-frequency microwave ablation (6 GHz) leads to a more concentrated ablation region.

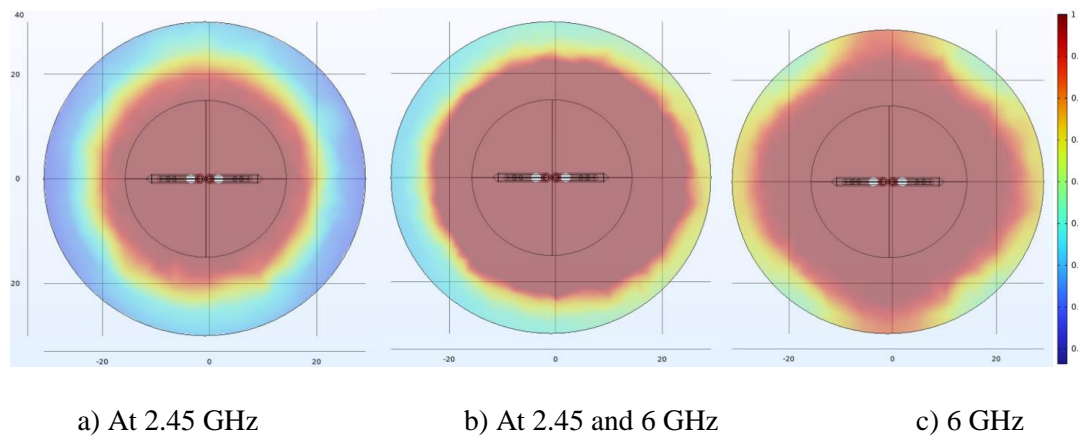


Figure 4.25 Ablation regions (top view) obtained by MWA using first order Arrhenius rate equation for fully deployed tines operated at 2.45 and 6 GHz for 15 W microwave power.

The dimensions of the ablation margins obtained from the numerical simulations of 3 cm-in-diameter hepatocellular carcinomas have been tabulated in Table 4.8. The MWA at 6 GHz reveals optimal ablation characteristics with 6 cm radial-axial length of ablation margin as against 5.7 cm for 2.45 GHz (both tines) and 5.9 cm for 2.45 and 6 GHz combination. Also, the ablation margin of 5.9 cm \times 5.8 cm with the trocar operated at 2.45 and 6 GHz combination can be considered to be significant against the conventional microwave frequency (2.45 GHz). Finally, the ablation margin of 6 cm in the radial transverse direction obtained when the trocar has been operated at 6 GHz (both tines) is even significant for treating large size tumors as compared to the other two combinations.

Table 4.8: *Minimum diameter of the tumor to be ablated during MWA using fully deployed tines*

S. No	Operating frequencies of the trocars	Diameter of the Hepatic Tumor (cm)	Radial axial length of the ablation margin (cm)	Radial transverse length of the ablation margin (cm)	Axial length of ablation margin (cm)
1	2.45 GHz	3	5.7	5.1	7.3
2	2.45 GHz & 6 GHz	3	5.9	5.8	5.2
3	6 GHz	3	6	6	3.9

Case study 2: MWA of HCC using the novel trocar with fully deployed and semi deployed tines

Temperature distribution plays an essential role in analyzing the cell necrosis during thermal ablation therapies. Figures 4.26 (a) (front view) and 4.26 (b) (top view) show the simulation geometry of the temperature monitoring points on the tumor edge. Figure 4.27 (a) shows the temperature rise at points 1, 2, 3 and 4 along the tumor edge for semi and fully deployed tines supplied with energy at 2.45 GHz. The rise in temperature at point 1 is higher than at points 2, 3 and 4 indicating complete tissue necrosis occurred at point 1. This is because the fully deployed tine is pointing towards 1st point leading to more energy deposition surrounding it. Further, Fig. 4.27 (b) shows the temperature rise at points 1, 2, 3 and 4 along the tumor edge at 2.45 and 6 GHz. The fully deployed tine is supplied with energy at 6 GHz, followed by semi deployed tine at 2.45 GHz. The temperature rise at point 1 which is near to 1st tine (operated at 6 GHz) is higher as compared to the temperature rise at points 2, 3 and 4. Figure 4.27 (c) shows the temperature rise at points 1, 2, 3 and 4 along the tumor edge when the tines are operated at 6 (1st tine) and 2.45 GHz (2nd tine) frequencies. The fully deployed tine has been supplied with energy at 2.45 GHz, followed by semi deployed tine at 6 GHz. The temperature rise at all the points follow a similar trend with a slight variation in the values. This is because the energy radiated into the tissue by the fully deployed tine operated at 2.45 GHz is becoming equal to the energy radiated by the semi deployed tine operated at 6 GHz. The rise in temperature at all points when both the tine are operated at 6 GHz has been shown in Fig. 4.27 (d). It can be seen that similar trend has been noticed with an exception that, the temperature rise at points 1 and 2 along the orientation of the tine are higher than the temperature rise at points 3 and 4. Figure 4.27 (e) shows the variation of temperature with time for the tissue at point 1, when the trocar is operated at 2.45 and 6 GHz. The ablation temperature is achieved within 2 minutes 30 seconds of treatment when the trocar is operated at 6 GHz, while it is 8 minutes when the trocar is operated at 2.45 GHz at point 1. This is due to the fact that the tumor shows better energy absorption properties at higher microwave frequency.

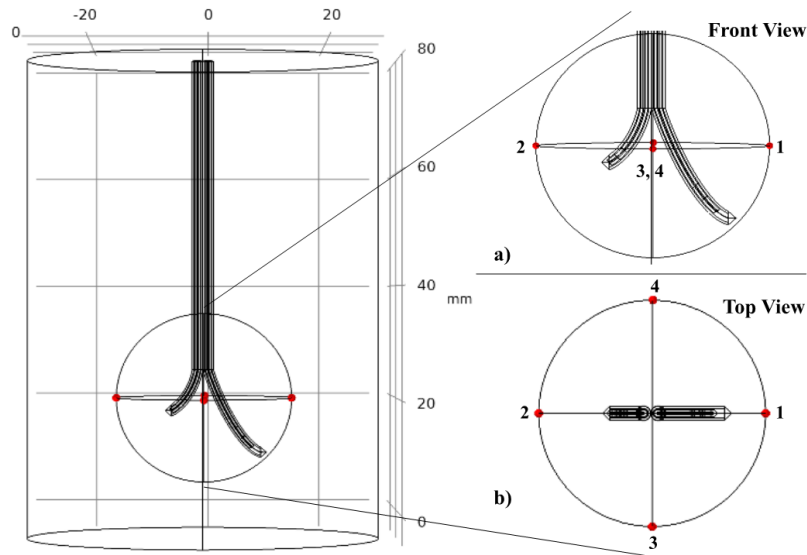
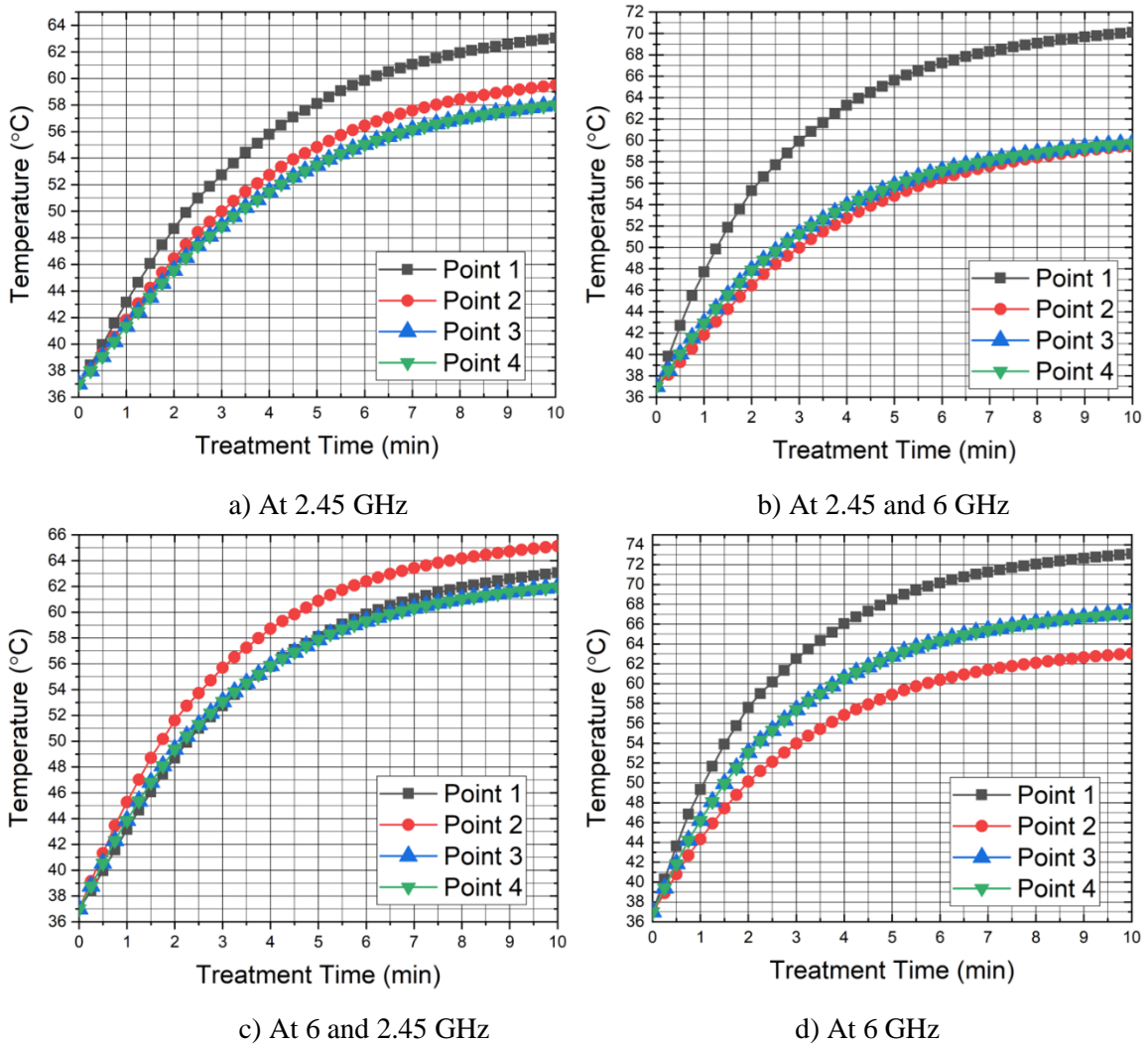
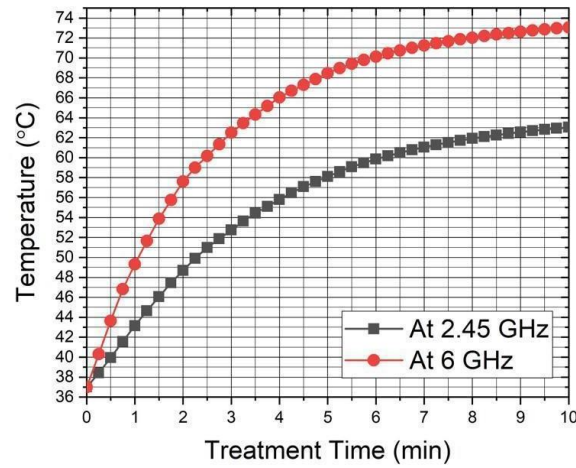


Figure 4.26 Temperature distribution points at the radial edge of the tumor. (a) positions of the temperature monitoring points (front view). (b) positions of the temperature monitoring points (top view).





e) At point 1

Figure 4.27 Temperature rise with time near the edge of the tumor for semi and fully deployed tines operated at: (a) 2.45 GHz (both tines), (b) 2.45 GHz (left-side tine) and 6 GHz (right-side tine), (c) 6 GHz (left-side tine) and 2.45 GHz (right-side tine), (d) 6 GHz (both tines) and (e) At point 1.

The novel trocar has been inserted into the tissue in such a way that one tine is fully deployed and the other tine is semi deployed, as shown in Figs. 4.28 (front view) and 4.29 (top view). Figures 4.28 and 4.29 show the ablation regions obtained by a fully deployed and semi deployed tines with energy supplied at different combinations of frequencies at 15 W for 10 minutes: a) 2.45 GHz (both tines), b) 2.45 GHz (left tine) and 6 GHz (right tine), c) 6 GHz (left tine) and 2.45 GHz (right tine), and d) 6 GHz (both tines).

It can be seen from Fig. 4.28 (a) that, the ablation region obtained is of teardrop shape with more ablation region towards the fully deployed tine. At this frequency (2.45 GHz), MWA causes backward heating of the trocar and hence collateral damage to the healthy tissue along the length of the trocar occurs. An addition of cooling system is required in order to overcome the backward heating of the trocar [74]. Further, variation of frequencies at which energy supplied to the tines leads to irregular or axisymmetric ablation regions. It can be seen from Fig. 4.28 (b) that a nearly spherical ablation region with less collateral damage to the trocar has been achieved for case (b). However, an irregular and asymmetric ablation region has been achieved for case (c). Also, it can be seen from Fig. 4.28 (c) that a large size shaped ablation region with more back heating of the trocar has been achieved. It is due to the fact that, the change in deploying length of the tine does not show the effect on the energy radiated into the tissue at higher frequency (6 GHz). To limit the amount of energy into the tissue at higher frequency MWA, the power of the supplied energy has to be reduced as compared to the power supplied at the conventional frequency [76]. Further, an oval-shaped ablation region has been achieved for case (d). From the results, it can be concluded that the tines operated at

high frequency (6 GHz) do less collateral damage to the tissue than those operated at conventional frequencies (2.45 GHz).

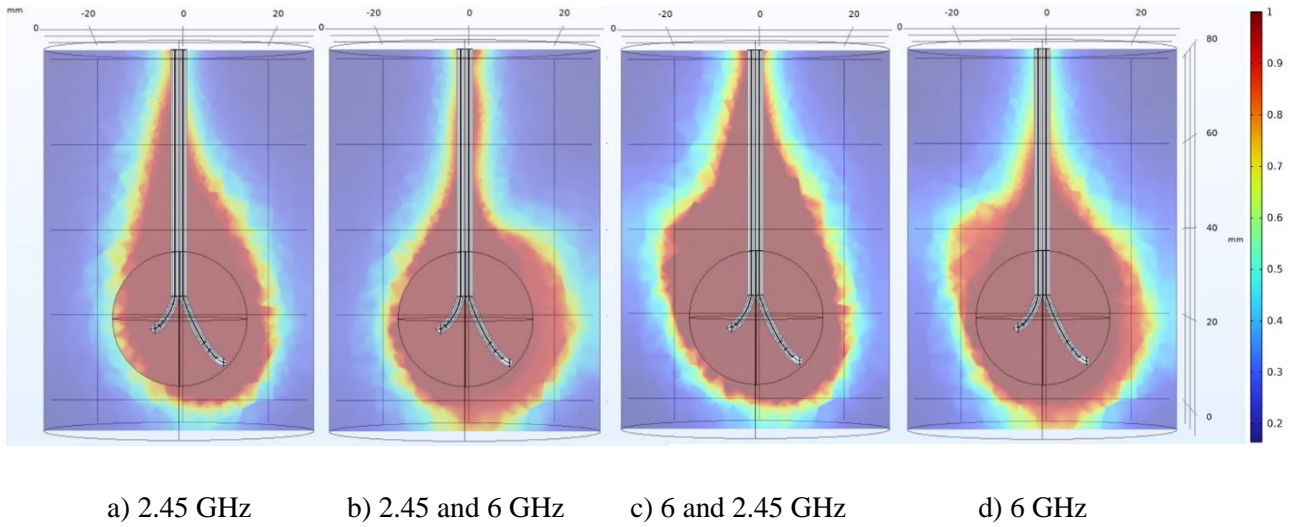


Figure 4.28 Ablation regions (front view) obtained by MWA using first order Arrhenius rate equation for fully (1st) deployed and semi (2nd) deployed tines operated at 2.45 and 6 GHz for 15 W microwave power.

The top view of the ablation region has been shown in Fig. 4.29. Please note that, 1st tine is semi deployed and 2nd tine is fully deployed. An incomplete tumor ablation region of elliptical shape has been achieved when both the tines are operated at 2.45 GHz (see Fig. 4.29 (a)). Further, it can be seen from Fig. 4.29 (b) that an irregular and incomplete tumor ablation region (ovate shape) has been achieved when the tines are operated at 2.45 GHz (1st tine) and 6 GHz (2nd tine) frequencies. A broad ovate shaped ablation region (complete tumor ablation) has been achieved (see Fig. 4.29 (c)) when the tines are operated at 6 GHz (1st tine) and 2.45 GHz (2nd tine). Finally, both the tines operated at 6 GHz leads to a much spherical shaped large ablation region as compared to the earlier cases.

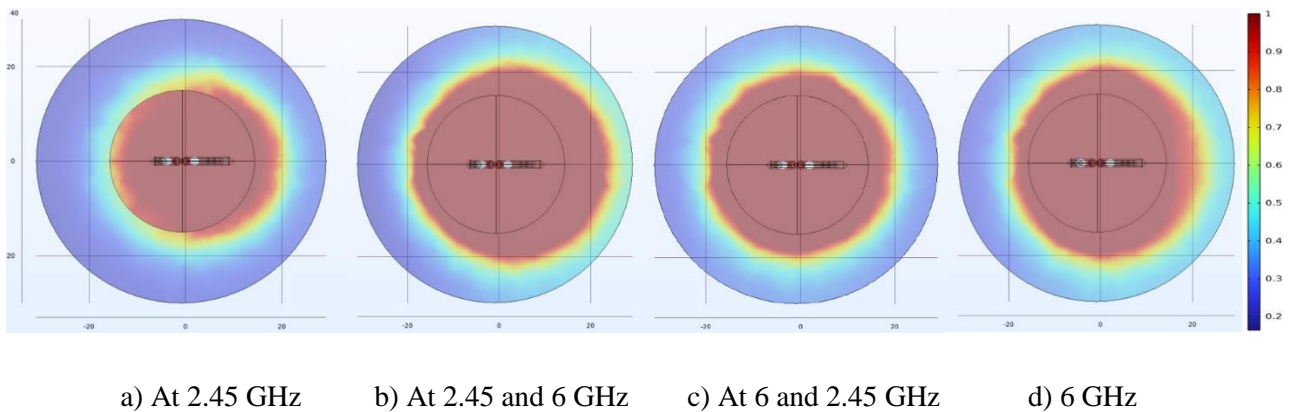


Figure 4.29 Ablation regions (top view) obtained by MWA using first order Arrhenius rate equation for fully (1st) deployed and semi (2nd) deployed tines operated at 2.45 and 6 GHz for 15 W microwave power.

The minimum diameter of the tumor ablated and its corresponding dimensions of the ablation boundary have been provided in Table 4.9. The MWA at 6 GHz reveals optimal ablation characteristics with 6 cm radial-axial length of ablation margin as against 4.4 cm of 2.45 GHz, 4.6 cm for 2.45/6 and 5.3 for 6/2.45 GHz frequency combinations. The trocar operated at 2.45 and 6 GHz combination is considered to be more significant than both the tines operated at 2.45 GHz frequency (ablation margin of $4.9 \text{ cm} \times 5.3 \text{ cm} \pm 0.1 \text{ cm}$). Further, it can be seen from Table 4.9 that both tines operated at 6 GHz has produced an ablation margin of 3.2 cm which can be considered to be more advantageous against all the said combinations. From the results, it can be concluded that by reducing the deploying length of the tine, the ablation region can also be reduced, making the novel trocar suitable for treating 4.4 to 5.8 cm diameter tumors of spherical and irregular shapes.

Table 4.9: *Minimum diameter of the tumor to be ablated during MWA of semi and fully deployed tines*

S. No	Tines operating frequencies	Diameter of the Hepatic Tumor (cm)	Radial axial length of ablation margin (cm)	Radial transverse length of ablation margin (cm)	Axial ablation margin (cm)
1	2.45 GHz	3	4.1	4.4	6.5
2	2.45 GHz & 6 GHz	3	5.9	5.2	4.2
3	6 GHz & 2.45 GHz	3	5.9	5.3	6.2
4	6 GHz	3	6	5.8	4.2

Case study 3: MWA of HCC using the novel trocar with semi deployed tines

Figures 4.30 (a) (front view) and 4.31 (b) (top view) depicts the computational geometry of the tumor embedded hepatic gland with temperature study points on the tumor edge. The rise in temperature at all the four points of the tumor edge have been shown in Fig. 4.31 (a) for the case of 2.45 GHz (both tines). The temperature rise at points 1 and 2 are higher than at points 3 and 4, indicating oval shaped ablation region. The maximum temperature obtained at all the points is less than 60°C and hence a case of incomplete tissue necrosis. Figure 4.31 (b) shows the temperature rise at all four points (1, 2, 3 and 4) when the tines are maintained at 2.45 GHz (1st tine) and 6 GHz (2nd tine). The temperature rise at point 1 (6 GHz) is more than the temperature rise at point 2 (2.45 GHz). The penetration depth of waves into the tissue is less at 6 GHz as compared to the tine at 2.45 GHz frequency making high energy deposition in smaller regions. This leads to generation of larger spherical ablation region at higher temperatures. Further, Fig. 4.31 (c) describes the temperature rise at points 1, 2, 3 and 4 along the circular edge of the tumor for the semi deployed tines operating at 6 GHz. The temperature rise at all the points is nearly identical with slightly higher temperature points 1 and 2 in line with the tine tips than at points 3 and 4. Figure 4.31 (d) shows the variation of

temperature with time for the tissue at point 1, when the trocar is operated at 2.45 and 6 GHz. The maximum value of temperature rise is obtained for trocar operated at 6 GHz rather than with 2.45 GHz.

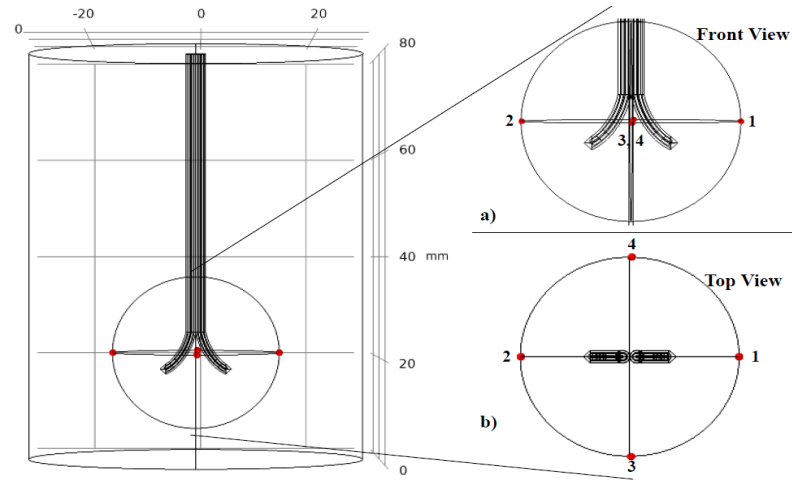


Figure 4.30 Temperature distribution points on the radial edge of the tumor. (a) positions of the temperature monitoring points (front view). (b) positions of the temperature monitoring points (top view).

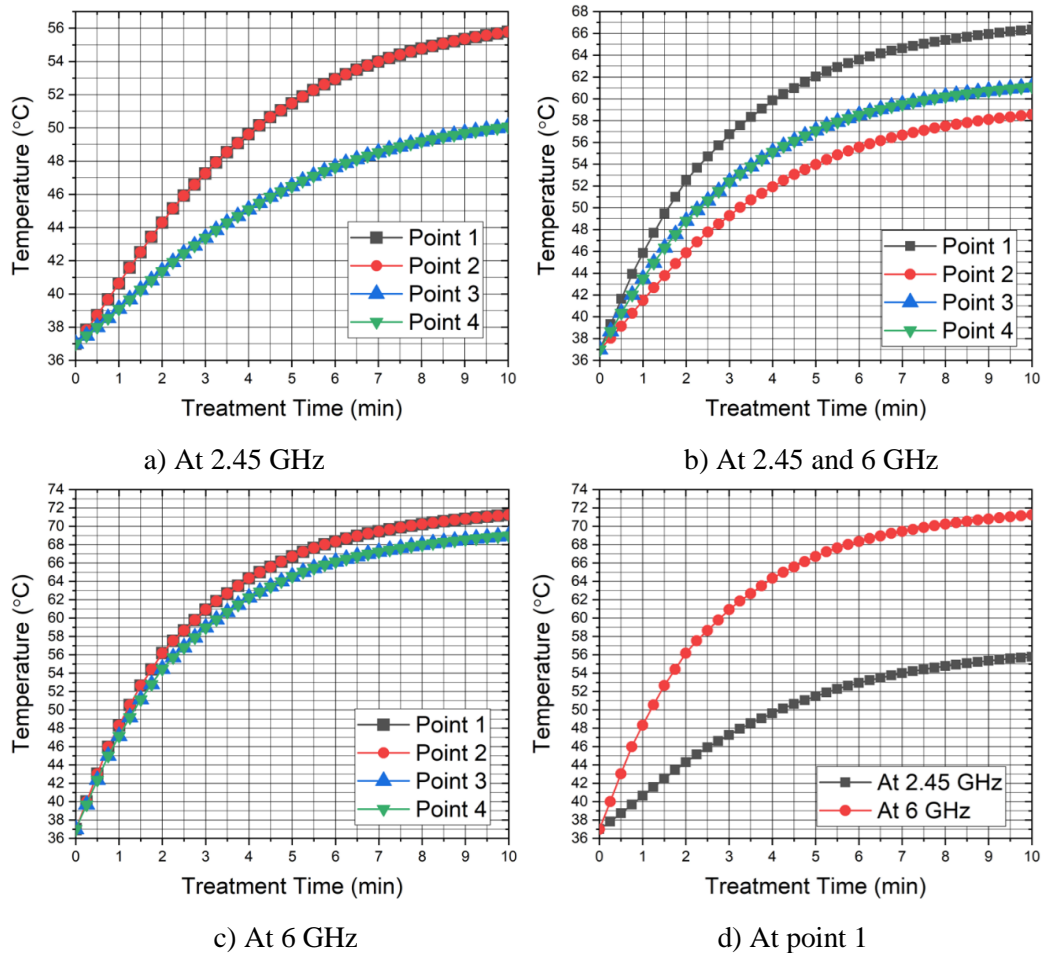
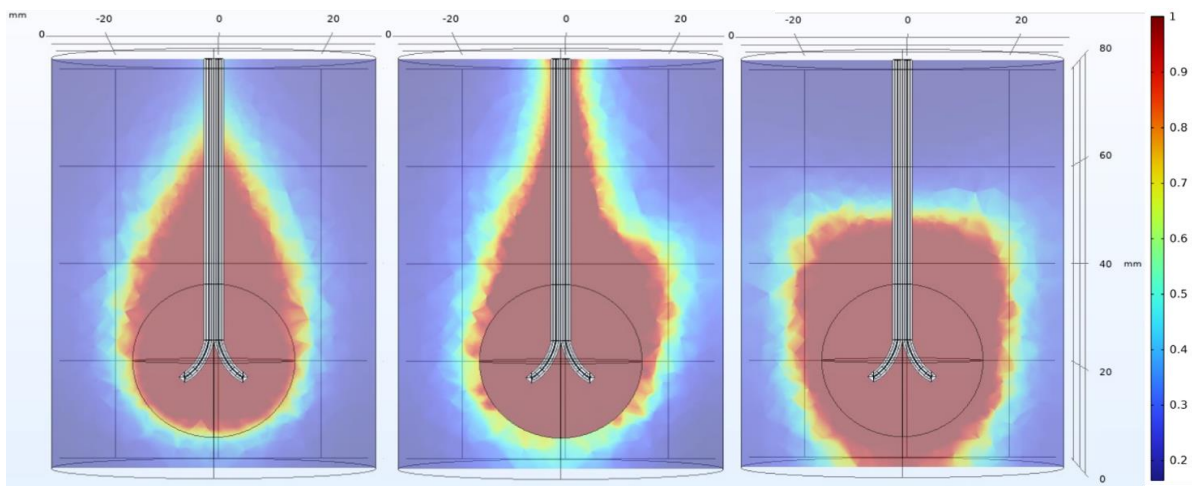


Figure 4.31 Temperature rise with time at four points near the edge of the tumor for semi-deployed tines operated at: (a) 2.45 GHz (both tines), (b) 2.45 GHz (left-side tine) and 6 GHz (right-side tine), (c) 6 GHz (both tines) and (d) At point 1.

In this section, the case of both tines deployed partially (semi) has been considered, as shown in Figs. 4.32 and 4.33. Further, the front view and the top view of the ablation regions have been shown in Fig. 4.32 and Fig. 4.33, respectively. The combination of frequencies considered have been: (a) 2.45 GHz (both tines), (b) 2.45 GHz (left tine) and 6 GHz (right tine), (c) 6 GHz (both tines) at 15 W for 10 minutes.

It can be seen from Fig. 4.32 (a) that, a teardrop-shaped incomplete tumor ablation region has been obtained with the tine operated at 2.45 GHz, and caused more damage to the healthy tissue. An asymmetrical ablation pattern has been attained by the novel trocar when the energy supplied has been to the tines at different frequencies (2.45 and 6 GHz), as can be seen from Fig. 4.32 (b). It can be further seen that backward heating is more prominent when the 1st tine has been operated at 2.45 GHz. The backward heating problem can be sorted out by deploying cool tip tines [74]. Finally, a larger ablation volume can be achieved when both the tines are operated at 6 GHz frequency (see Fig. 4.32 (c)).



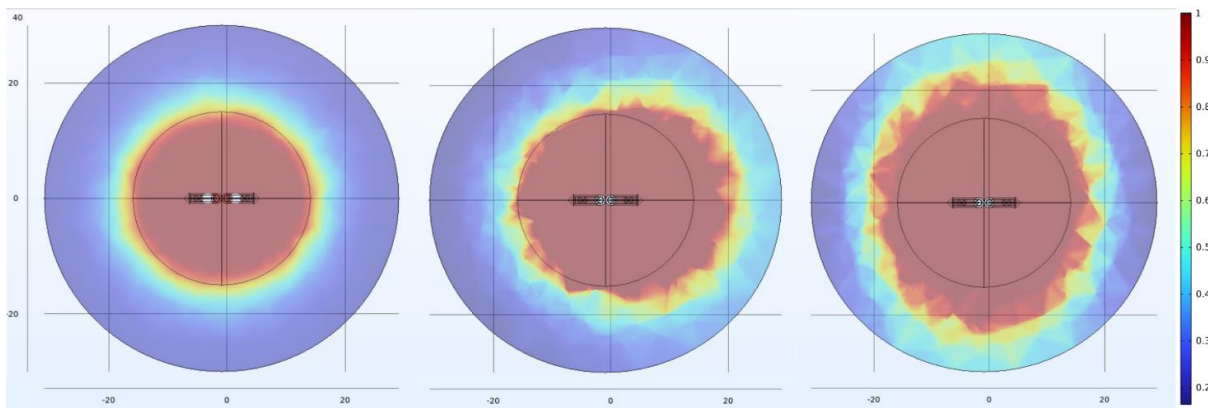
a) At 2.45 GHz

b) At 2.45 and 6 GHz

c) At 6 GHz

Figure 4.32 Ablation regions (front view) obtained by MWA using first order Arrhenius rate equation for semi deployed tines operated at 2.45 and 6 GHz for 15 W microwave power.

The top view of the ablation regions has been shown in Fig. 4.33. An elliptical shaped ablation region of incomplete tumor ablation can be seen from Fig. 4.33 (a) when the trocar has been supplied with energy at 2.45 GHz (both tines). A broad oval-shaped ablation region has been achieved when the tines are operated at 2.45 GHz (left-side tine) and 6 GHz (right-side tine), as can be seen from Fig. 4.33 (b). Further, it can be seen from Fig. 4.33 (c) that a spherical-shaped ablation region with complete tumor ablation has been obtained when the tines are operated at 6 GHz frequency.



a) At 2.45 GHz

b) At 2.45 and 6 GHz

c) At 6 GHz

Figure 4.33 Ablation regions (top view) obtained by MWA using first order Arrhenius rate equation for semi deployed tines operated at 2.45 and 6 GHz for 15 W microwave power.

Ablation margins (radial-axial and transverse lengths) obtained in case study 3 (semi deployed tines) have been detailed in Table 4.10. The details of ablation margins (4.2 to 5.5 cm-in-diameter tumor) obtained in the radial axial direction when both the tines have been supplied with energy at various combinations of frequencies (2.45 and 6 GHz) have been presented. Further, it is evident from the data given in Table 4.10 that, the optimal ablation region with ablation margins of 5.5 cm \times 6 cm diameter has been obtained when both the tines have been operated at 6 GHz frequency. It can be concluded from the results that MWA using a novel trocar at 2.45 GHz (both tines) is suitable for ablating smaller diameter tumors, i.e., tumors having diameter less than 3 cm.

The results suggest that the novel trocar is suitable for treating small-sized tumors of 3 cm diameter tumors having spherical and irregular shape. Further, with variation in the microwave power and ablation time, the novel trocar will be able to treat tumors less than 2 cm in diameter, making it suitable for treating tumors of all-sizes.

Table 4.10: *Minimum diameter of the tumor to be ablated during MWA using semi deployed tines*

S. No	Tines operating frequencies	Diameter of the Hepatic Tumor (cm)	Radial axial length of ablation margin (cm)	Radial transverse length of ablation margin (cm)	Axial ablation margin (cm)
1	2.45 GHz	3	4.2	4.2	6
2	2.45 GHz & 6 GHz	3	4.5	4.4	6.2
3	6 GHz	3	6	5.5	6.3

Hepatic gland Tissue Contraction during Microwave Ablation Procedure

The tissue deformation for a new design trocar for three deploying conditions of the tine has been presented in Fig. 4.34.

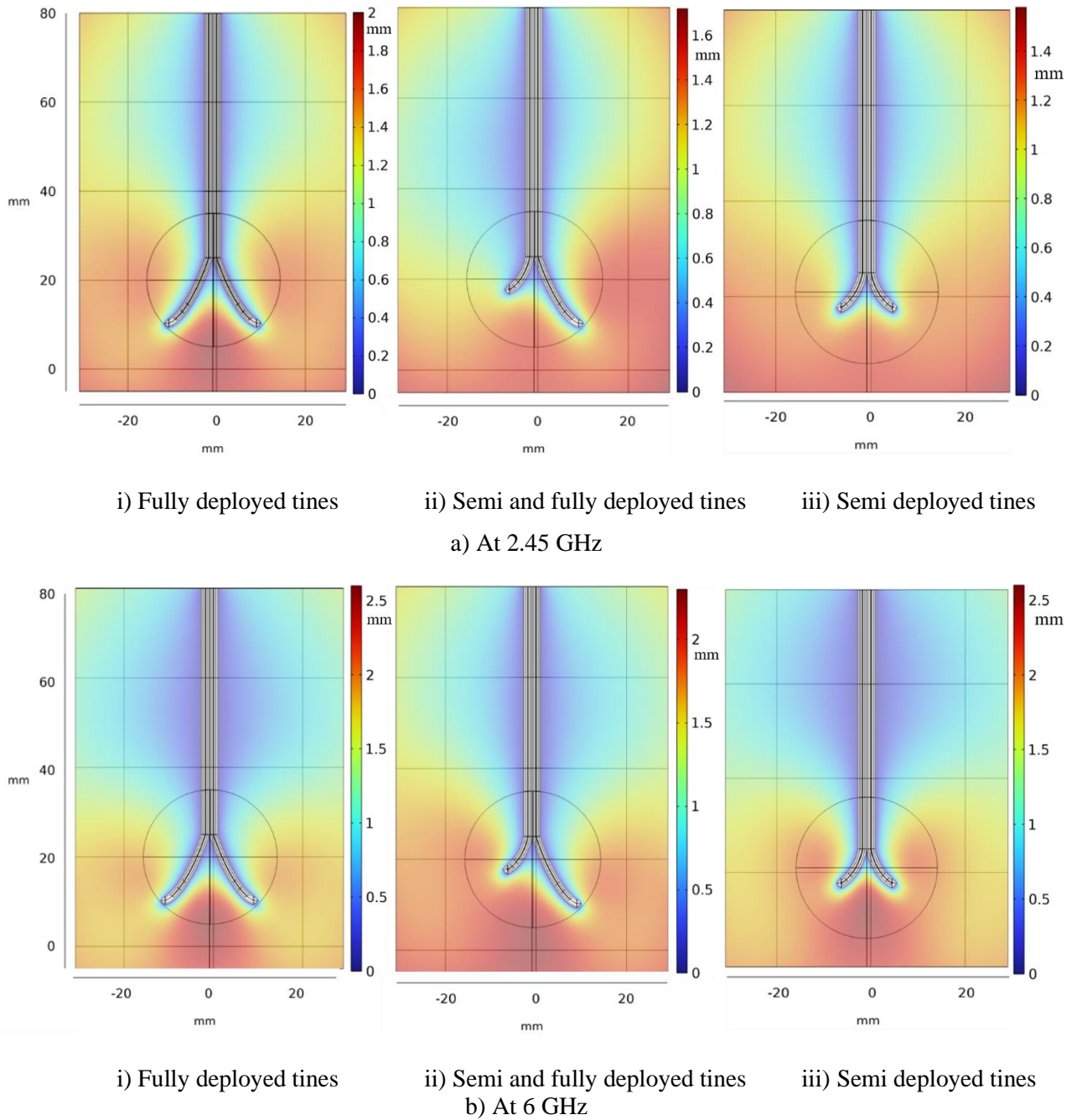


Figure 4.34 Tissue contraction obtained during MWA for three deploying conditions of the tine operated at a) 2.45 and b) 6 GHz for 15 W microwave power

Figure 4.34 shows that the maximum amount of tissue displacement (contraction) occurs near the trocar. This is due to the fact that tissue contraction is directly proportional to the rise in the temperature, which is maximum near the trocar. The tissue shrinkage is more during MWA at 6 GHz frequency as compared to 2.45 GHz frequency. The tissue

contraction near the tumor region at 2.45 GHz is 1.6 mm (see Fig. 4.34 (a) (i)). This is followed by 2 mm (see Fig. 4.34 (b) (i)) for the trocar operated at 6 GHz for fully deployed tines conditions. Similarly, the tissue contraction is 1.3 mm at 2.45 GHz and 2 mm at 6 GHz for semi-deployed tines (see Figs. 4.34 (a) (iii) and Fig. 4.34 (b) (iii)), respectively. From Figs. 4.34 (a) (ii) and 4.34 (b) (iii), it can be seen that the tissue deformation is more towards the fully deployed tine than the semi-deployed tine. It can be concluded from these results that the tissue contraction is more with high operating microwave energy frequency and is located within the concentrated region. By taking the account of tissue contraction, the actual extent of ablation will further increase by 1 to 2 mm than the actual extent.

Discussion:

This study presents a design theory for a MWA trocar used in the field of hyperthermia. The proposed trocar consists of a flexible dual tine that can be deployed independently and supplied with energy at 2.45/6 GHz. The current design is expected to address the problems associated with inappropriate positioning of the trocar into the tissue (Fig. 3.13). This is one of the major problems encountered in clinical practice during MWA. Once the trocar is inserted into the tumour, both the tines can be deployed based on the target region and the ablation volume to be achieved. Further, the frequency of the supplied energy (2.45 and 6 GHz) can be varied among the tines. In the present study, we have considered three deploying conditions of the tines of a trocar: i) both are fully deployed, ii) one is fully deployed and other one is semi-deployed, and iii) both are semi-deployed (Figs. 4.25, 4.29 and 4.33). For an ablation duration of 10 minutes with constant input power of 15 W at 2.45/6 GHz the fully deployed trocar gives a maximum ablation region of 4 cm to 3.3 cm in diameter (Figs. 4.25 and 4.26 and Table 4.8). Backward heating was generally lowest when the trocar was operated at 6 GHz, compared to 2.45 GHz.

Further, variation in frequency among the tines results in obtaining regular and irregular ablation regions. The MWA at 6 GHz frequency results in a spherical ablation region (Fig. 4.26). The deployment of the trocar tines can be varied between fully and partially deployed conditions. Figures 4.29 and 4.30 show the ablation regions obtained by fully deployed and semi deployed tines with energy supplied at different combinations of frequencies. The variation in the deployment length of the tine into the tissue results in obtaining irregular ablation areas. An asymmetrical ablation pattern has been achieved by the trocar when energy has been supplied to the tines at different frequencies (2.45 and 6 GHz). The trocar operated at 2.45 and 6 GHz combination is considered more significant than the tines operated at 2.45 GHz frequency (Figs. 4.29 and 4.30). The proposed trocar is also suitable for treating small-sized tumors of 2.5 cm in diameter, with a spherical or irregular shape under semi-deployed tines conditions (Figs. 16 and 17). Further, it can be

seen from Table 4.9 that both tines operated at 6 GHz have produced an ablation extent of 3.2 cm which can be considered to be more advantageous against all the said combinations.

In addition, estimating the extent of tissue contraction, which is evident during MWA, helps in predicting the actual ablation region. The tissue contraction is directly proportional to the increase in temperature during microwave ablation. The tissue deformation obtained using the proposed trocar design for three deploying conditions of the tine has been presented in Fig. 4.35. The maximum amount of tissue displacement (contraction) occurs near the trocar. The tissue shrinkage is greater at 6 GHz frequency when using MWA than it is at 2.45 GHz frequency, and it is located within the concentrated region. Further, the extent of ablation will increase by 1 to 2 mm more than the actual extent when tissue contraction is taken into account.

Advantages

From the proposed trocar, deploying length of the flexible tine will be varied as per the requirement of the ablation region. It overcomes the problem associated with the inapt positioning of the trocar into the tissue. The proposed trocar can replace the use of multiple trocars in treating large-size tumors. Further, the trocar operating conditions can be varied based on the tumor shape, nearby blood vessel presence, and the trocar's precise insertion. The power and ablation time of the trocar can be varied along with the frequencies to achieve different ablation regions.

Limitations

The present study considered multiple MWA trocars operated at 2.45 GHz and 6 GHz energy frequency with 15 W microwave input power. Further, the studies can be expanded by considering the impact of power and ablation time at different energy frequencies on the ablation outcome. Further modifications to the numerically developed antenna, viz., addition of a cooling system, wave reflectors, multiple slots, and external graphene coating to enhance the ablation volume characteristics, are needed. To optimize the computational modelling, the present study does not include structural changes in the tissues. Further, the present design is not suitable for small tumors (< 2cm) due to increased diameter of the trocar. There will be an increase in the operational procedure by using novel trocar since the working parameters will be decided after the trocar is placed into the tissue. The major limitation of the present study is the lack of experimental validation of the trocar that can operate at 6 GHz frequency which is not available in the market for clinical applications.

Summary/ Conclusions

The highest values of the ablation region have been observed for the liver, colon metastatic liver and breast cancerous tissues as compared with other organs at the same operating conditions. The positioning of the trocar is more important for the breast, liver, and kidney, as they produce a more rapid zone of heating in a shorter span of time. The present study may create a new path in the ablation of large tumors with multiple trocars of all shapes by sparing healthy tissue. This study may help in overcoming the problems associated with the inapt positioning of the trocar and undesired ablation region, and establishes a better treatment planning system for treating large-size tumors. Non-parallel trocar insertion with a variation of energy frequencies, power and ablation time results in ablating tumors irrespective of their shape, location and apt trocar positioning.

A numerical analysis of the performance of novel MWA trocar has been presented in this article. The trocar consists of a dual tine antenna with energy supplied to the tines at equal/ different frequencies (viz., 2.45 GHz and 6 GHz). The trocar operating condition can be varied based on the tumor shape, nearby blood vessel presence, and the trocar's precise insertion. It can replace the use of multiple trocars in treating large-size tumors. The novel trocar at high frequency (viz., 6 GHz) on both the tines leads to a sizeable spherical ablation region (i.e., 3 cm diameter tumors) with less treatment time (4 min), and the ablation region can be further enhanced to 4.5 cm in diameter by the addition of cooling system. Irregularly shaped ablation region can also be achieved by operating both tines at different frequencies. Further, the power and ablation time can be varied along with the frequencies to achieve different ablation regions. The findings that have been presented suggest that novel MWA trocar can be used to obtain enhanced tumor ablation volume, which is one of the major criteria for the treatment planning system.

Future Scope

The future scope of the thesis can be expanded in several directions to enhance the applicability and effectiveness of the dual tine dual frequency trocar for clinical applications.

1. **Practical Manufacturing:** The research can delve deeper into the practical aspects of manufacturing the dual tine dual frequency trocar. This could involve researching cost-effective materials, efficient production processes, and quality control measures to ensure its widespread availability for clinical use.
2. **Integrate Cooling System:** A promising avenue for research is the integration of a cooling system within the trocar. Investigate how cooling mechanisms, such as liquid or air cooling,

can be incorporated to improve the trocar's performance, particularly in terms of reducing tissue damage and enhancing precision during ablation.

3. **Wave Reflectors:** Explore the design and implementation of wave reflectors within the trocar to optimize the propagation of microwave energy. Investigate how different reflector configurations can be used to shape and direct the energy for more effective tissue ablation.
4. **Multiple Slots:** Research the benefits and challenges associated with incorporating multiple slots within the trocar. Analyse how varying the number, size, and placement of slots can affect ablation volume and efficiency.
5. **External Graphene Coating:** Investigate the potential of external graphene coatings for the trocar. Explore how graphene's unique properties, such as high thermal conductivity and mechanical strength, can enhance the trocar's performance and longevity.
6. **6 GHz Frequency MWA Trocar:** This could be a groundbreaking direction for furthering the research work. Explore the feasibility of developing an internally cooled MWA trocar operating at 6 GHz frequency, which is currently not widely available for clinical practices. Investigate the advantages of this frequency range, such as deeper tissue penetration or reduced interference.
7. **Medical Imaging Integration:** Consider replacing the uniform numerical modeling with advanced medical imaging techniques. Explore how techniques like MRI, CT scans, or ultrasound can be used in conjunction with the trocar for real-time visualization and monitoring of the ablation process. This could significantly improve precision and safety during procedures.

References/Bibliography

- [1] M.J. Thun, J.O. DeLancey, M.M. Center, A. Jemal, E.M. Ward, The global burden of cancer: priorities for prevention, *Carcinogenesis*. 31 (2010) 100–110. <https://doi.org/10.1093/CARCIN/BGP263>.
- [2] H. Sung, J. Ferlay, R.L. Siegel, M. Laversanne, I. Soerjomataram, A. Jemal, F. Bray, Global Cancer Statistics 2020: GLOBOCAN Estimates of Incidence and Mortality Worldwide for 36 Cancers in 185 Countries, *CA Cancer J Clin*. 71 (2021) 209–249. <https://doi.org/10.3322/CAAC.21660>.
- [3] F. Bray, J. Ferlay, I. Soerjomataram, R.L. Siegel, L.A. Torre, A. Jemal, Global cancer statistics 2018: GLOBOCAN estimates of incidence and mortality worldwide for 36 cancers in 185 countries, *CA Cancer J Clin*. 68 (2018) 394–424. <https://doi.org/10.3322/caac.21492>.
- [4] H.G. Prigerson, Y. Bao, M.A. Shah, M. Elizabeth Paulk, T.W. LeBlanc, B.J. Schneider, M.M. Garrido, M. Carrington Reid, D.A. Berlin, K.B. Adelson, A.I. Neugut, P.K. Maclejewski, Chemotherapy Use, Performance Status, and Quality of Life at the End of Life, *JAMA Oncol*. 1 (2015) 778–784. <https://doi.org/10.1001/JAMAONCOL.2015.2378>.
- [5] M. Ge, H. Jiang, X. Huang, Y. Zhou, D. Zhi, G. Zhao, Y. Chen, L. Wang, B. Qiu, A multi-slot coaxial microwave antenna for liver tumor ablation, *Phys Med Biol*. 63 (2018). <https://doi.org/10.1088/1361-6560/AAD9C5>.
- [6] A.J. Gosalia, P. Martin, P.D. Jones, Advances and future directions in the treatment of hepatocellular carcinoma, *Gastroenterol Hepatol (N Y)*. 13 (2017).
- [7] A. Raza, G.K. Sood, Hepatocellular carcinoma review: Current treatment, and evidence-based medicine, *World J Gastroenterol*. 20 (2014) 4115–4127. <https://doi.org/10.3748/wjg.v20.i15.4115>.
- [8] C. Brace, Thermal tumor ablation in clinical use, *IEEE Pulse*. 2 (2011) 28–38. <https://doi.org/10.1109/MPUL.2011.942603>.
- [9] C.J. Diederich, Thermal ablation and high-temperature thermal therapy: Overview of technology and clinical implementation, in: *International Journal of Hyperthermia*, Int J Hyperthermia, 2005: pp. 745–753. <https://doi.org/10.1080/02656730500271692>.
- [10] R. V. Davalos, L.M. Mir, B. Rubinsky, Tissue Ablation with Irreversible Electroporation, *Annals of Biomedical Engineering* 2005 33:2. 33 (2005) 223–231. <https://doi.org/10.1007/S10439-005-8981-8>.
- [11] R. Nuccitelli, U. Pliquett, X. Chen, W. Ford, R. James Swanson, S.J. Beebe, J.F. Kolb, K.H. Schoenbach, Nanosecond pulsed electric fields cause melanomas to self-destruct, *Biochem Biophys Res Commun*. 343 (2006) 351–360. <https://doi.org/10.1016/J.BBRC.2006.02.181>.
- [12] S. Singh, R. Repaka, A. Al-Jumaily, Sensitivity analysis of critical parameters affecting the efficacy of microwave ablation using Taguchi method, *International Journal of RF and Microwave Computer-Aided Engineering*. 29 (2019) e21581. <https://doi.org/10.1002/mmce.21581>.
- [13] R. Ramanathan, R.J. Leveillee, Ablative therapies for renal tumors., *Ther Adv Urol*. 2 (2010) 51–68. <https://doi.org/10.1177/1756287210366708>.
- [14] M. Chaichanyut, S. Tungjitkusolmun, Microwave Ablation Using Four-Tine Antenna: Effects of Blood Flow Velocity, Vessel Location, and Total Displacement on Porous Hepatic Cancer Tissue, *Comput Math Methods Med*. 2016 (2016). <https://doi.org/10.1155/2016/4846738>.

- [15] H. Ren, E. Campos-Nanez, Z. Yaniv, F. Banovac, H. Abeledo, N. Hata, K. Cleary, Treatment planning and image guidance for radiofrequency ablation of large tumors, *IEEE J Biomed Health Inform.* 18 (2014) 920–928. <https://doi.org/10.1109/JBHI.2013.2287202>.
- [16] C.J. Simon, D.E. Dupuy, W.W. Mayo-Smith, Microwave Ablation: Principles and Applications1, <https://doi.org/10.1148/Rg.25si055501>. 25 (2005). <https://doi.org/10.1148/RG.25SI055501>.
- [17] R.A. Bercich, D.R. Duffy, P.P. Irazoqui, Far-field RF powering of implantable devices: Safety considerations, *IEEE Trans Biomed Eng.* 60 (2013) 2107–2112. <https://doi.org/10.1109/TBME.2013.2246787>.
- [18] WO2008044000A1 - Surgical antenna - Google Patents, (n.d.). <https://patents.google.com/patent/WO2008044000A1/en?q=WO2008%2f044000> (accessed September 5, 2023).
- [19] J. Cho, J. Yoon, S. Cho, K. Kwon, S. Lim, D. Kim, E.S. Lee, C.H. Kim, J.W. Choi, C. Cheon, Y. Kwon, In-vivo measurements of the dielectric properties of breast carcinoma xenografted on nude mice, *Int J Cancer.* 119 (2006) 593–598. <https://doi.org/10.1002/ijc.21896>.
- [20] M. Radmilović-Radjenović, M. Sabo, M. Prnova, L. Šoltes, B. Radjenović, Finite Element Analysis of the Microwave Ablation Method for Enhanced Lung Cancer Treatment, *Cancers* 2021, Vol. 13, Page 3500. 13 (2021) 3500. <https://doi.org/10.3390/CANCERS13143500>.
- [21] N. He, W. Wang, Z. Ji, C. Li, B. Huang, Microwave Ablation: An Experimental Comparative Study on Internally Cooled Antenna versus Non-internally Cooled Antenna in Liver Models, *Acad Radiol.* 17 (2010) 894–899. <https://doi.org/10.1016/J.ACRA.2010.03.005>.
- [22] O. Seror, Ablative therapies: Advantages and disadvantages of radiofrequency, cryotherapy, microwave and electroporation methods, or how to choose the right method for an individual patient?, *Diagn Interv Imaging.* 96 (2015) 617–624. <https://doi.org/10.1016/J.DIII.2015.04.007>.
- [23] C. Floridi, I. De Bernardi, F. Fontana, A. Muollo, • Anna, M. Ierardi, A. Agostini, P. Fonio, E. Squillaci, • Luca Brunese, C. Fugazzola, G. Carrafiello, Microwave ablation of renal tumors: state of the art and development trends, *VASCULAR AND INTERVENTIONAL RADIOLOGY.* (n.d.). <https://doi.org/10.1007/s11547-014-0426-8>.
- [24] X. Wu, B. Liu, B. Xu, Theoretical evaluation of high frequency microwave ablation applied in cancer therapy, *Appl Therm Eng.* 107 (2016) 501–507. <https://doi.org/10.1016/j.applthermaleng.2016.07.010>.
- [25] M. Kuang, M.D. Lu, X.Y. Xie, H.X. Xu, L.Q. Mo, G.J. Liu, Z.F. Xu, Y.L. Zheng, J.Y. Liang, Liver Cancer: Increased Microwave Delivery to Ablation Zone with Cooled-Shaft Antenna—Experimental and Clinical Studies1, <https://doi.org/10.1148/Radiol.2423052028>. 242 (2007) 914–924. <https://doi.org/10.1148/RADIOL.2423052028>.
- [26] A.Z. Ibitoye, T. Orotoye, E.O. Nwoye, M.A. Aweda, Analysis of efficiency of different antennas for microwave ablation using simulation and experimental methods, *Egyptian Journal of Basic and Applied Sciences.* 5 (2018) 24–30. <https://doi.org/10.1016/J.EJBAS.2018.01.005>.
- [27] J.X. Audet, J.C. Bolomey, C. Pichot, D.D. N'Guyen, M. Robillard, M. Chive, Y. Leroy, Electrical Characteristics of Waveguide Applicators for Medical Applications, <http://dx.doi.org/10.1080/16070658.1980.11689200>. 15 (2016) 177–186. <https://doi.org/10.1080/16070658.1980.11689200>.
- [28] S.S. Stuchly, M.A. Stuchly, MULTIMODE SQUARE WAVEGUIDE APPLICATORS FOR MEDICAL APPLICATIONS OF MICROWAVE POWER, (n.d.).

- [29] F. Izzo, V. Granata, R. Grassi, R. Fusco, R. Palaia, P. Delrio, G. Carrafiello, D. Azoulay, A. Petrillo, S.A. Curley, Radiofrequency Ablation and Microwave Ablation in Liver Tumors: An Update, (2019). <https://doi.org/10.1634/theoncologist.2018-0337>.
- [30] D. Liu, C.L. Brace, Numerical simulation of microwave ablation incorporating tissue contraction based on thermal dose, *Phys Med Biol.* 62 (2017) 2070–2086. <https://doi.org/10.1088/1361-6560/aa5de4>.
- [31] Z. Zhao, F. Wu, Minimally-invasive thermal ablation of early-stage breast cancer: A systemic review, *European Journal of Surgical Oncology.* 36 (2010) 1149–1155. <https://doi.org/10.1016/j.ejso.2010.09.012>.
- [32] T.J. Vogl, L.M. Basten, N.E.A. Nour-Eldin, B. Kaltenbach, B. Bodelle, J.L. Wichmann, H. Ackermann, N.N.N. Naguib, Evaluation of microwave ablation of liver malignancy with enabled constant spatial energy control to achieve a predictable spherical ablation zone, *International Journal of Hyperthermia.* 34 (2018) 492–500. <https://doi.org/10.1080/02656736.2017.1358408>.
- [33] M.G. Lubner, C.L. Brace, J.L. Hinshaw, F.T. Lee, Microwave Tumor Ablation: Mechanism of Action, Clinical Results and Devices How Microwave Ablation works, (2010). <https://doi.org/10.1016/j.jvir.2010.04.007>.
- [34] G.D. Dodd, M.S. Frank, M. Aribandi, S. Chopra, K.N. Chintapalli, Radiofrequency Thermal Ablation, <http://dx.doi.org/10.2214/Ajr.177.4.1770777>. 177 (2012) 777–782. <https://doi.org/10.2214/AJR.177.4.1770777>.
- [35] H.H. Pennes, Analysis of Tissue and Arterial Blood Temperatures in the Resting Human Forearm, <https://doi.org/10.1152/Jappl.1948.1.2.93>. 1 (1948) 93–122. <https://doi.org/10.1152/JAPPL.1948.1.2.93>.
- [36] F.C. HENRIQUES, Studies of thermal injury; the predictability and the significance of thermally induced rate processes leading to irreversible epidermal injury., *Arch Pathol (Chic).* 43 (1947) 489–502. <https://europepmc.org/article/med/20243514> (accessed April 4, 2022).
- [37] N. Salas, Jr., F. Manns, J.-M.A. Parel, P.J. Milne, D.B. Denham, D.S. Robinson, Predictions of tissue denaturation during experimental laser interstitial thermotherapy for breast tumors, in: *Lasers in Surgery: Advanced Characterization, Therapeutics, and Systems XIII*, SPIE, 2003: p. 444. <https://doi.org/10.1117/12.485165>.
- [38] J. Sebek, S. Curto, R. Bortel, P. Prakash, Analysis of minimally invasive directional antennas for microwave tissue ablation, *International Journal of Hyperthermia.* 33 (2017) 51–60. <https://doi.org/10.1080/02656736.2016.1195519>.
- [39] C. Stureson, S. Andersson-Engels, A mathematical model for predicting the temperature distribution in laser-induced hyperthermia. Experimental evaluation and applications, *Phys Med Biol.* 40 (1995) 2037. <https://doi.org/10.1088/0031-9155/40/12/003>.
- [40] D. Yang, M.C. Converse, D.M. Mahvi, J.G. Webster, Measurement and analysis of tissue temperature during microwave liver ablation, *IEEE Trans Biomed Eng.* 54 (2007) 150–155. <https://doi.org/10.1109/TBME.2006.884647>.
- [41] M. Selmi, A.A. Bin Dukhyil, H. Belmabrouk, Numerical analysis of human cancer therapy using microwave ablation, *Applied Sciences (Switzerland).* 10 (2020). <https://doi.org/10.3390/APP10010211>.
- [42] A. Dekker, *Electrical engineering materials.*, Prentice-Hall, Englewood Cliffs N.J., 1959.
- [43] M. Cavagnaro, R. Pinto, V. Lopresto, Numerical models to evaluate the temperature increase induced by ex vivo microwave thermal ablation, *Phys Med Biol.* 60 (2015) 3287. <https://doi.org/10.1088/0031-9155/60/8/3287>.
- [44] P. Keangin, P. Rattanadecho, T. Wessapan, An analysis of heat transfer in liver tissue during microwave ablation using single and double slot antenna, *International*

- Communications in Heat and Mass Transfer. 38 (2011) 757–766.
<https://doi.org/10.1016/j.icheatmasstransfer.2011.03.027>.
- [45] V. Satish, J. Kumar, R. Repaka, Analysis of ablation volume produced during microwave ablation of breast cancerous lesion using fourier and non-fourier models, in: ASME International Mechanical Engineering Congress and Exposition, Proceedings (IMECE), American Society of Mechanical Engineers (ASME), 2019.
<https://doi.org/10.1115/IMECE2019-10800>.
 - [46] OVERVIEW » IT'IS Foundation, (n.d.). <https://itis.swiss/virtual-population/tissue-properties/overview/> (accessed October 4, 2022).
 - [47] C. Song, A. Alijani, T. Frank, G.B. Hanna, A. Cuschieri, Mechanical properties of the human abdominal wall measured in vivo during insufflation for laparoscopic surgery, *Surg Endosc.* 20 (2006) 987–990. <https://doi.org/10.1007/S00464-005-0676-6>.
 - [48] B. Hinz, Mechanical Aspects of Lung Fibrosis, <https://doi.org/10.1513/Pats.201202-017AW>. 9 (2012) 137–147. <https://doi.org/10.1513/PATS.201202-017AW>.
 - [49] W.C. Yeh, P.C. Li, Y.M. Jeng, H.C. Hsu, P.L. Kuo, M.L. Li, P.M. Yang, H.L. Po, Elastic modulus measurements of human liver and correlation with pathology, *Ultrasound Med Biol.* 28 (2002) 467–474. [https://doi.org/10.1016/S0301-5629\(02\)00489-1](https://doi.org/10.1016/S0301-5629(02)00489-1).
 - [50] D. Massalou, C. Masson, S. Afquir, P. Baqué, P.J. Arnoux, T. Bège, Mechanical effects of load speed on the human colon, *J Biomech.* 91 (2019) 102–108.
<https://doi.org/10.1016/J.JBIOMECH.2019.05.012>.
 - [51] A. Karimi, A. Shojaei, Measurement of the Mechanical Properties of the Human Kidney, *IRBM.* 38 (2017) 292–297. <https://doi.org/10.1016/J.IRBM.2017.08.001>.
 - [52] S. Singh, R. Repaka, THERMAL CHARACTERIZATION USING FOURIER AND NON-FOURIER CONDUCTION DURING RADIOFREQUENCY ABLATION OF BREAST TUMOR, *Multiphase Science and Technology.* 30 (2018) 207–219.
<https://doi.org/10.1615/MULTSCIENTECHN.2018021352>.
 - [53] B. Hinz, Mechanical Aspects of Lung Fibrosis, <https://doi.org/10.1513/Pats.201202-017AW>. 9 (2012) 137–147. <https://doi.org/10.1513/PATS.201202-017AW>.
 - [54] C. Song, A. Alijani, T. Frank, G.B. Hanna, A. Cuschieri, Mechanical properties of the human abdominal wall measured in vivo during insufflation for laparoscopic surgery, *Surgical Endoscopy and Other Interventional Techniques.* 20 (2006) 987–990.
<https://doi.org/10.1007/S00464-005-0676-6/METRICS>.
 - [55] R. Opik, A. Hunt, A. Ristolainen, P.M. Aubin, M. Kruusmaa, Development of high fidelity liver and kidney phantom organs for use with robotic surgical systems, *Proceedings of the IEEE RAS and EMBS International Conference on Biomedical Robotics and Biomechatronics.* (2012) 425–430. <https://doi.org/10.1109/BIOROB.2012.6290831>.
 - [56] D. Massalou, C. Masson, S. Afquir, P. Baqué, P.J. Arnoux, T. Bège, Mechanical effects of load speed on the human colon, *J Biomech.* 91 (2019) 102–108.
<https://doi.org/10.1016/J.JBIOMECH.2019.05.012>.
 - [57] V. Satish, R. Repaka, Microwave ablation trocar for ablating cancerous tumors: a numerical analysis, *Med Biol Eng Comput.* (2023). <https://doi.org/10.1007/S11517-023-02781-7>.
 - [58] H. Fallahi, P. Prakash, Antenna Designs for Microwave Tissue Ablation, *Critical Reviews™ in Biomedical Engineering.* 46 (2018) 495–521.
<https://doi.org/10.1615/CRITREVBIOSEDENG.2018028554>.
 - [59] Z. Makovich, J.R. Logemann, L. Chen, R. Mhaskar, J. Choi, N. Parikh, G. El-Haddad, B. Kis, Liver tumor ablation in difficult locations: Microwave ablation of perivascular and subdiaphragmatic hepatocellular carcinoma, *Clin Imaging.* 71 (2021) 170–177.
<https://doi.org/10.1016/J.CLINIMAG.2020.11.010>.

- [60] K. SAITO, T. TANIGUCHI, H. YOSHIMURA, K. ITO, Estimation of SAR Distribution of a Tip-Split Array Applicator for Microwave Coagulation Therapy Using the Finite Element Method, *IEICE TRANSACTIONS on Electronics*. E84-C (2001) 948–954.
- [61] I. Chang, U.N.- Biomedical, undefined 2004, Thermal modeling of lesion growth with radiofrequency ablation devices, *Biomedical-Engineering-Online* (n.d.).
<https://biomedical-engineering-online.biomedcentral.com/articles/10.1186/1475-925X-3-27> (accessed November 27, 2022).
- [62] G. Deshazer, P. Prakash, D. Merck, D. Haemmerich, Experimental measurement of microwave ablation heating pattern and comparison to computer simulations, *Https://Doi.Org/10.1080/02656736.2016.1206630*. 33 (2016) 74–82.
<https://doi.org/10.1080/02656736.2016.1206630>.
- [63] P. Prakash, M.C. Converse, J.G. Webster, D.M. Mahvi, An Optimal Sliding Choke Antenna for Hepatic Microwave Ablation, *IEEE Trans Biomed Eng*. 56 (2009) 2470–2476.
<https://doi.org/10.1109/TBME.2009.2025264>.
- [64] P. Wang, M.C. Converse, J.G. Webster, D.M. Mahvi, “Improved” Calculation of reflection coefficient for coaxial antennas with feed gap effect, *IEEE Trans Antennas Propag*. 57 (2009) 559–563. <https://doi.org/10.1109/TAP.2008.2011411>.
- [65] K. Saito, Y. Hayashi, H. Yoshimura, K. Ito, Heating characteristics of array applicator composed of two coaxial-slot antennas for microwave coagulation therapy, *IEEE Trans Microw Theory Tech*. 48 (2000) 1800–1806. <https://doi.org/10.1109/22.883857>.
- [66] I. Paolucci, S.J.S. Ruiter, J. Freedman, D. Candinas, K.P. de Jong, S. Weber, P. Tinguely, Volumetric analyses of ablation dimensions in microwave ablation for colorectal liver metastases, *International Journal of Hyperthermia*. 39 (2022) 639–648.
https://doi.org/10.1080/02656736.2021.1965224/SUPPL_FILE/IHYT_A_1965224_SM3163.PDF.
- [67] F. Fiore, V. Stoia, F. Somma, Surgical recurrence of solitary fibrous tumor of the pleura treated with microwave (MW) thermoablation: A case report, *Thorac Cancer*. 11 (2020) 443–446. <https://doi.org/10.1111/1759-7714.13263>.
- [68] Solero Microwave Tissue Ablation System - AngioDynamics, (n.d.).
<https://www.angiodynamics.com/product/solero-microwave-tissue-ablation-system/> (accessed May 10, 2023).
- [69] M.C. Giglio, E. Garofalo, R. Montalti, A. Vanlander, R.I. Troisi, The learning curve of laparoscopic ablation of liver tumors: A technically demanding procedure requiring dedicated training, *European Journal of Surgical Oncology*. 47 (2021) 2579–2585.
<https://doi.org/10.1016/J.EJSO.2021.05.032>.
- [70] V. Satish, R. Repaka, Microwave Ablation Trocar Operated at Dual Tine Dual-Frequency: A Numerical Analysis, *J Eng Sci Med Diagn Ther*. 6 (2023).
<https://doi.org/10.1115/1.4056410>.
- [71] V. Satish, R. Repaka, Safety and efficacy of intracavitary microwave ablation in hepatic gland tumours: Numerical and in vitro studies,
Https://Doi.Org/10.1177/09544119231179136. (2023) 095441192311791.
<https://doi.org/10.1177/09544119231179136>.
- [72] Z. Muludi, B. Aswoyo, Truncated microstrip square patch array antenna 2 × 2 elements with circular polarization for S-band microwave frequency, *Proceedings IES-ETA 2017 - International Electronics Symposium on Engineering Technology and Applications*. 2017-December (2017) 87–92. <https://doi.org/10.1109/ELECSYM.2017.8240384>.
- [73] C. Murat, M. Palandoken, I. Kaya, A. Kaya, A novel ISM band reflector type applicator design for microwave ablation systems, *Https://Doi.Org/10.1080/15368378.2021.1885434*. 40 (2021) 286–300. <https://doi.org/10.1080/15368378.2021.1885434>.

- [74] E.M. Knavel, J.L. Hinshaw, M.G. Lubner, A. Andreano, T.F. Warner, F.T. Lee, C.L. Brace, High-powered gas-cooled microwave ablation: Shaft cooling creates an effective stick function without altering the ablation zone, *American Journal of Roentgenology*. 198 (2012). <https://doi.org/10.2214/AJR.11.6503>.
- [75] D. Yang, J.M. Bertram, M.C. Converse, A.P. O'Rourke, J.G. Webster, S.C. Hagness, J.A. Will, D.M. Mahvi, A floating sleeve antenna yields localized hepatic microwave ablation, *IEEE Trans Biomed Eng.* 53 (2006) 533–537. <https://doi.org/10.1109/TBME.2005.869794>.
- [76] J. Yoon, J. Cho, N. Kim, D.D. Kim, E. Lee, C. Cheon, Y. Kwon, High-frequency microwave ablation method for enhanced cancer treatment with minimized collateral damage, *Int J Cancer*. 129 (2011) 1970–1978. <https://doi.org/10.1002/IJC.25845>.